BENEFICIAL USE OF BIOMASS AND COAL COMBUSTION RESIDUALS

A Dissertation
Presented to
The Academic Faculty

by

Xenia Wirth

In Partial Fulfillment
of the Requirements for the Degree
of Doctorate of Philosophy in the
School of Civil and Environmental Engineering

Georgia Institute of Technology
July 2019

BENEFICIAL USE OF BIOMASS AND COAL COMBUSTION RESIDUALS

Approved by:

Dr. Susan Burns, Advisor
School of Civil and Environmental Engineering
Georgia Institute of Technology

Dr. J. David Frost
School of Civil and Environmental Engineering
Georgia Institute of Technology

Dr. Sheng Dai
School of Civil and Environmental Engineering
Georgia Institute of Technology

Dr. Martial Taillefert
School of Earth and Atmospheric Sciences
Georgia Institute of Technology

Dr. Robert Bachus
Senior Principal Engineer
Geosyntec Consultants

Date Approved: July 1, 2019

To my grandparents, who first interested me in science

ACKNOWLEDGEMENTS

I would first and foremost like to thank my advisor, Dr. Susan Burns, without whose initiative and support, this work would not have been possible. She reached out to me when I was a 4th year undergraduate student in her course, asking me if I would consider staying on as a graduate research assistant. I happily accepted a semester of undergraduate research working with her lab, and the rest is history. She opened a new life pathway for me, and I cannot thank her enough for her initiative and support over these last six years.

I would also like to extend my sincerest thanks to my family, friends, and my fellow Geo-students for their unwavering support during this long journey. The encouragement they provided kept me focused and determined, even in the most challenging moments. I will treasure the memories I made during my tenure as a PhD student as I graduate, assume my role as an assistant professor, and embrace life's continuing challenges. I look forward to future adventures with all who I have had the pleasure of interacting with during my PhD.

I would like to thank the Geosystems faculty, other CEE faculty, and the academic support staff of Mason, SEB, the Structure's Lab, and Daniel Lab for their support, both technical and non-technical, over the years. Without your advice, expertise, and encouragement, my research would not have been possible.

And finally, I would like to thank Southern Company for not only their financial support and encouragement but for all of their advice and expertise. Their perspectives

were invaluable for understanding how my research in the laboratory fit into the larger world of coal and biomass combustion and waste disposal.

TABLE OF CONTENTS

LIST OF TABLES

LIST OF FIGURES

LIST OF SYMBOLS AND ABBREVIATIONS

AR	as-received
ASTM	American Society of Testing and Materials
BA	biomass fly ash
CBD	citrate bicarbonate dithionite
CCR	coal combustion residual
C_u	coefficient of uniformity
DI	deionized
EDS	electron dispersive spectroscopy
FA	coal fly ash
FBB	fluidized bed boiler
G_s	specific gravity
HCFA	high carbon content coal fly ash
ICP-OES	inductively coupled plasma optical emission spectrometry
LL	liquid limit
LOI	loss on ignition
POC	primary oxide content
SAI	strength activity index
SCM	supplementary cementitious material
SEM	scanning electron microscope
SSA	specific surface area
SWCC	soil water characteristic curve
TC	total carbon content, measured by TOC analyzer

TGA	thermogravimetry
TGA TL	total mass loss, measured by thermogravimetry
TGA OC	mass loss due to organic carbon content, measured by thermogravimetry
TOC	total organic carbon content, measured by TOC analyzer
WFA	weathered coal fly ash
XRD	x-ray diffraction
XRF	x-ray fluorescence

SUMMARY

The work performed in this dissertation focused on the beneficial use of coal and biomass combustion residuals. The alternative fly ashes tested in this study ranged from high-carbon content coal fly ash, to previously geologically disposed weathered coal fly ash, to ash from biomass that has been co-fired with coal, to woody biomass fly ash. However, the bulk of this dissertation was focused on geologically disposed weathered coal fly ash and woody biomass fly ash. These ashes were collected from power generation facilities in the southeastern and central United States. They were extensively characterized using mineralogical and thermal techniques, including thermogravimetry, x-ray diffraction, scanning electron microscope with electron dispersive spectroscopy, laser particle size analysis, and x-ray fluorescence, among others.

Characterization revealed morphologies specific to weathered coal fly ashes and to biomass fly ashes. Weathered fly ashes classified as Class F coal fly ashes with variable organic carbon content. They had, on average, more hydrated mineral phases than unweathered Class F fly ashes, most likely because they were wet-disposed and exposed to precipitation. Volatile mineral phases present in weathered ash included hydrated calcium sulfates, hydrated clays, portlandite, carbonates, iron oxides, and unburned carbon. Woody biomass fly ash from a full scale, biomass only power generation facility (PN) was a high-calcium, low-organic material whose properties were consistent across multiple combustion cycles. The fine-grained particle sizes, low specific surface area, and low organic carbon were attributed to the combustion conditions in the fluidized bed boiler; the PN ash had a lower unburned carbon content, a lower specific surface area, a higher specific gravity, and a

lower median particle size than three other woody biomass ashes produced at facilities with other boiler configurations.

The beneficial use of weathered fly ashes requires the dewatering and mining of ash impoundment facilities, which necessitates an understanding of the fly ash saturated and unsaturated hydraulic properties. In pursuit of this understanding, a detailed study on the saturated and unsaturated characteristics of a treated high-water-retention capacity weathered coal fly ash (PY) was performed. Hydraulic conductivity testing was performed in a flexible-wall, falling-head permeameter, and unsaturated behavior was quantified through soil-water-retention curves with the assistance of external laboratory DBS&A. Investigation of the hydraulic behavior of the ash samples was conducted after a series of chemical and physical treatments. Color change of the as-received PY sample that occurred during thermal treatment was due to the transformation of kaolinite present in the ash into non-crystalline metakaolin and crystalline hematite (and potentially mullite and cristobalite). This transformation was confirmed by the shift in crystalline phases from kaolinite to hematite in x-ray diffraction analyses. All PY samples had a hydraulic conductivity on the order of 10^{-5} or 10^{-6} cm/s, which was consistent with literature on silts. The only treatment that had a significant influence on saturated hydraulic conductivity was the iron removal treatment using the CBD process (sample Y_CBD). The removal of crystalline and surface iron species and the inclusion of sodium compounds in the fly ash decreased the hydraulic conductivity by an order of magnitude.

The as-received PY sample had unsaturated behavior consistent with fine-grained silt; its water-retention profile was characterized by a shallow drainage curve and a high residual water content. Its high water-retention capacity was due to both kaolinite and diatom

frustules present in the ash. The calcined PY sample (Y_C) displayed unsaturated characteristics of a silty (high air-entry pressure) and sandy material (sharp drainage curve, low residual water content). Calcining the ash transformed the kaolinite into metakaolin and reduced its water-retention capacity. However, the as-received PY ash, the acid-treated sample (Y_A), and Y_CBD displayed silt-like drainage characteristics, reflected in a shallower drainage curve and higher residual water content. The acid (Y_A) and iron removal (Y_CBD) treatments did not influence either the kaolinite or the diatom frustules and so did not reduce the water-retention capacity of PY.

After weathered and biomass fly ash samples were characterized, potential beneficial use alternatives were explored, including use in concrete as supplementary cementitious materials and as sorbents for Pb(II) removal from aqueous solutions. Weathered coal fly ashes met ASTM C618 requirements for chemical, physical, and mechanical properties for Class F fly ashes, though some of these ashes had LOI values that exceeded 6%. When used in concrete mortars, 9 of 13 weathered ash samples met the strength requirements at 7 or 28 days. These ashes had the potential for use in concrete as supplementary cementitious materials. However, the effectiveness of weathered coal fly ashes in sorption applications was limited. These ashes had a limited total removal capacity for Pb(II) (<6 mg/g). However, woody biomass fly ashes showed high removal capacity for aqueous Pb(II) species. Removal of Pb(II) using biomass fly ashes included a combination of sorption to carbon functional groups and precipitation of lead sulfates and hydroxides. Geochemical modeling analysis using PHREEQC confirmed that the high equilibrium pH and high soluble cation concentrations of biomass fly ash contributed to Pb(II)

precipitation. Wastewater treatment applications may be a beneficial use sector for woody biomass fly ash if metal removal is the primary objective for the treatment.

In summary, the work performed in this study of biomass and weathered coal fly ash indicated that:

- Weathered coal fly ashes from impoundment facilities in the southeastern and central United States were Class F fly ashes, with variable LOI contents
- Weathered coal fly ashes contained more hydrated mineral phases than unweathered coal fly ash, due to disposal conditions in impoundment facilities
- Biomass fly ash from a biomass-only facility equipped with a fluidized bed boiler consisted of a low carbon, high-calcium, silt-sized material with aluminosilicate spheres
- The saturated hydraulic conductivity of a high water-retention capacity weathered coal fly ash was on the order of 10^{-5} cm/s, and it displayed unsaturated hydraulic behavior representative of both sand (low air-entry pressure) and silt (shallow drainage curve, high residual moisture content)
- The high water-retention capacity of a weathered fly ash sample was due to kaolinite and diatom frustules present in the ash
- Iron reduction and removal using the CBD process was the most influential treatment on the saturated hydraulic conductivity, but calcining the ash at 800°C was the most effective treatment for reducing the water-retention capacity of the as-received weathered fly ash

- Weathered fly ashes retained amorphous, potentially reactive pozzolanic silica after weathering and performed well as SCMs in concrete applications
- Biomass fly ashes were effective for removal of Pb(II) from aqueous solutions, by a combination of precipitation and sorption to carbon functional groups

Overall, weathered coal fly ashes could potentially be used as an additional source of coal fly ash for concrete applications, once they have been reclaimed from the ash pond. The weathered ashes analyzed in this dissertation fulfilled the ASTM C618 requirements to be beneficially used as a supplementary cementitious material. Using weathered coal fly ash as an SCM would supplement seasonal shortages of freshly-produced coal fly ash.

A full-scale, biomass-only power generation facility consistently produces a biomass fly ash characterized by high calcium content, low carbon content, and silt-sized particles. This material could potentially be beneficially used in applications where a high-calcium content is favorable (soil solidification/stabilization, agricultural amendments, and buffering of acidic waste streams). Additionally, this material was effective for removing Pb(II) from aqueous solutions and could be potentially used in wastewater treatment. Beneficially using biomass fly ash would provide additional economic incentive for the combustion of renewable fuels.

CHAPTER 1. INTRODUCTION

1.1 Research Motivation

Ash disposal facility engineering failures in the 21st century (Tennessee Valley Authority, 2008; Duke Energy, 2014) have brought ash disposal practices under federal scrutiny in recent years. In October of 2015, the Environmental Protection Agency published a final ruling on disposal of coal combustion residuals (CCRs) that formally classified CCRs as non-hazardous waste regulated under the Resource Conservation and Recovery Act (RCRA) Subtitle D (the same category as municipal solid waste (MSW)) [1]. As part of the final ruling, the EPA published minimum criteria for CCR disposal for all disposal facilities (new and currently existing), including location restrictions, design and operations management, groundwater monitoring controls, closure and post-closure care, and recordkeeping [1]. Similar to MSW disposal, states are able to impose disposal requirements in addition to the federal regulations. For example, North Carolina has imposed additional restrictions on top of the federal guidelines and requires existing impoundments to be "clean-closed" (the pond must be emptied completely, and the CCR material moved to lined facilities and/or landfills). Other facilities in the southeastern United States have opted for "close-in-place" where impoundments that are not currently receiving new ash are capped and monitored according to post-closure care criteria. A combination of these closure options is found throughout the United States which provides an opportunity to study the engineering, environmental, and morphological properties of weathered CCRs.

The combination of “clean-closed” and “closed-in-place” construction has brought particular attention to the hydraulic properties of weathered, geologically-disposed fly ash. CCRs are typically wet-sluiced to permanent impoundments by mixing bottom ash (a sand sized material) and fly ash (a silt sized material) with water and pumping the slurry to an impoundment. Consequently, ponded CCRs are partially-to-fully saturated, and the standing water table may be above the surface of the disposed material. Dewatering ash disposal facilities is a time-consuming and energy-intensive process that relies heavily on an understanding of the hydrologic environment within and surrounding the disposal facility. However, the literature is sparse on the unsaturated and saturated hydraulic properties of weathered fly ash. Research questions remain to determine how weathered fly ash responds to the partially-saturated conditions experienced during impoundment dewatering. A deeper understanding of the hydrogeological interactions between fly ash and water would be beneficial for applications related to ash pond dewatering.

Weathered fly ash that is being removed from its impoundment and transported to a new disposal location may have the potential to be processed, stored, and beneficially used. However, there is currently limited data in the literature on how long-term weathering changes the mineralogy and morphology of fly ash. These changes can impact the beneficial use of weathered ash in the concrete sector, which is currently the largest sector for beneficial use of fly ash [2]. Ash that is not suitable for beneficial use in concrete may find additional beneficial use opportunities elsewhere; for example, high-carbon content ash, while undesirable for concrete mixtures, may be a good adsorbent for heavy metals and organics. Additionally, reclaimed ashes may be used for the extraction of rare earth

elements. Exploring beneficial use opportunities for weathered fly ash may offset some of the environmental and economic costs of “clean-closure”.

Biomass combustion refers to the combustion of fuel products derived from natural sources, including but not limited to wood products, plant wastes, agricultural residue, and municipal solid wastes [3]. Biomass is considered a mostly renewable, mostly carbon-neutral fuel source because the plants have metabolized CO_2 [4,5]. However, there are still questions concerning the effectiveness of biomass as a major fuel source and the unintended consequences of combustion [4,6,7]. Biomass combustion produces some of the same waste products as coal combustion, which must then be geologically disposed or beneficially used. Although the use of biomass fly ash in concrete applications in the United States is currently barred because the ASTM standard C618 specifies 100% coal fly ash, the use of biomass fly ash as a carbon-based sorbent should be explored [8]. Biomass fly ash could be an effective adsorbent of heavy metals in aqueous solutions, for applications in wastewater and drinking water treatment [9]. Beneficially using biomass fly ash wastes would encourage the use of biomass as a renewable energy combustion alternative to coal combustion. The costs associated with ash disposal would decrease, as the residual product is sold for alternative benefit.

1.2 Research Scope

This work focuses on the characterization, beneficial use, and hydraulic properties of biomass and coal combustion residuals. Beneficial use alternatives for weathered coal and biomass fly ashes were focused on two sectors: concrete and wastewater treatment. Unsaturated and saturated hydraulic properties of weathered fly ash were studied for one

particular sample of weathered ash that was observed by plant operations personnel to have unusually high water-retention capabilities.

Fifty-five samples of fly ash (24 biomass ash (BA), 30 weathered coal fly ash (WFA), and 1 unweathered coal fly ash (FA)) were collected and characterized for various chapters of this study. These samples were taken from five coal ash disposal sites in the southeastern and central United States and one biomass-only, full-scale combustion facility in Texas (Table 1). PW, PM, PY, and PV samples were sampled from the surfaces of ash impoundments (less than 10 feet below ground surface). BH samples were taken from two boreholes (up to 60 feet below ground surface), and in future chapters will be labeled as BH2 (3 samples) and BH10 (9 samples).

Table 1. Fly Ash Samples and Firing Conditions

Plant ID	Location	Capacity (MW)	Boiler Configuration[1]	Type of Ash
PW	Georgia	952	TF	WFA (10), FA (1)
PM	Georgia	163	TF	WFA (5)
BH	Alabama	705	OWF	WFA (12)
PY	Georgia	952	TF	WFA (1)
PV	Indiana	250	OWF	WFA (2)
PN	Texas	70-100	FB	BA (24)

[1]OWF = opposed wall fired; TF = tangentially fired; FB = fluidized bed

The samples were analyzed using the following investigative techniques:

- particle size distribution by laser diffraction (Malvern 3000 Hydro EV)
- specific gravity by helium pycnometer (Quantachrome ULTRAPYC 1200e) because water pycnometer was not appropriate for ash particles that floated
- semi-quantitative mineral and amorphous phase classification by x-ray diffraction (Panalytical Empyrean)

- carbon content by loss-on-ignition in a muffle furnace and a total organic carbon analyzer (Shimadzu TOC-V SSM-5000A)
- specific surface area by N_2 adsorption (Micromeritics ASAP 2020) and methylene blue adsorption [10]
- elemental composition and morphology by scanning electron microscope and electron dispersive spectroscopy, for qualitative analysis of fly ash morphologies (Hitachi SU8010; Zeiss Ultra 60)
- elemental oxide composition by x-ray fluorescence (Philips PW 2400)
- volatile/combustible mineral composition by thermogravimetry (Exstar TG/DTA7300)

The work performed in this study was designed to provide insight into the following properties and engineering behaviors:

- potential chemical and morphological changes in fly ash due to weathering
- the variation in biomass ash morphology from ash produced at different facilities
- the unsaturated and saturated hydraulic properties of untreated and treated weathered fly ash
- the beneficial use of weathered fly ash as a supplementary cementitious material (SCM) in concrete
- the use of alternative fly ashes for heavy metal sorption and predictive modeling of removal behavior based on ash/water chemistry

This dissertation is part of a greater project to characterize and explore the beneficial use of many types of alternative ashes, including: high carbon content coal fly ash (HCFA),

pure biomass fly ash (BA), ash from coal combusted with small quantities of biomass (biomass ≤ 15%) (CA), and weathered coal fly ash (WFA). Past researchers Yeboah [11] and Shearer [12] were responsible for characterizing HCFA, BA, and CA samples, along with recently-produced coal fly ash (FA). These researchers examined the beneficial use of these materials in sorption, fired-brick, alkali-activated geopolymer, and concrete applications [11–14]. This work expands upon previous work by characterizing: (a) 26 BA samples that were produced at a full-scale, biomass-only power generation facility (PN) and (b) 30 weathered coal fly ashes (WFA) samples that were reclaimed from five ash disposal impoundments. The previous work on sorption was expanded by including a thermodynamically-derived Langmuir sorption model and determining Pb(II) sorption capacity for 2 WFA samples. The previous work on beneficial use of ash in concrete was expanded to include 13 WFA samples. Additional, new work was done on saturated and unsaturated hydraulic properties of the PY WFA sample. A complete summary of the work performed by each researcher involved in the project is listed below (

Table 2).

Table 2. Summary of the Study of Alternative Ashes

Researcher		Yeboah [11]	Shearer [12]	Wirth	Benkeser
Characterization of pure biomass, co-fired, and high carbon content coal fly ashes		(1) FA (4) HCFA (8) CA (3) BA			
Beneficial use of pure biomass, co-fired, and coal fly ashes	Fired brick production	(1) HCFA (1) CFA (3) BFA			
	Adsorption of Pb(II), As(V), and Se(VI)	(1) HCFA (2) CA (3) BA (2) AC			
	Alkali-activated geopolymers	(1) HCFA (1) FA			
	Concrete		(1) FA (2) HCFA (3) CFA (1) BA		
Characterization of pure biomass and weathered coal fly ash				(1) FA (30) WFA (24) BA	
Beneficial use of pure biomass and weathered coal fly ash	Adsorption modeling of Pb(II)			(2) WFA (4) BA (1) HCFA	
	Concrete			(13) WFA	(13) WFA
Saturated and unsaturated hydraulic properties of weathered coal fly ash				(1) WFA	

The following chapter provides a literature review of coal and biomass fly ash morphology, chemistry, and geotechnical engineering properties and an overview of the current regulatory environment for CCR disposal. Characterization of WFA samples is presented in Chapter 3. The characterization of BA samples from PN, compared to laboratory combustion of PN wood mixtures, and 3 BA samples characterized by researcher Yeboah [11], is summarized in Chapter 4. Chapter 5 presents the saturated and unsaturated hydraulic properties of the PY WFA sample, after chemical and physical treatments. The use of alternative fly ashes in concrete as supplementary cementitious materials is

presented in Chapter 6. Finally, Chapter 7 summarizes the sorption capacity of BA, WFA, and HCFA samples for Pb(II).

CHAPTER 2. LITERATURE REVIEW

2.1 Combustion Products

2.1.1 Coal Combustion

Fly ash is a waste product resulting from the generation of electrical power through the combustion of fuel. Coal, biomass, or a combination of solid fuels is used as the fuel source to create steam that rotates turbines, generating electricity. For the remainder of this manuscript, power generation facilities will be classified by the type of boiler: stoker-fired, fossil-fuel fired, or fluidized-bed [15,16]. Stoker-fired boilers combust fuel which is inserted into the firing chamber on a fuel bed comprised primarily of active fuel and fuel ash. For coal combustion, larger chunks of coal are used as the fuel. Fossil-fuel fired boilers refer to large-capacity boilers that burn coal that has been previously pulverized to a fine powder (less than 0.075 mm) because the crushed coal particles burn more efficiently than larger chunks of coal [15,16]. This is referred to specifically as pulverized-coal combustion. Various geometries of coal and air injection burners are used in pulverized-coal combustion, including tangentially-fired, opposed-wall fired, and front-wall fired [15]; these terms will be used later when summarizing firing conditions of various power generation facilities. The last category of boiler, fluidized-bed boilers, is used for efficient combustion of a wide range of fuels (including biomass fuels) at lower combustion temperatures [15]. These boilers have the advantage that the incoming fuel does not need to be pulverized to a powder. Fuel particles are suspended in a fluidized bed of inert materials (sand, limestone, fuel ash, etc.), and combustion is stimulated using an upwards-flowing stream of combustion gas (air) [15].

After coal or biomass is combusted in the boiler, waste materials are removed from the chamber either by gravity deposition or filtration. Larger ash particles (ranging in size from very small gravel to fine sand) are removed from the combustion bed by gravity deposition into a collecting bin. Bottom ash, economizer ash, and surge ash compose the larger ash particles. Ash particles in the 1-1000 μm range are light enough to float in the convection air currents within the combustion chamber. These particles are referred to as fly ash because they are light enough to "fly" with the flue gases. They are removed with filtration devices, including electrostatic precipitators (ESP) and baghouse filters [16]. For ESP filtration, fly ash particles are given an electric charge and are then removed from the flue gases when they pass through an electric field [16]. Baghouse filters are finely-woven glass fiber (or other material) filter bags that trap the fly ash particles as the flue gases pass through [16]. After filtration using either method, the fly ash particles are then deposited in hoppers and stored temporarily on-site in ash silos.

2.1.2 Formation of Cenospheres and Plerospheres

The formation of hollow (cenospheres) and filled (plerospheres) aluminosilicate spheres (the primary morphology found in fly ash) is a result of the high-temperature, rapid combustion in the boiler. The exterior surface of the fuel particle is exposed to the high temperatures (typically greater than 800°C), which allows it to become molten. Thermal degradation or dehydration of mineral phases in the fuel generates H_2O and CO_2; the expansion of the heated gases stretches the molten surface while rapidly heating the core [17]. The rapidly-heating core either completely boils away, leaving hollow spheres (cenospheres), or microspheres are formed within the expanded shell (plerospheres) [17]. During this expansion process, the lightweight spheres are also rising with the flue gases

and cooling, fixing the characteristic spherical shape of the aluminosilicate spheres. The characteristic time for sphere formation is estimated to take approximately 1,000 μsec for a 10 μm-sized particle [17].

2.1.3 CCR Production and Usage

In 2017, approximately 111 million tons of coal combustion residuals (CCRs) were produced in the United States [2]. The term CCRs encompasses all waste products of the coal combustion industry including fly ash, bottom ash, boiler slag, fluidized bed combustion (FBC) ash, gypsum, and other flue gas desulfurization (FGD) products. Approximately 62 million tons of ash waste products (fly ash, bottom ash, and FBC ash) (60% of the total waste stream) were generated in 2017; fly ash accounts for 34% of the total CCRs generated [2]. Approximately 60% of the produced coal fly ash was beneficially used, mostly in concrete applications, as fill for embankments, and in mining applications [2]. The unused fly and bottom ashes were disposed in ash ponds or landfills.

An upsurge in domestic natural gas usage in the United States in the past decade has contributed to a decrease in coal combustion for electricity. As a result of market forces, natural gas combustion for energy generation has increased from approximately 800 million MWh (megawatt hours) in 2006 (20% of the total energy generated) to approximately 1.3 billion MWh in 2017 (32%) [18]. In contrast, coal combustion has dropped from a 50% share of the total energy generated in 2006 to 29% in 2017 [18]. Consequently, fly ash production levels have dropped in 2017 to levels not seen since the early 1990s (less than 40 million tons), and the downward trend is likely to continue [2]. However, the production rate is dropping faster than the beneficial use rate, as the percent

usage of fly ash that is beneficially used has increased to 63% in 2017 [2]. Overall, fly ash usage is outpacing production, especially during periods of reduced energy demand (in the U.S. spring and fall months). Fly ash is used as a supplementary cementitious material (SCM) in concrete, including 14 million tons of fly ash in 2017 [2]. Fly ash, as a replacement for Portland cement (15-25% by mass), increases the quantity of the cementitious binder phase and therefore increases concrete durability without the addition of more costly Portland cement [19–22]. The concrete industry has become reliant on good quality coal fly ash for its technical and economic benefits, and the downward production trend may force concrete manufactures to find alternative supplementary cementitious materials (SCMs) and/or import ash from other countries.

2.2 Mineralogical Properties of Fly Ash

2.2.1 Coal Fly Ash

Although variability in combustion conditions and coal source generate some expected heterogeneity in fly ash composition, some predominant characteristics generally represent the material. Morphologically, coal fly ashes are comprised of lightweight aluminosilicate spheres and porous, irregular ellipsoids of unburned carbon (the leftover residual organic carbon from incomplete combustion). In terms of inorganic composition, coal fly ash is enriched in aluminum, iron, and silica and is more depleted in alkaline, alkaline-earth metals, and halogens than fly ash derived from biomass sources, mostly likely due to the subterranean alteration of organic matter in coal over millions of years [23]. Because the primary inorganic constituents in coal fly ash are typically silica, aluminum, and iron oxides, industries that use fly ash regularly (power generation facilities,

concrete manufacturers, etc.) use primary oxide content (POC), the sum of the silica, aluminum, and iron oxides content, as a general reference for classifying fly ash. In the U.S., the ASTM standard C618 uses POC as one of the requirements to classify fly ash as Class C (POC > 50%), and Class F (POC > 70%) [8]. Irrespective of coal source or specific combustion conditions, the POC is consistently greater than 50% across a variety of 178 North American coal ashes [24]. Calcium oxide content remains constant, but moisture content and alkaline content display of the highest variability in coal ashes [24].

The unburned carbon content in fly ash is often represented by its loss-on-ignition (LOI) value. A LOI test is a bulk mass loss combustion test that provides an approximation of unburned carbon content in fly ash, though the technique also includes mass loss due to mineral volatilization [25,26]. This parameter is widely used in the ash industries for reporting on both ash quality and boiler efficiency. For example, ashes with LOI over 6% are not suitable for use in U.S. concrete, unless acceptable performance standards are provided by the seller [8] because unburned carbon content negatively impacts concrete performance [26–28]. This test and the implications of LOI on concrete performance will be discussed in greater detail in Chapters 3 and 5 in the manuscript. In the same study of 178 fly ashes referenced earlier, LOI of fly ashes were in the range of <1% to 40% [24], though advances in boiler and combustion technologies have most likely reduced the average LOI in recent years.

Coal fly ash particles range between 1-200 μm in diameter, though most particles are smaller than 75 μm [13,29–31]. The smaller and smallest particles are spherical in shape, hollow (cenospheres) or filled (plerospheres), lightweight, and are composed of glassy

aluminosilicates [13,17,30]. However, glassy cenospheres are often larger as well, with one study finding that approximately 70%[1] of cenospheres from four different power plants in Australia had particle diameters between 45-150 μm [32]. Larger, non-spherical, porous unburned carbon structures have higher specific surface areas than the other morphologies found in coal fly ash [13,29], but overall, the specific surface area of coal fly ashes is low, with some variability. Even high-carbon content coal fly ashes display surface areas of less than 10 m^2/g [13].

X-ray diffraction (XRD) analysis shows mullite, hematite, magnetite, and quartz as some of the major crystalline components in coal fly ashes, along with some amorphous, potentially reactive silica identified as an "amorphous hump" between angles 15° and 40° 2Θ [13,30,33,34]. Mullite is more equally distributed among various size fractions than the other crystalline groups [30] and represents the most prominent Al-containing crystalline phase in low-calcium fly ashes [24]. Hematite is more prevalent in low-calcium fly ashes but magnetite concentration is equally distributed among low, intermediate and high-calcium content ash [24]. Although quartz is a siliceous material, it is non-reactive and cannot be used as a natural pozzolan for cement and concrete applications [24]. However, amorphous, reactive silica can also be identified using x-ray diffraction.

2.2.2 Biomass Fly Ash

Fly ash produced from biomass combustion is heterogeneous because the term 'biomass' encompasses a large variety of heterogeneous fuels. Biomass includes most organic materials that are not already encompassed by fossil fuels. Overarching categories

[1] By weight

of biomass fuel include woody biomass, herbaceous and agricultural biomass, aquatic biomass, animal and human waste biomass, industrial biomass waste, and biomass blends [4]. Because the composition of biomass material is variable even within a certain group, a thorough compositional analysis must be performed for each biomass fuel source. Woody biomass, as the name suggests, is composed of wood material derived from natural wood products (coniferous or deciduous) including chips, sawmill, pellets, briquettes, tree limbs, bark and foliage, among others. However, industrialized wood products (wood pellets, waste from paper and plywood industries) are not generally included in this category because industrialized wood products often contain high amounts of anthropogenic phases resulting from paints, detergents, contaminants, additives, and remnants from the glass, paper, ceramic and rubber industries [4,35]. The general elemental composition of woody biomass is approximately 50% carbon, 40-50% oxygen, 6% hydrogen and other trace elements including inorganic alkaline earth minerals, silicon, sulfur, and nitrogen [35,36]. Woody biomass displays higher C and Ca concentrations and lower concentrations of ash, Cl, K, N, S and Si than other biomass products [4]. Salts exist as cations bound to organic acids in cell walls or as phosphates, carbonates, silicates, and sulfates [37,38]. Silica content is often higher in bark than in wood, most likely due to soil contamination and embedment in the bark pore crevices by both natural and anthropogenic sources (i.e. wind, water, harvesting methods, processing, or transport) [4,37,39]

Biomass fly ash, like the parent biomass, is a highly heterogeneous material whose composition is dependent on a variety of factors, including but not limited to: (1) the type of biomass; (2) combustion conditions; and (3) the transportation and storage of the waste ash [4]. Biomass ashes have been shown to have higher concentrations of alkaline-earth

elements and lower percentages of sulfur, iron, and aluminum compared to coal fly ashes [5,13,40,41]. The alkaline earth elements are bioavailable and could be used productively for soil improvement and plant health [23]. In turn, there is a significant range in the silicon oxide content between biomass varieties, again highlighting the inherent variability of biomass materials [42,43]. Herbaceous materials have been shown to have higher ash yield than woody biomass, and wood foliage and outer features (small branches, twigs, and bark) yield higher ash content than the large wood stems or stumps [40,43]. Combustion temperatures and mineralogical composition also influence the ash content. Biomass ash particle sizes can range from less than 1μm to greater than 1mm. The largest particle sizes are often attributed to the organic, unburned carbon fraction [5,43]. Higher specific surface areas in biomass ash samples have also been linked to these larger, more porous carbon structures [13]. In contrast, the smallest-sized fractions are more enriched in volatized trace elements [40,41,43].

2.3 Geotechnical Properties of Coal Fly Ash

In geotechnical terms, fly ash is a predominately silt sized material (2-75μm particle diameter) with low plasticity [16,44–47]. The pH of ten representative coal ash samples from the United States, Europe, and Asia ranges between 6 and 12 [44]. Maximum dry unit weights of coal fly ashes tested by a variety of researchers range from 11.9 to 18.7 kN/m^3 and optimum water content range from 13 to 32% [16,47–49]. Kim et al. [48] suggests that the large difference between compaction parameters of two coal fly ashes (14.8 kN/m^3 and 17.5 kN/m^3) is related to their specific gravities (2.32 and 2.81, respectively). The hydraulic conductivity of fly ash is similar to silt, ranging from 10^{-4} – 10^{-7} cm/s, though most fly

ashes fall within the 10^{-4} to 10^{-6} cm/s range [16,44,45,48,50]. The friction angle for coal fly ash has been found to range from 22-47° [16,44 and references therein].

The specific gravity of coal fly ash has a much larger range (1.90-3.10) than natural soils (2.60-2.75) [16,44,45,48]. The specific gravity of 178 North American coal fly ashes fell within the 1.85-2.89 range, influenced by the percentages of inorganic constituents in the ash (iron oxides and unburned carbon content) and "Type I occluded voids" inside the hollow cenospheres [16,24,31,44,51–53]. A more detailed discussion of specific gravity is presented in Chapter 3, in which mineralogical reasons for this wide range are analyzed in greater detail. This range in specific gravity separates fly ash from natural sands, silts, and clays.

2.4 CCR Disposal

The federal regulations concerning the geologic disposal of CCRs were altered in October 2015, when the Environmental Protection Agency published the final rule entitled: 'Disposal of Coal Combustion Residuals from Electric Utilities' [1]. These regulations stipulate the requirements for ash disposal to mitigate potential environmental hazards. CCPs have been formally classified as non-hazardous waste, to be disposed under Subtitle D of the Resource Conservation and Recovery Act (RCRA). All ash disposal ponds must follow the new requirements for ash disposal unless the ash pond is dewatered and capped within three years [1]. On-site disposal units are the most typical method of CCR disposal, though some facilities transport their ash for disposal off-site. To facilitate transport to disposal locations, ash is typically mixed with water and pumped (wet-sluiced) though it

may be dry disposed [1]. Approximately 1,000 surface impoundments or ash landfills were active when the new regulations were published in April 2015.

The surface impoundments or ash landfills that cannot meet certain performance requirements for groundwater contamination, location, or structural integrity must either retrofit or close within five years, though extensions can be requested [1]. This regulation does not include municipal solid waste (MSW) landfills that also include CCRs. The disposal owner or operator is not allowed to dispose of ash "in uppermost aquifers, wetlands, within fault areas, seismic impact zones, and unstable areas" [1]. Any new disposal structure must be built with a composite geomembrane/compacted soil liner or an alternate composite liner and include a leachate collection and monitoring system. Older facilities without composite liners must meet all groundwater monitoring criteria [1]. To fulfill regulations relating to structural integrity, the owner or operator must: (1) conduct hazard assessments of potential failure of the ash ponds; (2) bring in a professional engineer to conduct structural stability assessments to document that disposal operations are consistent with good engineering practice; and (3) conduct safety factor assessments to determine pond slope stability [1]. In addition, the facility must meet operations criteria that address air pollution, hydraulic capacity requirements, periodic inspections, and run-on/run-off controls.

CHAPTER 3. MINERAL PHASES AND CARBON CONTENT IN WEATHERED FLY ASHES

3.1 Introduction

In the United States, an upsurge in natural gas production has contributed to a decrease in the burning of coal and a corresponding decrease in the production of fly ash. This has driven the concrete and cement industry to consider alternative ash products, such as imported ash and legacy ash reclaimed from waste ponds. Reclaimed, previously disposed fly ash is a potential new source of coal fly ash that is being examined for use as a supplementary cementitious material (SCM). However, ASTM C618 has strict limits on mineralogy, fineness, and loss-on-ignition (LOI) [8]. It is worthwhile to investigate how exposure to water during disposal and final storage has impacted the resultant coal fly ash and if weathered fly ash fulfills ASTM C618 requirements.

Water is the primary driver for ash weathering and the formation of tertiary mineral phases during disposal and permanent storage [54] because fly ashes are often sluiced (mixed as a slurry and pumped) to disposal facilities. Afterwards, weathering occurs primarily at two elevation zones within the pond: near surface (where they are exposed to surface water) and at the phreatic level [55–57]. The most influential weathering processes in the pond are hydration, carbonation, hydrolysis, and dissolution/precipitation [57,58], with hydration and dissolution/precipitation changing the ash mineralogy in as little as two weeks [58]. Tertiary mineral phases that have been found in weathered fly ashes include carbonates, portlandite (hydrated lime), amorphous clays (from glass hydrolysis),

chlorides, calcium-rich minerals (calcium sulfates, ettringite, and thaumasite) and amorphous iron oxides [54,57,59,60]. Ash that has had prolonged exposure to water is also typically less alkaline than unweathered fly ash, as soluble alkaline metals are dissolved and washed from the ash surface [56]. Because many of the weathering processes in ash ponds are governed by interactions with water, ash that has been dry-disposed takes longer to weather than wet-disposed fly ash [57,61].

The LOI method is a relatively simple procedure that quantifies the total amount of combustible minerals in fly ash, including unburned carbon [62], which is important because reducing the unburned carbon content in fly ash is necessary to limit sorption of air-entraining agents (AEA) that are used to stabilize air bubbles in concrete. The AEAs are attracted to the non-polar surfaces of the unburned carbon particles in fly ash [63] but are not sorbed at significant levels within the interior pore space. Small carbon particles, with high surface area to volume ratios, are the most problematic unburned carbon particles in fly ash because these particles have high quantities of accessible surface area to sorb AEAs [64]. Large AEA molecules cannot access the internal pore network of highly porous carbon particles, so fly ash that contains many large, highly porous unburned carbon particles are better for use in concrete due to their low surface area to volume ratio. The cost of producing concrete increases when fly ash has a large volume of small unburned carbon particles because sorption of AEAs occurs, requiring more AEAs to achieve a distributed network of air bubbles. The cost increases due to the expense of the admixtures.

ASTM C618 sets an LOI maximum at 6%, unless laboratory tests or performance metrics are provided which allow for an absolute maximum of 12% [8,62]. LOI is a bulk mass loss combustion measurement that includes mass loss due to the combustion of unburned

carbon, the main concern, but also due to volatilization of calcium and carbonate minerals and aromatic hydrocarbons, and water loss of the bulk ash and mineral constituents (such as the transformation of gypsum to anhydrite) [25,62,65]. Although the measurement quantifies the loss of volatiles, it is impossible to tell directly from an LOI measurement what types of volatile minerals are present in fly ash. It is incorrect to make assumptions about the mineral constituents of a weathered fly ash compared to an unweathered fly ash, simply on the basis of LOI value.

Alternative methods of measuring mass loss can provide additional information about volatile mineral content [25,26,28,63,66]. For example, dual-atmosphere thermogravimetry analysis (TGA) is effective because volatile mineral phases are combusted in an inert atmosphere and unburned carbon content is combusted in an oxidizing atmosphere [63]. TGA can be used to measure mass loss at the temperature ranges in which bonded water (200-400 °C), the decomposition of calcium hydroxides (400-500 °C), the decomposition of carbonate minerals (500-800 °C), and the reduction of iron oxides (750-1000 °C) contribute to mass losses in fly ashes [26,28,63,65–77]. A dual-atmosphere TGA used in conjunction with mass spectroscopy is able to determine when specific elements are volatized during combustion [63]. Compared to LOI, thermogravimetry provides more detail on the heat-sensitive minerals in fly ash.

A total organic carbon (TOC) analyzer fitted with a solid sample module excludes measurement of volatile mineral phases by measuring carbon using infrared detection [13,68,70,78]. The total carbon (TC) is converted to CO_2 via high-temperature combustion (900 °C), and the amount of CO_2 produced is measured by a non-dispersive infrared detector [79]. The inorganic carbon (IC) is converted to CO_2 through acidification with

phosphoric acid at 200 °C and is measured by the same detector. The subtraction of IC from TC is the total organic carbon (TOC) and is assumed to represent the unburned carbon content. Because a TOC analyzer only measures CO_2, this method excludes mass loss due to bound water loss in hydrated mineral phases (e.g. gypsum) or decomposition of non-carbonaceous phases (e.g. iron oxides).

Many mineral phases that form during ash weathering (hydrated sulfates, hydrated clays, and carbonates) decompose during high-temperature thermal treatment [26,28,63,65,71] and contribute to the LOI. Although these minerals are likely to be present in larger quantities in weathered ash compared to unweathered ash, but LOI provides no information about the type and quantity of volatile minerals in fly ash. This study uses multiple characterization tools and combustion methods to determine how the organic and mineral constituents of weathered fly ash differ from that of unweathered fly ash.

3.2 Materials and Methods

3.2.1 Analyzed Samples

Fly ash samples were taken from three different power generation facilities in the southeastern United States (PW, PM, and BH). All plants burned eastern bituminous coals. PW-labeled samples are a combination of fly ash and bottom ash that were disposed on-site through hydraulic sluicing into ash ponds. Samples were taken from the ash delta, at a depth of 0.15-0.9 m (0.5-3 ft) bgs (below ground surface), where there was no standing water. The surficial ash crust was removed before sampling. PW samples were disposed because there was not sufficient market demand to dry-collect all of the produced ash. One sample of unweathered, dry-stored fly ash (PW_F) was also collected from the same

facility as weathered samples. Because little is known of the historical record of combustion conditions and coal source, other than the type of coal, boiler configuration, and MW output, the unweathered fly ash serves only as a general comparison to weathered samples [80].

PM-labeled samples were taken from a second power plant that is no longer active. The ash pond received a combination of bottom ash and fly ash from 1980-2015. After coal combustion, the residual bottom ash and fly ash were hydraulically sluiced to the wet-storage facility in separate streams and combined at the drainage inlet. Samples were taken at depths between 0.15 – 1.5 m (0.5-5 ft) bgs within the wet-storage facility and are most likely fewer than 10 years old, according to plant operations personnel. Ash produced at this facility was disposed because it was not consistently of marketable quality (LOI was consistently over 6%).

BH-labeled samples were taken from two boreholes in a wet-storage facility next to a power plant. Samples were taken at a range of depths, up to 16 m (53 ft) bgs using a split spoon sampler and are estimated to be between 20 and 40 years old, according to plant operations personnel. During sampling, a layer of bottom ash approximately 3 m (10 ft) thick was placed on top of the disposed ash to form a stable platform and to allow access for borehole sampling equipment. Samples used for analysis were taken at depths below 3.4 m (11 ft) bgs to ensure that they were not contaminated by the construction access material layer. The depths reported for the borehole samples note ground surface as the level below the 3 m (10 ft) thick working platform of bottom ash. Ash produced at this facility was disposed because it was also not consistently of marketable quality.

All weathered samples (PW, PM, and BH) were weathered under southeastern U.S. climate conditions (humid subtropical) in saturated to partially saturated conditions [81]. All samples were oven-dried overnight at 80 °C, ground with a mortar and pestle, and stored. To isolate the fly ash particles for analysis, samples that were a mixture of fly ash and bottom ash (PW1-6 and PW10) were sieved using a No. 200 (75 μm) sieve. Particles passing the No. 200 sieve were collected and used for analysis. No other alterations of the samples were performed before characterization. Characterization was performed according to the procedures outlined in the introduction. Grain size analysis is reported below as the median particle size (D_{50}) and a uniformity parameter (u) (1). The uniformity parameter is the measurement of absolute deviation from the median size of the distribution, d(x,0.5) (Equation 1).

$$u = \frac{\sum X_i |d(x, 0.5) - d_i|}{d(x, 0.5) \sum X_i} \quad (1)$$

Although there is a growing body of literature on weathered fly ash, much of it is focused on chemical changes due to weathering and geochemical modeling of weathering processes [55,57,80,82,83]. There is little information on engineering properties of weathered ash. Industries that are considering beneficially using weathered ash in bulk quantities (for earthen embankments, roadway fillers, etc.) would benefit from information concerning particle size and specific gravity. Weathered fly ash is a fine-grained material with primarily silt-sized (less than 75 μm) particles and a relatively uniform particle size distribution (Table 3; Table 4). Median particle size fluctuated between ashes from different disposal sites. Specific gravity also fluctuated in a similar manner, but these

fluctuations were found to be correlated to chemical properties of weathered ash (discussed in detail below).

Table 3. Physical Properties of PW and PM Samples

Sample	Depth (m bgs)	G_s	d_{50} (μm)	u
PW1	0.15-0.91	2.90	27.4	0.68
PW2	0.15-0.91	2.73	23.3	0.80
PW3	0.15-0.91	2.72	24.3	0.78
PW4	0.15-0.91	2.87	31.8	0.66
PW5	0.15-0.91	2.92	31.6	0.63
PW6	0.15-0.91	2.91	29.7	0.66
PW7	0.15-0.91	2.38	20.6	1.12
PW8	0.15-0.91	2.42	18.3	1.36
PW9	0.15-0.91	2.48	12.7	1.29
PW10	0.15-0.91	2.67	23.4	0.76
PW_F	n/a	2.50	18.0	0.97
PM1	0.15-1.52	2.26	45.7	0.83
PM2	0.15-1.52	2.26	28.2	1.54
PM3	0.15-1.52	2.39	24.5	0.91
PM4	0.15-1.52	2.35	23.8	1.19
PM5	0.15-1.52	2.38	30.5	1.05

Table 4. Physical Properties of BH Samples

Sample	Depth (m bgs)	Gs	d_{50} (μm)	u
BH10-1	0.30-0.91	2.24	160	0.63
BH10-2	3.29-3.90	2.20	207	1.23
BH10-3	3.90-4.51	2.19	167	0.95
BH10-4	6.37-6.98	2.20	144	1.48
BH10-5	9.93-10.6	2.21	272	1.65
BH10-6	10.6-11.2	2.20	245	1.52
BH10-7	13.0-13.6	2.19	144	0.82
BH10-8	15.4-16.0	2.10	65.7	1.09
BH10-9	15.4-16.0	2.22	108	0.78
BH2-1	1.83-2.44	2.40	76.4	1.11
BH2-2	6.55-7.16	2.34	88.3	1.07
BH2-3	15.5-16.2	2.35	74.2	1.02

3.2.2 Visual Analysis of Weathered Fly Ashes

A scanning electron microscope (Hitachi SU8010) was used to visually inspect weathered fly ash samples; several distinct particle types were identified. Larger, dark-colored, spheroidal particles that had a well-defined surface pore structure were unburned carbon particles (Figure 1a) [84]. The shallow weathered fly ash samples contained almost exclusively large, smooth-surfaced (no surface adsorption or deposition), honeycombed carbon structures whose pores contained small glassy cenospheres (Figure 1b and c). Similar structures have been identified as carbon particles by others researchers [13,64,85,86]. The porous carbon structure was preserved after weathering when samples were relatively young (aged fewer than 10 years); however, the BH weathered samples that were taken at greater depths within the wet-storage facility showed signs of carbon weathering. The carbon surface had a sheeted, feathery morphology with fewer surface pores though the embedded cenospheres were still visible, and the structure was still porous (Figure 1d).

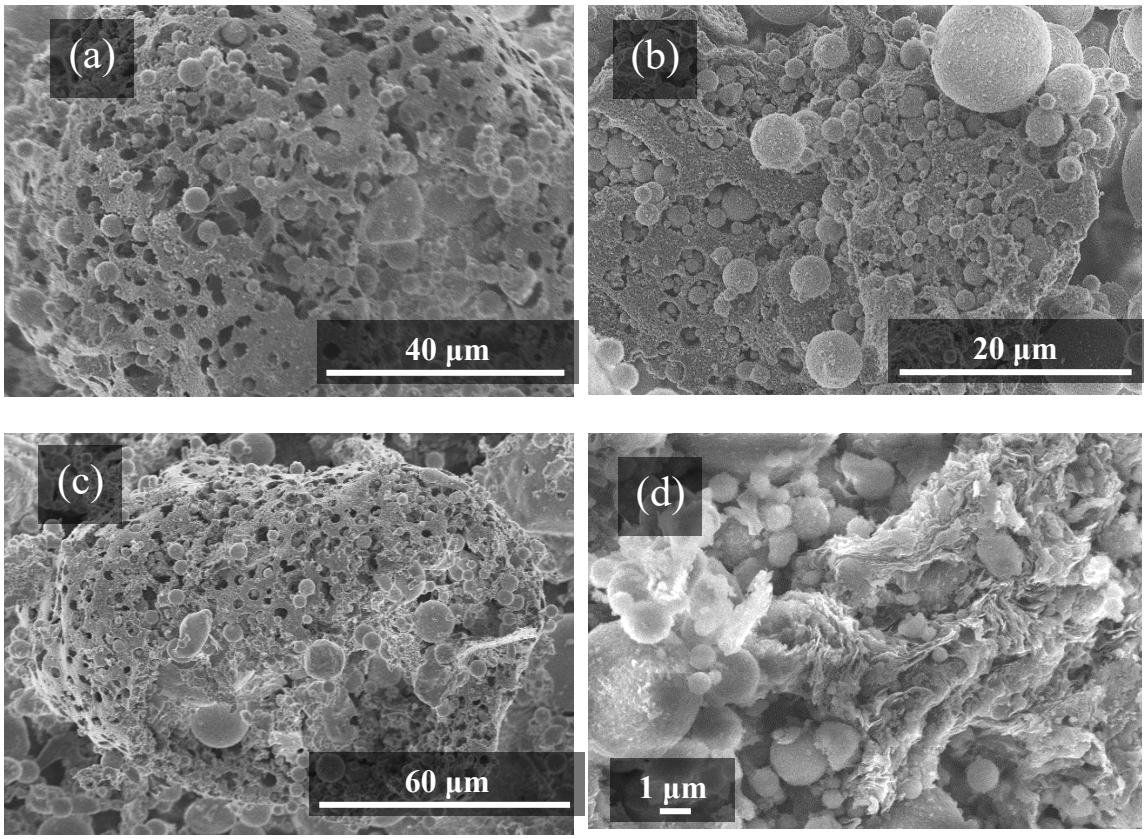

Figure 1. SEM images showing: (a) a carbon particle in a sample of unweathered PW fly ash, (b) a carbon particle in sample PW3 fly ash sample, (c) a carbon particle in sample PM2, and (d) a carbon particle in sample BH10 7

Similarly to unweathered fly ash, most of the structures found in weathered fly ash were aluminosilicate glassy spheres and unburned carbon particles [13]. However, in weathered ashes, ash particles were often found in larger agglomerates, with depositional bonding structures present as long "threads" (BH10 4 in Figure 2) or as large, amorphous clumps (PW1 in Figure 2) between particles. Fractured aluminosilicate spheres were common, and many fractured spheres were filled with smaller spheres (Figure 3). Some deposition directly onto the surface of aluminosilicate spheres was seen (PM3 in Figure 2; Figure 3), though many spheres have smooth surfaces free from precipitates. Past research has attributed deposition onto aluminosilicate spheres to weathering dissolution/precipitation processes [56,59]; however, surface depositions (anhydrite, hematite, and magnetite) have

also been shown on unweathered fly ashes [54]. SEM EDS analysis confirmed that common precipitates on aluminosilicate spheres in weathered ashes include calcium, sulfur, iron and oxygen and that iron oxides exist both as distinct, discrete particles (upper sphere in Figure 3) as well as precipitates on aluminosilicate spheres (lower, fractured sphere in Figure 3).

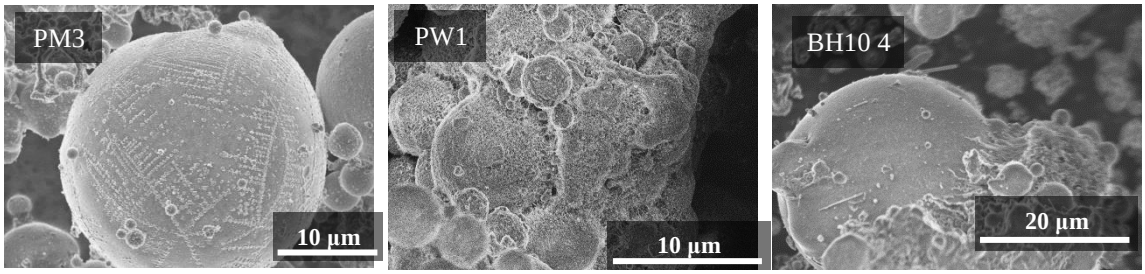

Figure 2. SEM micrographs showing various morphologies in weathered fly ash

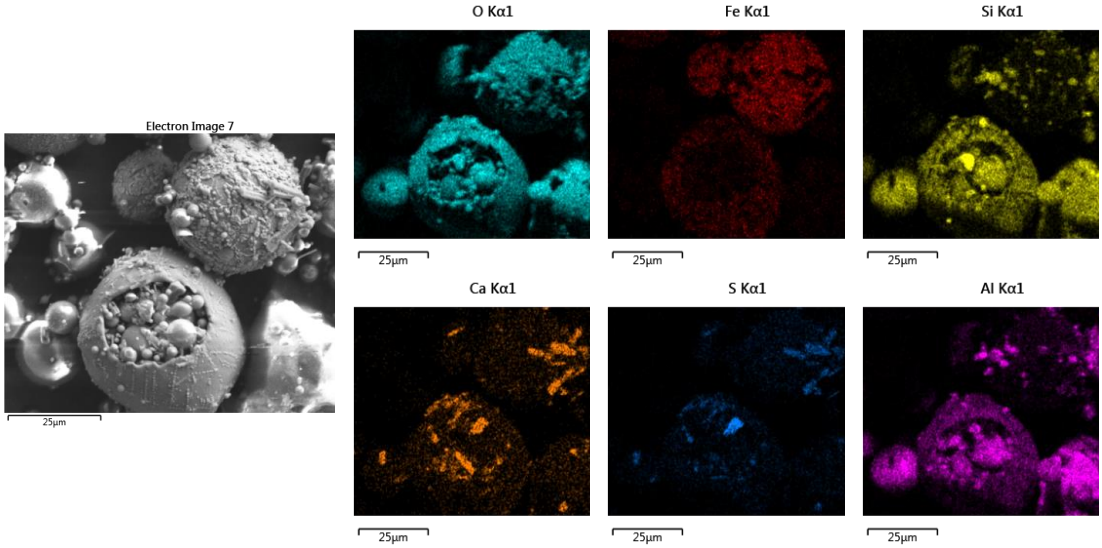

Figure 3. SEM EDS image showing the distribution of oxygen, iron, silicon, calcium, sulfur and aluminum in a sample of weathered fly ash

3.2.3 Carbon Analysis

Five different mass losses attributed to the combustion of carbon and other volatile minerals in the ash were compared including: loss-on-ignition (LOI), total carbon content (TC, from TOC analysis), total organic carbon content (TOC), total mass loss measured by

thermogravimetry analysis (TGA TL), and mass loss measured by thermogravimetry analysis after the atmosphere had been switched to compressed air (assumed to be the mass loss due to the unburned carbon content) (TGA OC). LOI was determined by heating samples in a muffle furnace according to ASTM D7348, Method B (combustion at 950 ℃) [62]. Total and inorganic carbon contents were determined using a Shimadzu TOC-V Analyzer fitted with a solid sample module. Inorganic and total carbon content were measured by acidification with 85% phosphoric acid at 200 °C and combustion at 950 °C, respectively, and total organic content (TOC) was determined by subtraction. Thermogravimetry samples were heated to 950 °C in a nitrogen atmosphere (flow rate of 100 cc/min) and then the atmosphere was changed to compressed air to allow for combustion of free carbon phases.

3.3 Results and Discussion

3.3.1 Mineral Phases in Weathered Fly Ashes

Weathered fly ashes were comprised primarily of silica, aluminum, and iron oxides (Table 5; Table 6); major crystalline phases were quartz, mullite, hematite and magnetite. Ash chemical properties (LOI, POC, CaO content, and Fe_2O_3 content) fell within the ranges for 178 unweathered North American coal fly ashes [24] and 13 unweathered co-fired and coal fly ashes analyzed by Yeboah [13], except for the high iron contents of 7 PW ashes (Figure 4). There were no clear trends in elemental composition with depth for the BH10 and BH2 samples and no significant differences in elemental composition between the PW unweathered ash and the weathered ashes; samples were a heterogeneous assortment that represented decades of coal combustion at multiple generation facilities.

Table 5. Oxide Content of PW and PM Ash Samples

Samples	SiO_2	Al_2O_3	Fe_2O_3	SO_3	CaO	Na_2O	MgO	K_2O	P_2O_5	TiO_2	SrO	BaO	POC (%)
PW1	37.4	17.0	38.8	0.54	1.10	0.41	0.55	1.82	0.16	0.93	0.07	0.07	93.2
PW2	43.7	19.8	27.7	0.30	1.83	0.51	1.01	2.18	0.14	1.08	0.08	0.09	91.2
PW3	46.6	21.2	23.8	0.10	1.62	0.60	0.83	2.34	0.20	1.16	0.08	0.11	91.7
PW4	41.1	18.6	32.9	0.11	1.60	0.44	0.79	1.99	0.15	1.01	0.07	0.10	92.6
PW5	54.5	25.3	11.1	0.16	1.78	0.66	1.00	2.87	0.21	1.31	0.09	0.12	91.0
PW6	38.5	17.4	36.9	0.12	1.55	0.48	0.66	1.83	0.17	0.99	0.08	0.09	92.7
PW7	39.5	17.3	35.3	0.26	1.98	0.46	0.64	1.80	0.18	1.00	0.08	0.09	92.2
PW8	55.6	26.0	10.2	0.12	1.64	0.68	1.00	2.93	0.25	1.36	0.09	0.13	91.8
PW9	54.4	24.5	12.3	0.12	1.89	0.77	0.97	2.83	0.22	1.33	0.09	0.11	91.3
PW10	40.1	17.9	34.7	0.28	1.43	0.41	0.67	1.89	0.16	1.06	0.08	0.09	92.6
PW_F	48.6	20.7	16.0	1.78	5.97	0.94	0.83	2.33	0.12	1.05	0.05	0.05	85.3
PM1	54.5	28.9	8.67	0.10	1.06	0.35	0.99	2.81	0.47	1.6	0.12	0.16	92.0
PM2	52.4	30.5	8.55	0.14	1.56	0.43	0.98	2.58	0.9	1.52	0.21	0.21	91.5
PM3	52.4	28.3	11.8	0.05	1.11	0.31	0.80	2.38	0.31	1.49	0.15	0.13	92.5
PM4	53.7	30.1	8.00	0.07	1.38	0.31	0.89	2.51	0.75	1.62	0.19	0.17	91.7
PM5	54.8	28.9	8.13	0.05	1.28	0.38	0.94	2.53	0.56	1.66	0.12	0.16	91.8

Table 6. Oxide Content of BH Ash Samples

Samples	SiO_2	Al_2O_3	Fe_2O_3	SO_3	CaO	Na_2O	MgO	K_2O	P_2O_5	TiO_2	SrO	BaO	POC (%)
BH10-1	61.8	23.5	5.97	0.29	3.19	0.49	1.25	2.29	0.54	1.21	0.13	0.15	91.3
BH10-2	60.2	26.2	4.99	0.28	2.27	0.41	1.18	2.5	0.71	1.34	0.14	0.19	91.4
BH10-3	61.0	25.1	5.14	0.25	2.41	0.47	1.26	2.51	0.68	1.27	0.15	0.17	91.2
BH10-4	55.8	29.7	5.11	0.31	2.51	0.39	1.26	2.61	0.54	1.63	0.12	0.20	90.6
BH10-5	53.7	29.6	5.90	0.37	3.30	0.49	1.40	2.56	0.66	1.59	0.15	0.24	89.2
BH10-6	53.6	29.7	5.79	0.39	3.21	0.53	1.33	2.57	0.68	1.58	0.14	0.24	89.2
BH10-7	59.2	26.8	4.94	0.27	2.49	0.47	1.20	2.46	0.74	1.42	0.16	0.20	91.0
BH10-8	54.8	31.3	4.69	0.11	1.99	0.54	1.12	2.63	0.75	1.68	0.17	0.26	90.9
BH10-9	54.9	29.6	5.73	0.35	2.81	0.41	1.32	2.53	0.53	1.61	0.12	0.22	90.2
BH2-1	50.4	28.4	5.67	0.6	6.51	0.7	1.85	2.09	0.86	1.73	0.22	0.35	84.5
BH2-2	52.5	27.7	5.78	0.45	5.48	1.09	1.72	2.23	0.78	1.62	0.18	0.32	85.9
BH2-3	50.8	26.8	5.25	0.56	7.84	1.19	2.18	1.80	0.90	1.61	0.22	0.37	82.8

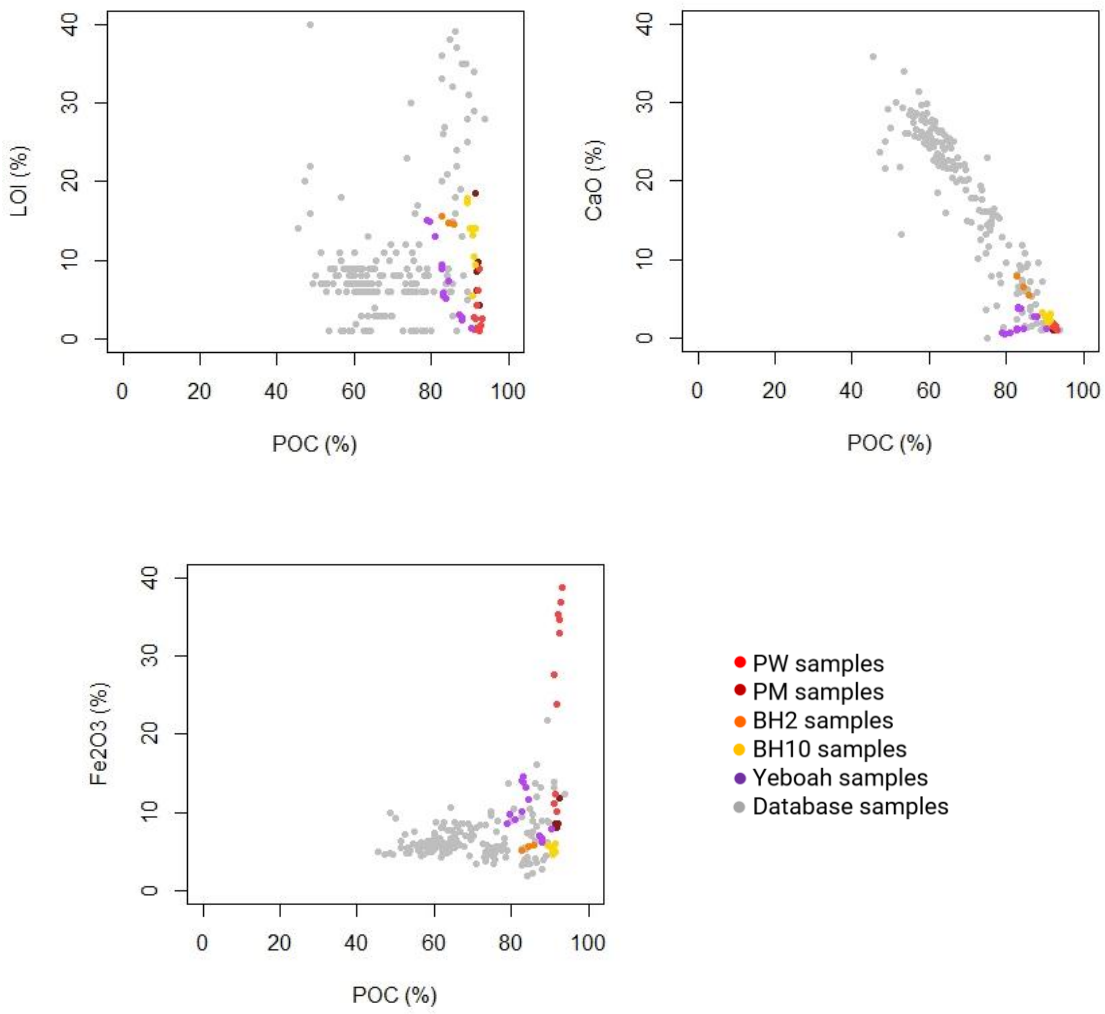

Figure 4. Weathered ash samples compared to a database of 178 North American coal fly ashes and 13 coal and co-fired ashes analyzed by Yeboah [13]

Changes during power generation combined with the influence of wet-storage and weathering processes (meteoric water, hydrology, temperature, and pondwater chemistry) make it difficult to distinguish which processes (coal source, combustion and/or weathering) are responsible for the heterogeneity in oxide composition in the weathered ashes [80]. However, all of the weathered ashes, whether newly weathered (PW, PM and shallow BH samples) or more severely weathered (deep BH samples), have a primary oxide content (POC) (sum of silicon, aluminum, and iron oxides) above 70%, a sulfur trioxide

content of less than 5%, a low calcium content, and an appropriate fineness level to be classified as Class F fly ashes, per ASTM C618 [8]. They have appropriate mineralogical compositions to be used as SCMs in concrete. The only chemical requirement that would potentially prohibit the use of these ashes as SCMs is an LOI over 6%. The BH samples, in particular, contain an LOI that was too high for use of these materials as SCMs in concrete. Additional testing (discussed in detail in Chapter 6) of the PW and PM samples confirm that these materials performed well as SCMs in concrete [87] and could be beneficially used to augment seasonal shortages of fresh fly ash.

3.3.2 Volatile Mineral Phases in Weathered Ashes

Thermogravimetry was used to identify volatile mineral phases in weathered fly ashes (Figure 5). The temperature of interest was plotted against the differential mass loss (DTG, µg/°C). DTG was normalized by heating rate because two different heating rates were applied in the method (20 °C/min below 105 °C, and 25 °C/min above 105 °C). Four different temperature ranges were chosen: (a) 200-400 °C, to capture mass loss due to bonded water in hydrated phases [63,65,73]; (b) 400-600 °C, to isolate mass loss due to portlandite dehydration [66,76]; (c) 400-800 °C, to capture mass loss due to carbonate decomposition [63,66,77]; and (d) 700-950 °C, to isolate mass loss due to iron oxide reduction and capture the switch to the oxidizing atmosphere when unburned carbon was combusted [63]. The ashes displayed in each sub-figure were chosen as representatives displaying certain mass loss characteristics.

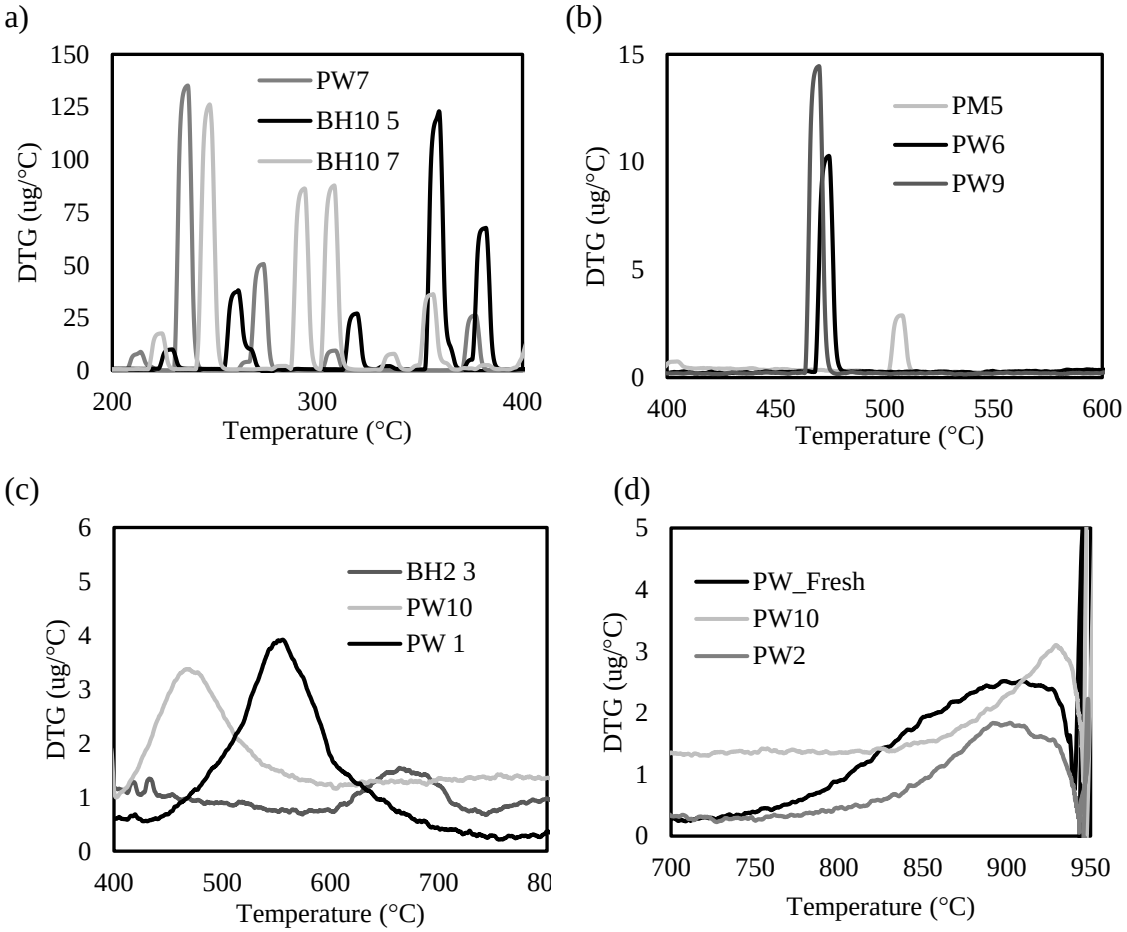

Figure 5. DTG vs. temperature for representative samples of weathered fly ash showing: (a) peaks representing mass loss due to bonded water in the range 200-400 °C; (b) peaks representing mass loss due to portlandite decomposition in the range 400-600 °C; (c) peaks representing mass loss due to carbonation in the range 400-800 °C; and (d) peaks representing mass loss due to potential iron oxide reduction above 750 °C and carbon content above 950 °C, when the atmosphere was switched to compressed air

Calcium phases contributed significantly to mass loss in weathered fly ashes. Mass losses characterized by sharp, distinct peaks were observed in the 200-400 °C range and in the 450-550 °C range (Figure 5). The mass loss in the 200-400 °C range was attributed to the loss of bound water in hydrated minerals, including gypsum, calcium sulfate hemihydrate ($CaSO_4 \cdot 0.5H_2O$), clays, and calcites [65,73–75]. TGA in isolation cannot confirm that the

hydrated minerals contained calcium, but calcium and sulfur were present in SEM EDS analyses (Figure 3; Figure 6). Furthermore, literature on weathered fly ashes indicates that many common tertiary mineral phases contain calcium [57]. A sharp DTG peak between 450-550 °C was attributed to portlandite decomposition [66]. A few weathered ash samples (PW4, PW6, PW9, and BH10 2) showed this distinct peak. An SEM image from BH10-2 showed a hexagonal, platy particle (Figure 7); a similarly-shaped particle was identified in a cement SEM analysis as portlandite [88]. Calcium minerals may have come from the parent coal, been introduced to the fly ashes as lime injections during combustion, or been due to contamination with flue gas desulfurization (FGD) gypsum during or after disposal. Regardless of source, hydrated calcium phases contribute significantly to bulk mass loss during thermal treatment of weathered fly ashes [63].

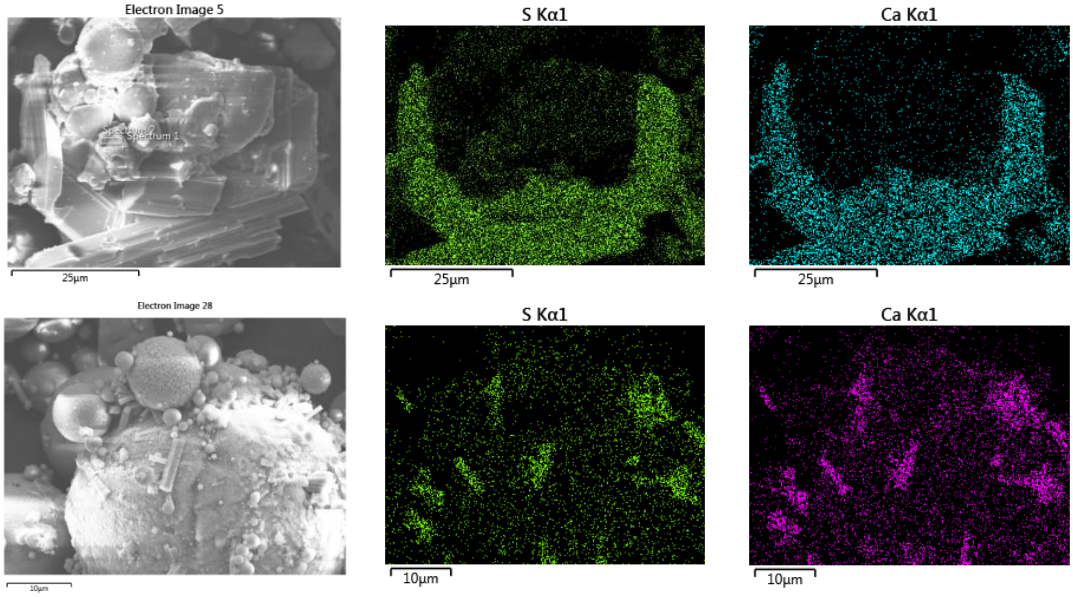

Figure 6. SEM EDS scans of calcium sulfate phases in PW1 (upper images) and PW5 (lower images)

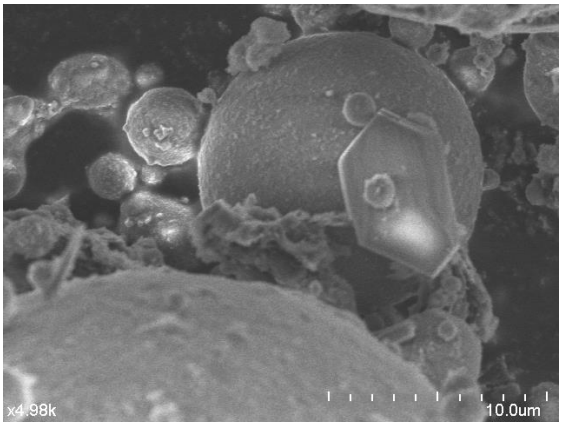

Figure 7. Hexagonal platy particle in an SEM image of BH10-2 that matches with SEM images of portlandite from SEM cement analyses performed by FHWA [88]

Carbonate peaks, in contrast to the sharp, narrow peaks characterizing bound water loss and portlandite decomposition, were broad and encompassed a range of possible mineral phases. Carbonate decomposition has been reported by others to be characterized by broad peaks in the range of 600-750 °C, though some carbonates begin decomposing at temperatures as low as 470 °C [28,63,68,69,77]. Magnesium, iron, lead, and combination Mg, Fe carbonates all begin decomposing before 650 °C [77]. Representative evidence of carbonate deposition is shown in Figure 5. The decompositions of PW10 and PW_F were unusual because the carbonate peaks occurred just after 400 °C. Although this temperature range may include portlandite decomposition, the broadness of the peak indicated its carbonate origin.

Potential reduction of ferric oxide to ferrous oxides by carbon was also observed in weathered fly ashes. The most prevalent examples, represented in Figure 5, are all from PW samples that also had a high iron content. In weathered ashes with high iron content, unburned carbon content may be underestimated because the iron reduction reaction consumes carbon [63]. Mohebbi et al. [63] recommend limiting TGA temperatures to 750°C to minimize iron reduction and improve carbon content estimates.

The total mass loss was quantified, including mass loss due to: (a) free moisture, which refers to excess water molecules on the surface of fly ash particles; (b) bound water, which refers to water molecules bound to mineral phases; (c) portlandite decomposition; (d) carbonates; (e) iron oxides; and (f) unburned carbon content, for the 27 weathered fly ashes and five samples (F1-F4 and PW_F) of unweathered, Class F fly ash. Samples F1-F4 were not extensively characterized, but the F classification was confirmed by XRF analysis. Unburned carbon and bound water contributed the most to mass loss in weathered fly ashes (Figure 8). Many weathered ashes were originally disposed because the power generation facility produced high LOI ashes, so the high unburned carbon content in weathered ashes was not surprising. In 6 of the 27 weathered ashes, greater than 6% of the total sample mass was lost due to volatilization of bound water; they had exceeded the 6% LOI limit specified in ASTM C618 before they had been combusted past 400 °C. Mass loss due to iron oxide reduction was significant in samples with high iron content (PW1, PW2, and PW10). Free moisture, portlandite decomposition, and carbonates contributed to mass loss in some cases (PW1, PW6, PW9, PW10, and BH10 8) but overall, it was minimal compared to mass loss due to bound water. In contrast, mass loss in unweathered fly ash (F1-F4 and PW_F) was primarily due to unburned carbon, iron oxides, and carbonates. Very little of the total mass loss was due to bound water; TGA quantification confirmed that hydrated mineral phases are much more likely to be found in wet-disposed weathered fly ashes than in unweathered dry-stored Class F fly ashes.

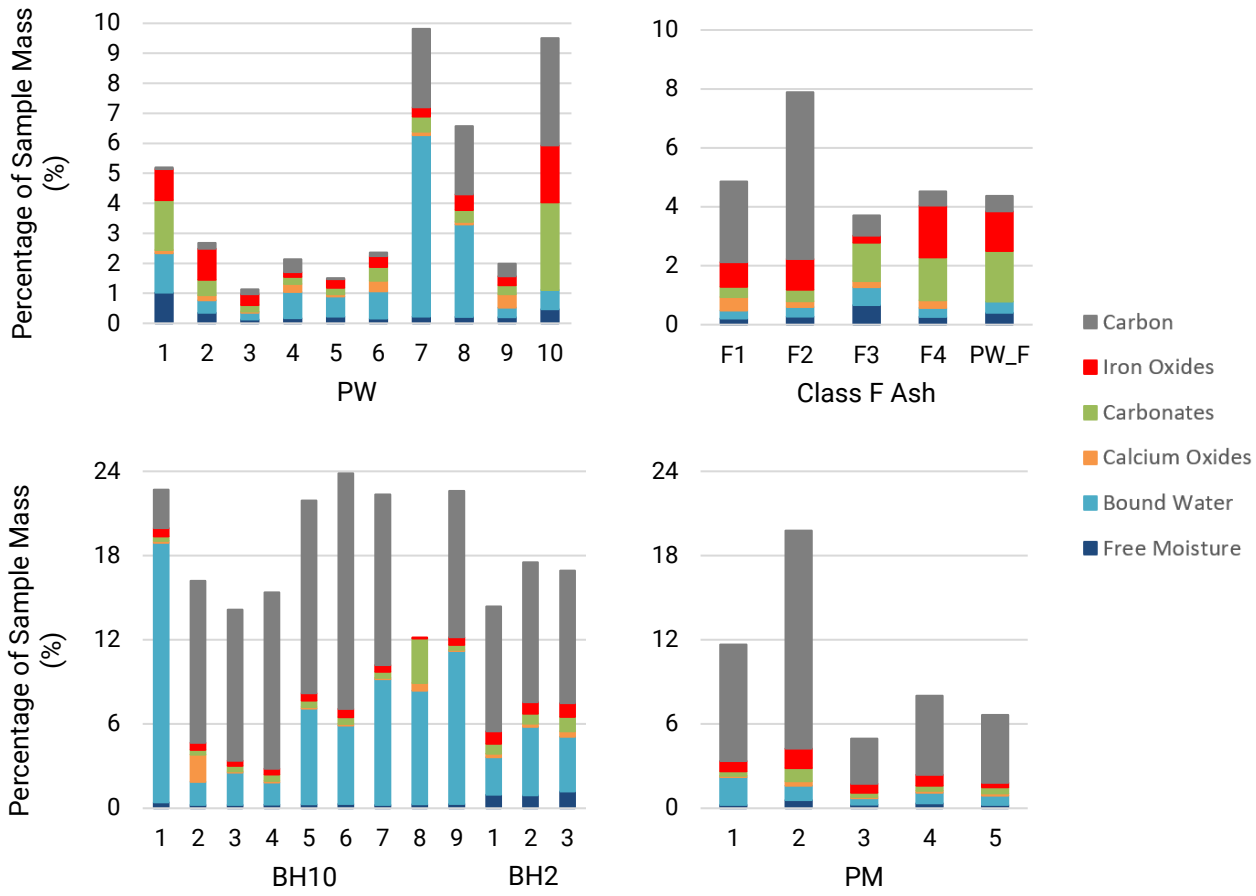

Figure 8. Sample mass loss during TGA for PW (upper left), BH (lower left), PM (lower right), and Class F unweathered (upper right) fly ashes, separated by category of volatile phase

3.3.3 Carbon Content in Weathered Ashes

Weathered fly ash was heterogeneous, and unburned carbon content varied not only in the different samples but also for the same sample when different methods were used. In nine samples taken from the same borehole (BH10), the range in reported carbon contents was from 0.00% (TGA OC, BH10 8) to 23.9% (TGA TL, BH10 6) (Table 7; Table 8). Similarly, the carbon contents in ten samples taken from the surface of the same ash wet storage facility ranged from 0.00% (TOC, PW5) to 9.81% (TGA TL, PW7).

Table 7. Carbon Content in PW and PM Weathered Fly Ash Samples

Sample	LOI (%) (@950 ºC)	TC (%)	TOC (%)	TGA TL (%)	TGA OC (%)
PW1	-[1]	0.54	0.48	5.19	0.05
PW2	3.90	1.55	1.55	2.68	0.19
PW3	0.17	0.14	0.14	1.14	0.17
PW4	0.72	0.47	0.47	2.14	0.43
PW5	0.65	0.00	0.00	1.51	0.03
PW6	0.78	0.25	0.25	2.36	0.11
PW7	3.37	3.00	3.00	9.81	2.62
PW8	2.58	2.96	2.96	6.58	2.27
PW9	1.55	0.89	0.89	1.98	0.41
PW10	8.65	5.05	5.05	9.50	3.57
PW_F	2.65	1.05	0.85	4.38	0.52
PM1	7.50	5.15	5.15	11.6	8.30
PM2	20.4	13.2	11.6	19.8	15.5
PM3	4.36	3.62	3.62	4.96	3.22
PM4	8.27	7.49	7.49	8.02	5.64
PM5	4.43	5.37	5.37	6.64	4.82

[1]Sample was consumed before an LOI test could be performed

Table 8. Carbon Content in BH Weathered Fly Ashes

Sample	LOI (%) (@950 ºC)	TC (%)	TOC (%)	TGA TL (%)	TGA OC (%)
BH10-1	5.33	4.14	4.11	22.7	2.74
BH10-2	12.4	12.2	12.2	16.2	11.5
BH10-3	14.2	10.1	10.1	14.2	10.8
BH10-4	13.2	13.9	13.9	15.4	12.6
BH10-5	17.4	21.0	21.0	21.9	13.7
BH10-6	16.6	16.7	16.7	23.9	16.8
BH10-7	12.6	11.6	11.6	22.4	12.2
BH10-8	4.96	4.15	4.15	12.1	0.00
BH10-9	12.9	12.3	12.3	22.6	10.4
BH2-1	18.5	10.3	10.2	14.4	8.89
BH2-2	14.1	11.2	11.2	17.5	9.95
BH2-3	16.6	10.9	10.9	16.9	9.42

This variability highlighted the challenge of selecting a representative value of unburned carbon content for a bulk quantity of weathered fly ash. In general, TGA TL was the highest mass loss measurement of the four techniques, and TGA OC was the lowest. All but one weathered fly ash sample (PW1) had equivalent TOC and TC measurements. Both LOI and TGA TL values were higher than TOC values for most of the weathered fly ashes (Figure 9). However, the TOC and TGA OC values were much more consistent (Figure 9). The deeper samples (particularly from BH10) showed higher LOI and TGA TL values than the surficial samples (Figure 9). The increased mass loss was due to both the higher unburned carbon content (as measured by TOC) and the hydrated mineral phases, because these ashes were sampled below the phreatic surface of the wet-storage facility. Inorganic carbon in the form of carbonates was detected in the TGA analysis, and the lack of inorganic carbon in the TOC analysis indicated that the quantity of carbonates was below the detection limit for the TOC analyzer. PM2 and BH10-5 had the greatest variation between TOC and TGA OC measurements and were confirmed as influential points that had a Cook's distance greater than 4/n. [89].

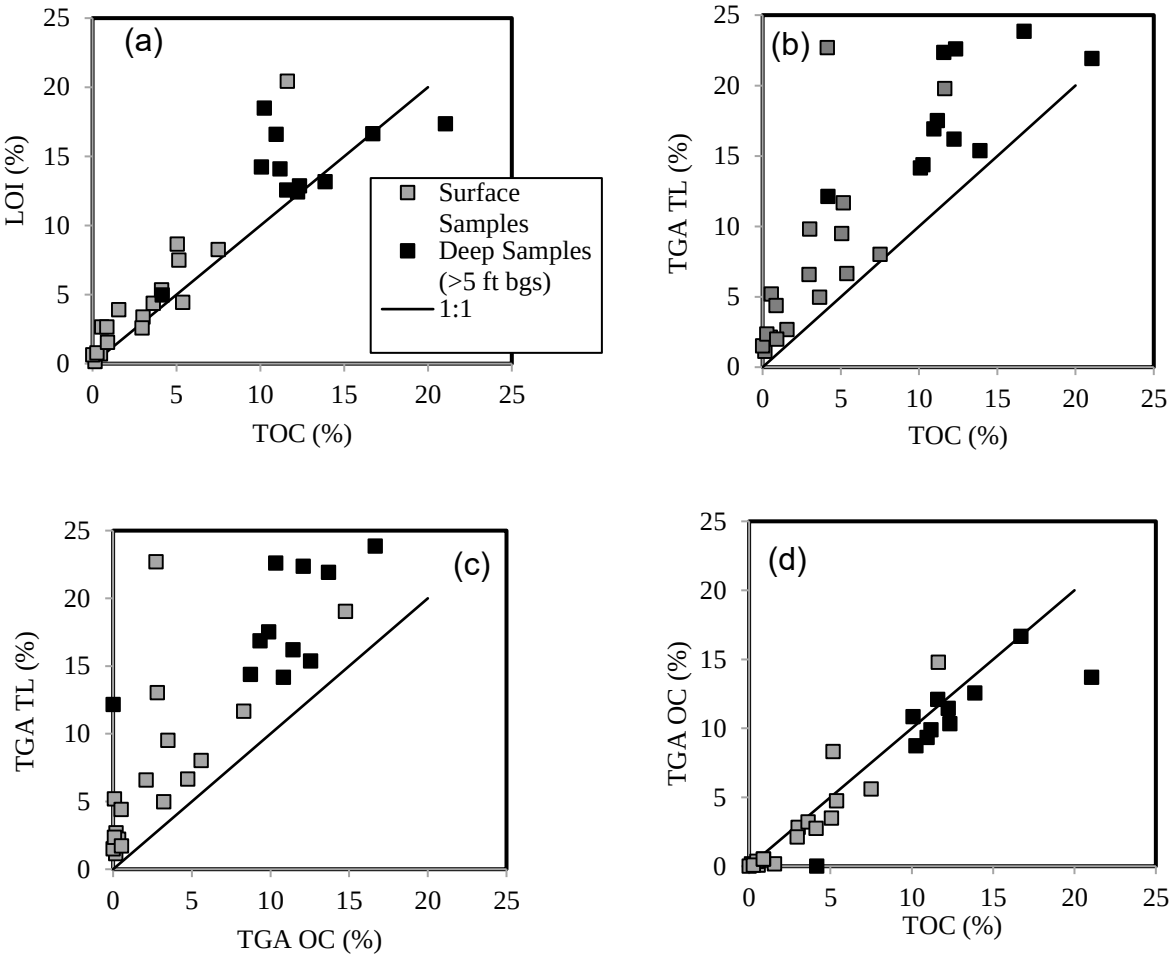

Figure 9. Comparison of measurements for total mass loss and organic carbon in weathered ash samples (assumed to be primarily due to combustion of carbon), including: (a) loss on ignition (LOI, Method B) vs. total organic carbon (TOC), (b) thermogravimetry total mass loss (TGA TL) vs. TOC, (c) TGA TL vs. thermogravimetric mass loss due to organic carbon (TGA OC), and (d) mass loss due to organic carbon, TGA OC vs. TGA OC

The variation between TGA TL and LOI (bulk mass loss) and TOC and TGA OC (unburned carbon content) was due primarily to the hydrated minerals in weathered fly ashes. This study confirmed the stipulation presented in ASTM D7438 that "LOI should not be used as an estimate of unburned carbon content in all combustion residues" [62]. Unburned carbon content in weathered fly ashes would be overpredicted by any bulk mass

loss method that does not separate combustion of carbon from the volatilization of hydrated mineral phases.

3.3.3.1 Carbon Content and Specific Gravity

The specific gravity of fly ash is a direct function of its mineralogy, and the specific gravity measured for weathered samples varied from 2.10 – 2.92, decreased with carbon (G_s ~ 1) content but was positively correlated with iron (G_s ~7) content (Figure 10), consistent with previous work [13,46]. Other researchers have also discussed how aluminosilicate spheres contribute to the range of specific gravity in fly ash [44]. However, the effect of cenospheres on specific gravity was not specifically addressed in this study because all ash samples contained spheres, and ashes were not compared to natural soils that do not contain them. The specific gravity was negatively correlated with carbon content (as measured by TOC) because the weathered fly ashes contained a significant percentage of carbon particles that were large, low density, highly porous particles with a low mass to volume ratio [13], e.g. the BH samples. In contrast, high specific gravities in the PW weathered ashes positively correlated with high iron contents, where seven of the ten PW samples had iron contents above 25%. These PW samples had some of the highest specific gravities of all 27 weathered samples.

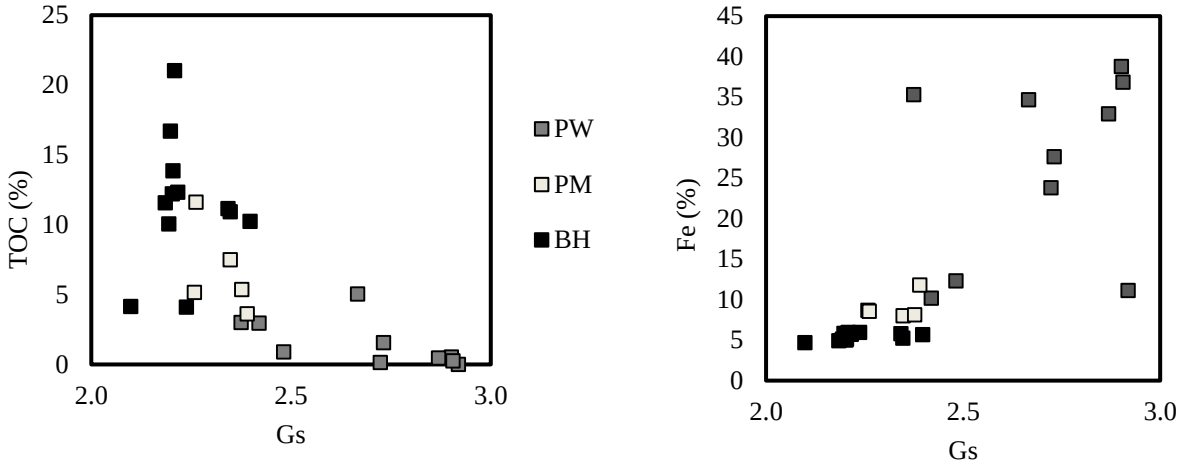

Figure 10. Relationship between (a) specific gravity and TOC for weathered ashes, and (b) specific gravity and iron content (as measured by XRF) for weathered samples

3.4 Conclusion

Tertiary mineral phases and unburned carbon content of twenty-seven samples of weathered fly ash were investigated. Volatile mineral phases in weathered fly ash include hydrated calcium sulfates, hydrated clays, portlandite, carbonates, iron oxides, and unburned carbon. Though the techniques used in this study cannot distinguish tertiary mineral phases from mineral phases formed during combustion or carried forward from the parent coal, literature on weathered fly ashes confirms that exposure to water during long-term disposal contributes to the formation of some of the phases found in the weathered ash samples used in this study, including hydrated calcium sulfates, amorphous clays, and carbonates. Quantification of TGA results indicates that weathered fly ashes have, on average, more hydrated mineral phases that unweathered fly ashes. In some weathered ash samples, greater than 6% of the total sample mass was lost due to dehydration (heating in the 200-400 ℃ range). In general, a weathered ash and an unweathered ash with a similar LOI may have significantly different mineralogies. Also, bulk mass loss combustion

methods such as LOI will fail to distinguish unburned carbon content from volatile minerals in weathered fly ashes.

Most of the BH samples in this study would be excluded from beneficial use in concrete applications because the LOI value was over 6%. However, all PW ashes and some PM ashes were candidates for use in concrete applications; they fulfilled the chemical and fineness requirements for Class F fly ashes in ASTM C618. Previous testing confirmed that these ashes have potential as SCMs in concrete [87]. For those samples with high LOI, further investigation using dual-atmosphere TGA or a TOC analyzer may indicate that the unburned carbon content is lower than the prescribed 6% ASTM limit. Additional testing on carbon content using methods than separate combustion of carbon from other volatile mineral phases may allow the beneficial use of additional reclaimed materials. The heterogeneous nature of reclaimed ash may make it challenging to find a consistently marketable product for beneficial use; however, reclaimed ashes should be considered as additional sources of Class F and Class C fly ashes for concrete applications.

Weathered fly ashes contained large, highly porous carbon particles, even after weathering. Samples that were disposed for longer than ten years had more degraded carbon structures and exposed carbon surfaces than younger samples. Additional morphologies in weathered fly ashes included fractured aluminosilicate spheres filled with smaller spheres, large agglomerates of particles with evidence of bonding between the particles, and precipitates on the surface of aluminosilicate spheres.

CHAPTER 4. CHARACTERIZATION OF BIOMASS FLY ASH FROM A FULL-SCALE, BIOMASS-ONLY COMBUSTION FACILITY

4.1 Introduction

Biomass fly ash is a heterogeneous waste material derived from the combustion of biomass fuel. Although biomass combustion represents a more carbon-neutral, renewable method of generating electricity, the biomass waste must still be beneficially used or geologically disposed. One of the challenges of using biomass ash beneficially is that the biomass fuel sources vary widely, and so does the corresponding ash [90]. However, biomass fly ashes produced from a full-scale, biomass-only facility may potentially be beneficially used, if the facility produces a consistent and marketable product.

Biomass ash is often used as a soil amendment in agricultural applications [41,91,92], as adding alkaline ash balances the acidic effects of introducing nitrogen fertilizers while simultaneously providing necessary nutrients for plant growth [92]. Biomass fly ashes have also been beneficially used as construction materials and sorbents [43]. Additional potential beneficial use alternatives for high-lime content biomass ash include mitigating acid mine drainage, encouraging the precipitation of heavy metals in water treatment applications, and working as solidifiers in solidification/stabilization applications [41,93–95]. Beneficially using biomass fly ash provides an additional economic incentive for incorporating more full-scale biomass-fueled power generation facilities into the U.S. energy market.

Woody biomass fly ash produced at a full-scale, biomass-only facility in Nacogdoches, Texas (PN) was selected as a pilot study. The power generation facility sources wood from an approximate 75-mile radius around the facility, including: (1) forest waste material (tree limbs, leaves, and needles) from lumber operations in surrounding forest land (mostly pinewood and hardwood); (2) sawmill waste and sawdust; and (3) urban wood waste primarily composed of treated wood pallets and leftover tree branches. The facility operates on a 90-day burn cycle and provides additional power to the city of Austin, Texas. When the facility is not actively combusting fuel and generating power, chipped wood fuel is collected and stored on site. The cyclical nature of power generation at this facility is an opportunity to study if ash chemistry and morphology remains consistent across multiple burn cycles.

A primary objective of this dissertation is the beneficial use of biomass fly ash. If certain combustion conditions or fuel mixtures produce biomass fly ashes with more marketable properties, power generation facilities with those configurations may be encouraged to beneficial use their material. Additionally, future biomass-only generation facilities may be designed more holistically to produce a marketable ash for specific beneficial use applications. In pursuit of identifying biomass generation facilities that produce potentially beneficially usable ash, this study was undertaken with three main objectives:

1. To investigate how boiler configuration influences ash morphology, by comparing woody biomass ash from three separate facilities with different boiler configurations
2. To investigate how woody biomass ash produced at a single generation facility varies across combustion cycles

3. To investigate how woody biomass ash morphology and chemistry compares to ash samples created from the same wood mixtures and combusted in the laboratory, to isolate if any ash morphologies are unique to combustion conditions produced by the fluidized-bed boiler.

4.2 Materials and Methods

PN biomass fly ash samples were collected from a dry-storage ash silo after combustion in a fluidized-bed boiler and filtration through a series of baghouse hoppers. The PN facility burned wood fuel after a 90-day collection period, and during the 2016-2017 year, sets of samples were collected during four burn cycles, February 2016 (PN_F), May 2016 (PN_M), November 2016 (PN_N) and April 2017 (PN_A) (Table 9). In May 2016, samples were collected for five days of the burn period, and each of these samples was analyzed separately. In November 2016 and March 2017, samples were taken each day for a nine-day period. For each sampling period, samples were taken from the ash silo on site after steady state combustion conditions had been reached. All samples were provided by Southern Company.

Table 9. Power Plant Location, Capacity, and Wood Mixture Used

	BP1	BP2	BP3	PN_F	PN_M	PN_N	PN_A
Year				2016	2016	2016	2017
Location	Vermont	Virginia	Georgia	Texas	Texas	Texas	Texas
Power Capacity (MW)	50	83	73	70	70-100	70	70
Wood Mixture	Forest, sawmill, urban wood waste	Logging, paper mill, sawmill	Sawmill	60/20/20[2] forest, sawmill, and urban wood waste	89/10/1 forest, sawmill, and urban wood waste	92/7.9/0.1 forest, sawmill, very little urban	80/5/15 forest, sawmill, urban
Boiler configuration[1]	TGS	FGS	RB	FBB	FBB	FBB	FBB
# of Samples	1	1	1	1	5	9	9
Temperature	-	-	-	1550C	1550C	1550C	1550C

[1]TGS = traveling grate stoker, FGS = fixed grate stoker; RB = recovery boiler; FBB = fluidized bed boiler
[2]percentages of each of the three wood types used, respectively

The samples from the Nacogdoches plant were compared to three samples of fly ash taken from other facilities (BP1, BP2, and BP3) and analyzed by Yeboah et al. [13]. Samples BP1 and BP2 were produced by biomass-only facilities, and sample BP3 originated from a test burn performed at a coal-burning facility. The power capacity at these facilities were 50MW, 83MW, and 73MW, respectively [13].

PN samples were also compared to fly ash combusted in the laboratory from the same fuel mixture. Samples of the three wood types used as fuel (forest, sawmill, and urban wood waste) were taken from the Nacogdoches facility, dried overnight, and stored. Wood mixtures of forest/sawmill/urban by weight were combusted in a muffle furnace at the same temperature as the fluidized-bed boiler (~840°C or 1550°F). They were combusted at a 10°C/min heating rate and held at 840°C for three hours. The chosen wood mixtures represented the wood mixtures used during each combustion cycle outlined in Table 9. The

resulting fly ash from each wood mixture was ground, stored, and analyzed using the same procedures as the as-received PN samples.

The ash samples were dried in an oven at 100°C overnight and stored until characterization. Physical and chemical characterization was performed using the techniques summarized in the introduction. Further characterization information for the BP samples is referenced elsewhere [13].

4.3 Results and Discussion

4.3.1 Comparison of BP and PN Samples

In general, biomass combustion produced a fly ash comprised primarily of porous unburned carbons and woody ash particles, although the morphologies varied between the BP and PN samples (Figure 11) [13]. BP samples were mostly unburned carbon, reflected in the SEM micrographs by large, porous particles that resembled, morphologically, the wood fuel source. In contrast, PN ash contained at least three distinct morphologies, including aluminosilicate cenospheres, woody ash particles, and angular silica particles [41]. Silica sand was used as a bed material in the fluidized-bed boiler at the PN facility, and contamination of the fly ash with very fine silica sand was expected. The presence of cenospheres indicated a higher temperature combustion than at the other power generation facilities because these structures only form at high combustion temperatures (typically greater than 800°C), where particle surfaces become molten, internal gases expand outwards (forming the characteristic spherical shape), and particles cool rapidly as they are carried through the gas stream [13,17]. It is possible for biomass combustion to produce

aluminosilicate spheres, given the appropriate combustion conditions, although they do not dominate the ash morphology like they do in coal fly ash.

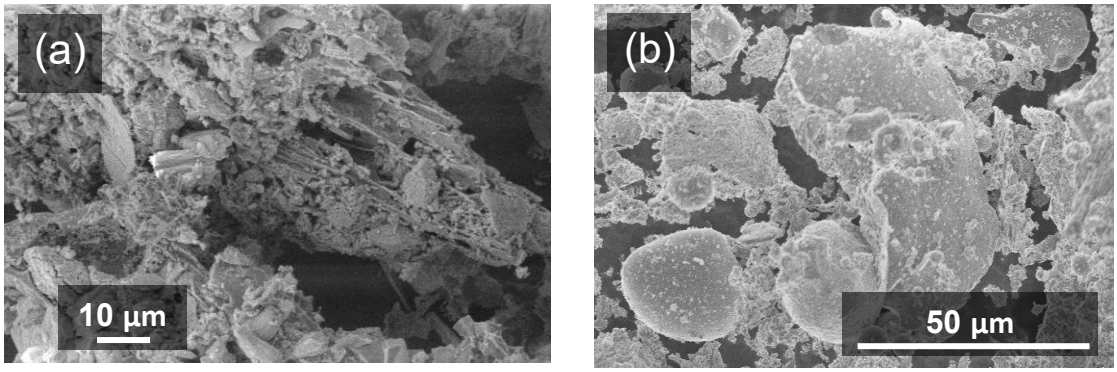

Figure 11. SEM micrographs showing: (a) the woody structure of a BP2 sample and (b) the combination of woody, angular, and spherical particles in the PN_F sample. Micrographs were used for descriptive analysis of ash morphologies

The unburned carbon content controlled the physical properties of the biomass ashes. The LOI values were between 10 and 20 times higher for the BP1-3 samples compared to the PN samples (Table 10). In the most extreme case, the BP3 sample had only 4% non-combustible materials by mass, compared to an average of 95.5% non-combustible materials for PN samples. Specific surface area followed a similar trend; BP1-3 samples had between 32 (BP1) and 194 (BP3) times greater SSA than the average of the PN samples. These results are not surprising; high-carbon content fly ashes have been found to also have high specific surface areas, as unburned carbon particles contained significant internal porosity [13]. Other physical properties that were significantly different between the BP1-3 samples and the PN samples include specific gravity (45-60% lower values found in the BP samples) and particle size distribution. The median particle sizes of the BP samples were between 6.5 (BP1) and 55.7 (BP3) times higher than the PN samples, and the particle size distribution of the BP samples was shifted towards higher particle sizes compared to the PN samples (Figure 12).

Table 10. Physical Properties of Biomass Fly Ash

	BP1[1]	BP2[1]	BP3[1]	PN_F	PN_M[2]	PN_N[2]	PN_A[2]
Wood Ratio	-	-	-	60/20/20	89/10/1	92/7.9/0.1	80/5/15
SSA (m^2/g)	116	180	687	1.33	3.99	-	-
G_s	1.87	1.62	1.27	2.80	2.74	2.76	2.88
LOI (%)	46.7	63.9	95.9	0.30	1.28	5.67	5.56
D_{50} (μm)	168	640	1440	32.3	25.8	22.7	25.9
C_u[3]	6.6	13.4	35.5	-	-	-	-
u[4]	-	-	-	1.40	0.88	0.95	0.97

[1]Yeboah et al. 2014 [13]
[2]averages of analyzed properties for multi-day sampling
[3]C_u: coefficient of uniformity= D_{60}/D_{10}
[4]Uniformity parameter for laser particle size diffraction

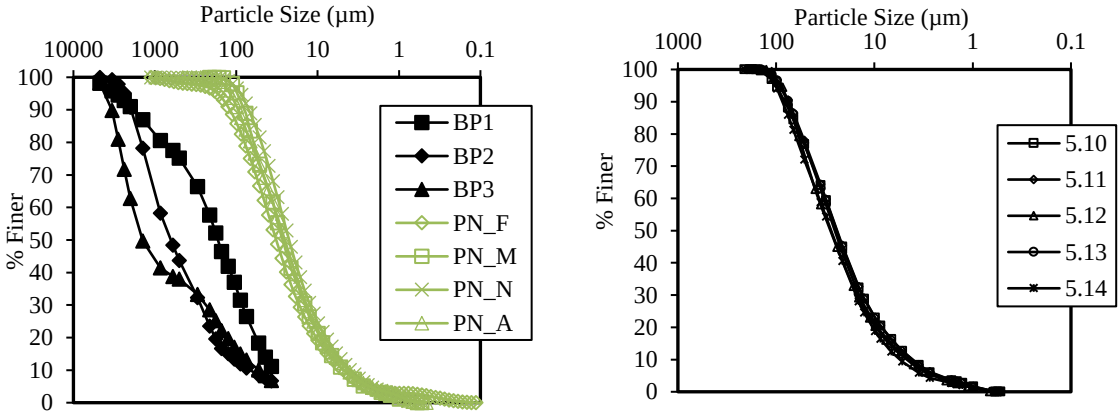

Figure 12. Particle size distribution of (left) seven BA samples (PN_x samples as an average over each sampling period) and (right) five PN samples taken over a five-day combustion period in May 2016, labeled by sampling date

Overall, PN samples had physical properties that approximated a typical coal fly ash, and BP samples did not [13,24,54]. The variation in physical properties was attributed to the quantity of unburned carbon in the fly ash, which is related to the efficiency of combustion in the boiler [96]. The larger, highly porous unburned carbon particles increased the overall specific surface area of the samples, decreased the specific gravity, increased the median particle size, and increased the LOI [13,97]. The larger percentage of unburned carbon indicated that firing conditions in the TGS, FGS, and RB configurations were less efficient than the FBB configuration [11,98,99]. Sorption applications may be the best beneficial

use alternatives for ashes produced in TGS, FGS, and RB boiler configurations because of their high carbon content and high specific surface area. In contrast, woody biomass combustion in a high-temperature FBB produced a fly ash with physical properties more consistent with typical Class F or Class C coal fly ash.

Chemical analysis revealed some variation between fly ashes combusted at different facilities. The silica content of the PN samples was considerably higher than the BP samples (between 6 and 60 times higher) (Table 11). The high silica content was a result of the inclusion of very fine silica particles either carried through the flue gases with the fly ash or partially melted and reformed as part of the ash matrix during combustion. The primary oxide content (POC) of the BP1-3 samples was too low and the LOI was too high to classify these ashes as a Class C or Class F fly ash, according to the chemical specifications of ASTM C618 [8]. Although the PN samples had a POC and LOI to classify as a Class F fly ash, the lack of amorphous silica in XRD scans indicated that the PN ash did not have potentially reactive, pozzolanic silica and may not be appropriate for use in concrete. All samples except BP3 had a high calcium content, compared to a typical Class F coal fly ash. The high calcium content is more indicative of a Class C ash than a Class F ash. Solidification/stabilization or agricultural applications may be appropriate beneficial use alternatives for PN ash because of its high alkaline content.

Table 11. Oxide Content of Biomass Fly Ash Samples

Major Oxides	BP1	BP2	BP3	PN_F	PN_M	PN_N	PN_A
SiO_2	6.43	10.63	1.74	67.9	67.6	59.4	64.9
Al_2O_3	0.75	2.06	0.27	4.61	4.71	4.65	3.67
Fe_2O_3	0.54	0.85	0.09	5.32	4.14	3.89	3.12
SO_3	2.88	1.1	0.44	0.75	0.93	8.37	1.44
CaO	24.12	14.47	1.16	14.6	15.4	19.3	17.6
Na_2O	0.4	bd[1]	bd	0.29	0.30	0.38	0.24
MgO	2.54	1.78	bd	0.97	1.30	2.01	1.96
K_2O	7.48	3.42	0.13	2.03	2.62	3.61	3.89
P_2O_5	2.18	0.98	0.07	0.47	0.60	1.04	1.02
TiO_2	0.07	0.17	0.01	0.48	0.43	0.42	0.38
SrO	0.09	bd	0.04	0.08	0.08	0.12	0.09
BaO	bd	bd	bd	0.08	0.09	0.13	0.14
LOI (%)	46.7	63.9	95.9	0.20	1.28	5.67	5.56
POC (%)	7.72	13.54	2.10	77.9	76.4	67.9	71.7

[1]below detection limit of instrument

Chemistries of biomass fly ash samples were compared to a database [24] of 178 coal and co-fired ashes (Figure 13). All PN samples fell within the range of coal and co-fired ashes for LOI, calcium content, and sulfur content. However, all BP samples fell outside the range in every category. Although all biomass samples had similar fuel sources, combustion with different boiler configurations played a significant role in determining the ash chemistry as well as morphology.

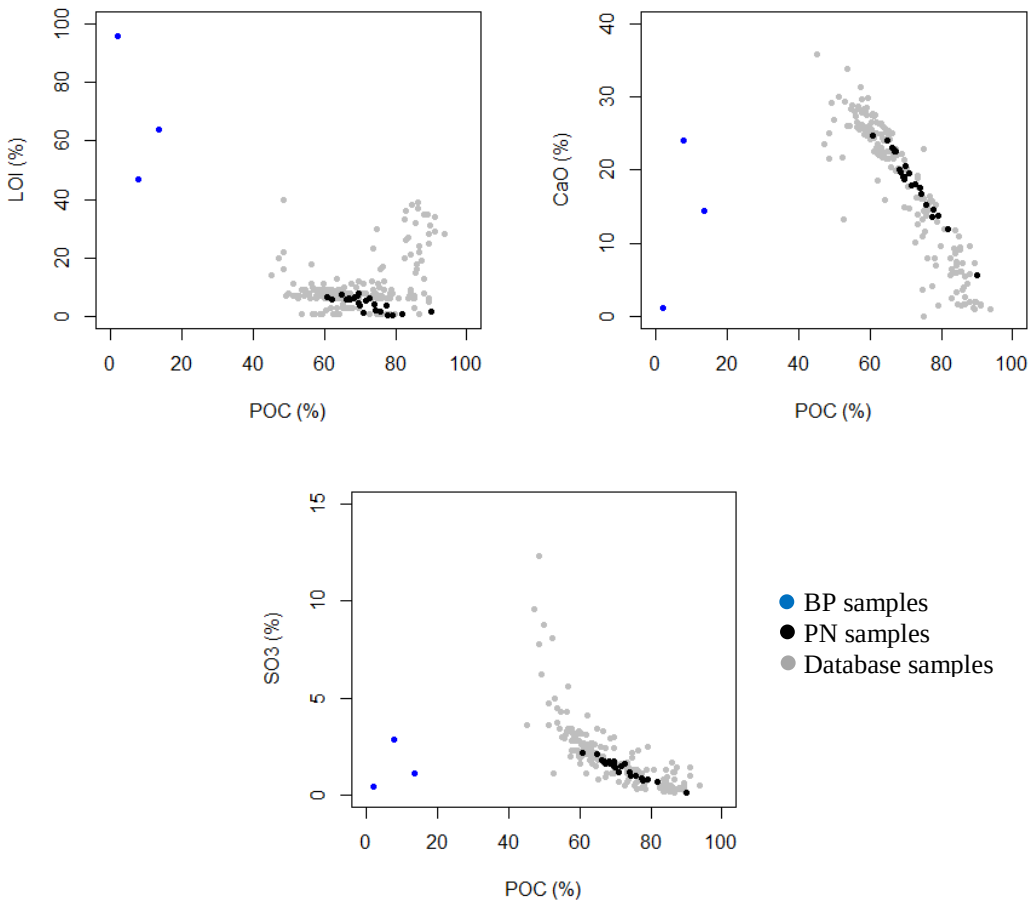

Figure 13. Comparison of LOI (upper left), CaO (upper right), and SO_3 (lower middle) content of BP and PN samples to a database of 178 coal and co-fired ashes [24]

Additional crystalline phases were found in the PN samples that were not present in the BP samples (Figure 14). Of the three BP samples and the 22 PN samples analyzed for crystalline content using XRD, 96% contained quartz, 92% contained calcite, and 80% contained lime. Crystalline lime was not found in the BP samples, but 90% of the PN samples contained lime. Arcanite was found in 20% of the biomass samples. 24% of samples contained hematite, and 16% contained anhydrite. Crystalline lime and anhydrite were also found in other biomass ashes [4,100,101]. 100% of the PN samples contained quartz, and 95% contained calcite. The crystalline chemistry of biomass fly ash confirmed that woody biomass ash contains more alkaline and alkaline-earth metals than coal fly ash.

X-ray diffraction (XRD) analyses on typical Class F fly ash included an amorphous hump between 15 and 35° 2θ, which indicated reactive, amorphous silica, a necessary pozzolanic component for concrete [102]. However, none of the biomass XRD scans had this feature, suggesting that these samples may be ineffective as supplementary cementitious materials in concrete (Figure 14). The ineffectiveness of sample BP1 was confirmed by the mortar testing performed in Chapter 5. Because these ashes do not contain amorphous silica, they are not expected to perform effectively as pozzolanic materials in concrete applications, though the high calcium content may allow them to be beneficially used in solidification/stabilization applications where self-hardening properties are advantageous [41].

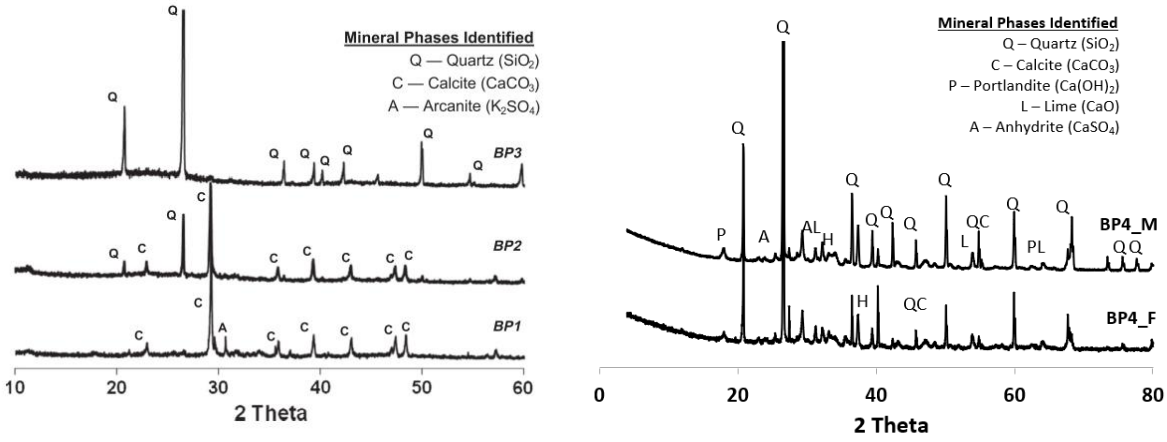

Figure 14. XRD scans of biomass fly ash samples, indicating that quartz, calcite, and arcanite are the major crystalline components in the BP1, BP2, and BP3 samples [13]. Crystalline lime, hematite, and anhydrite are additional compounds in the BP4 samples

4.3.2 Variation in PN Samples In Combustion Cycles

PN samples were taken from multiple 90-day burn cycles, to determine if biomass ash properties remained consistent during each burn period; each daily sample was

characterized independently. The particle size distribution and specific gravity were reasonably homogenous, indicating that the biomass fly ash has consistent physical properties across burn cycles (Table 12). The greatest variation was in LOI content; two of the burn periods had LOI over 5% (PN_N and PN_A), but the earlier burn periods (PN_F and PN_M) had LOI values less than 1.5%. Combustion may have been less efficient over time over the life cycle of the facility, or the longer burn period for the November and April runs led to slightly more variation in efficiency. Detailed characterization parameters are listed in Appendix B.

Table 12. Properties of PN Samples for Each Combustion Cycle

Sample ID		PN_F	PN_A	PN_M	PN_N
Burn Period		Feb 2016	April 2017	May 2016	Nov 2016
Wood Mix		60/20/20	80/5/15	89/10/1	92/7.9/0.1
# of samples		1	9	5	9
Gs	Average	2.80	2.87	2.74	2.78
	Std.Dev	n/a	0.09	0.08	0.10
	COV	n/a	0.033	0.025	0.036
d50 (um)	Average	32.3	28.3	25.8	22.7
	Std.Dev	n/a	12.62	1.91	1.03
	COV	n/a	0.445	0.066	0.045
LOI (%)	Average	0.4	5.56	1.28	5.67
	Std.Dev	n/a	1.89	0.66	1.09
	COV	n/a	0.341	0.461	0.192
CaO	Average	14.6	17.6	15.4	21.4
	Std.Dev	n/a	5.33	2.91	2.42
	COV	n/a	0.303	0.169	0.113
SiO_2	Average	67.9	64.9	67.6	59.4
	Std.Dev	n/a	8.84	5.14	4.39
	COV	n/a	0.136	0.068	0.074
SO_3	Average	0.75	1.44	0.93	1.65
	Std.Dev	n/a	0.58	0.20	0.28
	COV	n/a	0.406	0.192	0.168

There was evidence of angular silica particles and glassy aluminosilicate spheres in ash from every combustion cycle (Figure 15), and the feathery texture of the wood ash

remained visually consistent. Overall, the FBB boiler was efficient and produced a relatively consistent product during a single combustion cycle and across multiple combustion cycles. The PN biomass fly ash was a silt-sized, low organic, low sulfur, high calcium content fly ash across four different burn cycles. These results are encouraging for large-scale beneficial use of this material.

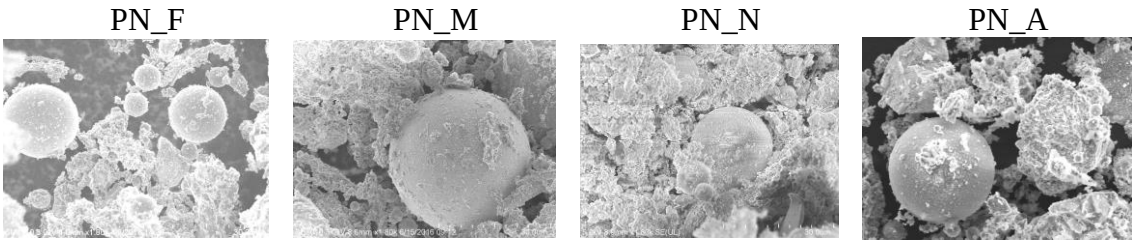

Figure 15. SEM micrographs showing aluminosilicate spheres in every burn cycle of PN ash. Micrographs were used for descriptive analysis of ash morphologies

4.3.3 Comparison to Lab-Combusted Fly Ash

Lab-combusted fly ashes exhibited similar physical characteristics to the PN samples (Table 13). The median particles sizes were, on average, 66% larger for the PN samples, compared to their lab combusted counterparts. However, the average LOI of the lab-combusted samples was over 5 times higher. The higher LOI value was found to be mass loss due to volatile mineral phases, not mass loss due to unburned carbon content. Representative samples (60/20/20, 92/7.9/0.1 and 0/0/100) were analyzed using dual atmosphere thermogravimetry (shown in Appendix B). The mass loss was shown to occur in the N_2 atmosphere, between 700-850°C and was identified to be the decomposition of carbonate minerals. The lab samples (as discussed in greater detail in the following paragraph) were more enriched in calcium phases compared to the PN samples, as calcium carbonate phases decompose in the 600-800°C range [100]. Negligible mass loss was

observed during combustion in a compressed air atmosphere, indicating that unburned carbon was efficiently combusted in the muffle furnace and was not responsible for the higher LOI values of the lab samples.

Table 13. Physical Properties of Lab-Combusted Samples

	60/20/20	80/5/15	89/10/1	92/7.9/0.1	100/0/0	0/100/0	0/0/100
G_s	2.91	2.79	-[1]	-[1]	-[1]	2.64	2.81
LOI (%)	30.0	14.9	19.4	13.4	0	24.0	25.0
D_{50} (μm)	13.4	21.3	18.7	20.8	19.1	14.2	17.0
u[4]	1.09	1.14	1.26	1.05	1.17	1.13	1.01

[1]sample was consumed before testing was performed

Lab-combusted samples also displayed a different morphology than their PN counterparts. They were composed entirely of woody ash particles (Figure 16), and there was no evidence of aluminosilicate spheres or angular silica in SEM micrographs of the lab-combusted samples. Clearly, the combustion conditions within the FB boiler were responsible for additional morphologies associated with PN samples, including the aluminosilicate spheres and the angular silica particles.

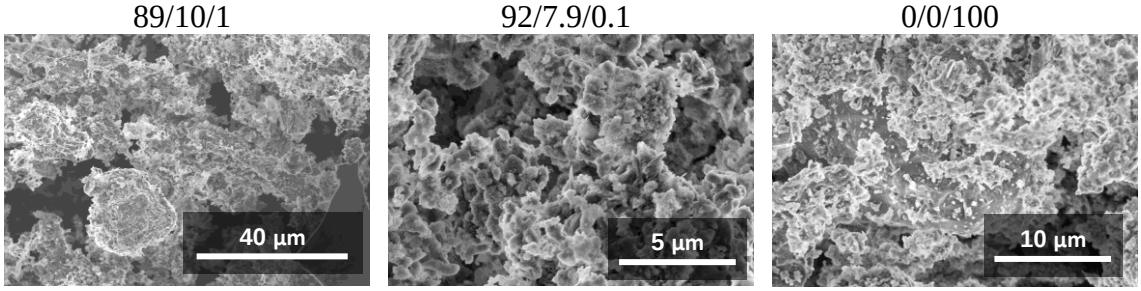

Figure 16. SEM micrographs showing morphology of lab-combusted samples

Overall, lab-combusted samples were enriched in silica, calcium, and other alkaline and alkaline earth oxides and contained limited quantities of iron and aluminum, similar to the PN samples (Table 14). However, the lab-combusted fly ashes were proportionally less enriched in silica and more enriched in calcium compared to the PN samples. This result further confirmed the earlier observation that fine silica sand was carried with the fly ash

in the flue gases, deposited in the baghouse hoppers, and contributed to the high quartz content of the PN samples. The sawmill ash had the highest calcium content of the three fuel sources, and the forest waste ash had the lowest. The lab-combusted simulation of PN_N (92% forest waste, 7.9% sawmill waste, and 0.1% urban wood waste) had a lower silica concentration compared to the other lab-combusted wood mixtures. This result may be due to the variation in the forest wood chips that were used for combustion.

Table 14. Oxide Content of Lab-Combusted Samples

	Lab Combusted Fuel Mixture Ratios						
Major Oxides	60/20/20	80/5/15	89/10/1	92/7.9/0.1	100/0/0	0/100/0	0/0/100
SiO_2	42.6	48.3	51.0	26.6	51.1	34.8	47.5
Al_2O_3	4.69	6.64	4.75	4.28	4.8	2.69	7.55
Fe_2O_3	3.48	2.98	5.15	2.19	5.52	2.81	2.79
SO_3	2.34	1.73	2.27	3.93	1.87	0.99	0.86
CaO	35.0	30.3	22.0	41.1	14.3	50.0	33.4
Na_2O	0.51	0.57	0.63	1.23	0.76	0.6	0.57
MgO	3.16	2.59	3.81	6.56	5.66	2.22	1.66
K_2O	5.11	4.14	6.4	8.63	9.5	3.32	2.37
P_2O_5	2	1.45	2.51	4.12	4.01	1.31	0.93
TiO_2	0.4	0.42	0.49	0.24	0.45	0.27	0.47
SrO	0.15	0.1	0.16	0.16	0.09	0.28	0.11
BaO	0.11	0.09	0.18	0.25	0.14	0.27	0.04
LOI (%)	30.0	14.9	19.4	13.4	0	24.0	25.0
POC (%)	50.74	57.93	60.88	33.1	61.4	40.26	57.82

The reduction in silica content, the corresponding percentage increase in alkaline and alkaline earth metal content, and the increase in LOI brought the lab-combusted samples outside the range of 197 coal and co-fired fly ashes (Figure 17). While the lab-combusted samples were not as extreme in morphology and chemistry as the BP samples, many of these samples have a POC that is too low and an LOI that is too high to classify as Class C or Class F fly ashes [8].

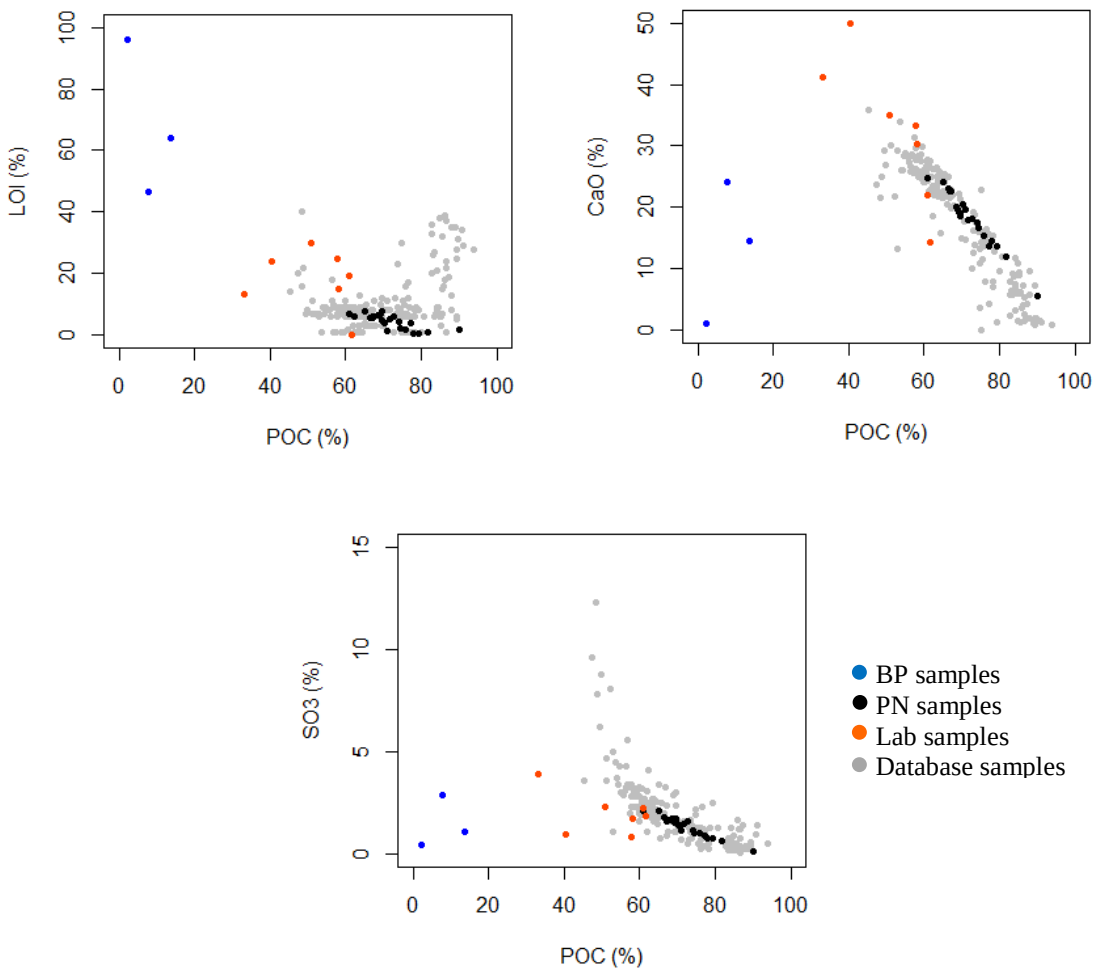

Figure 17. Comparison of LOI (upper left), CaO (upper right), and SO3 (lower middle) content for BP, PN, and lab samples compared to a database of 178 coal and co-fired ashes [24]

Lab samples had a similar crystalline composition as the PN samples (Figure 18). Quartz, calcium, and lime dominated, with quartz and calcite compromising greater than 70% of the total crystalline material in the ash. Minor and trace crystalline mineral phases included additional calcium phases (anhydrite, dolomite, and portlandite) and hematite. Again, no amorphous silica hump was present between 18 and 30° 2θ, indicating that these biomass ashes did not contain potentially reactive, pozzolanic silica [102].

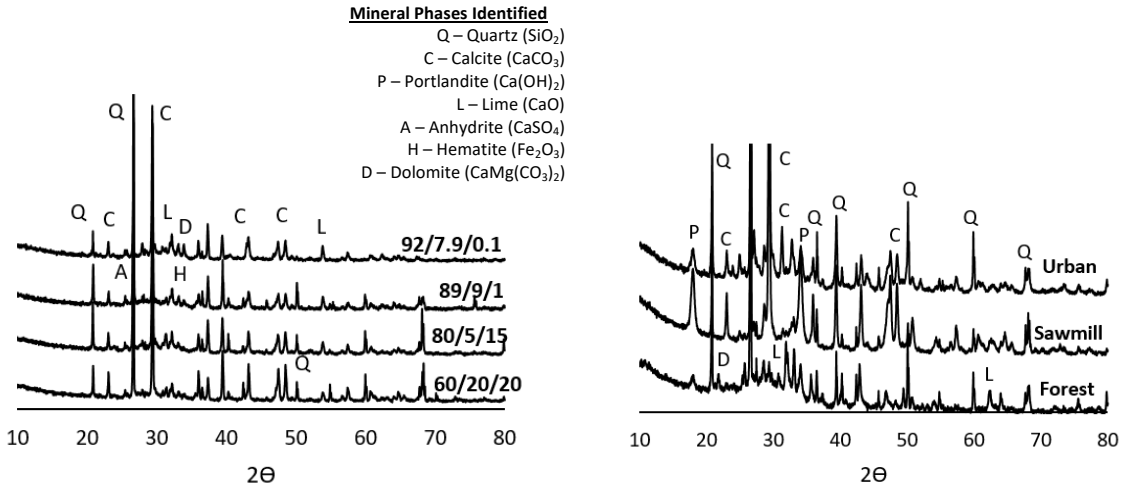

Figure 18. XRD scans of lab fly ash samples, indicating that quartz, calcite, and lime are the major crystalline components. Dolomite, hematite, portlandite, and anhydrite are additional crystalline components in lab samples

4.4 Conclusions

A full-scale, biomass-only power plant in Texas produced a significantly different fly ash compared to other biomass facilities and one test burn at a coal combustion facility. The PN facility produced an ash with a lower unburned carbon content, a lower specific surface area, a higher specific gravity and a lower median particle size. The PN biomass fly ash was very similar to coal fly ash physically, although the biomass ash contained higher concentrations of alkaline earth metals, especially calcium, and lower concentrations of aluminum and sulfur than typical coal ash. The BP samples did not meet the chemical requirements for a Class C or Class F fly ash, per ASTM C618, but the PN samples met all the chemical requirements for a Class F fly ash. However, XRD analysis confirmed that the samples contained only crystalline quartz and no potentially pozzolanic amorphous silica. These ashes may not be appropriate for beneficial use in concrete applications because they may not contribute extra pozzolanicity to the concrete.

The physical and chemical properties of the PN samples were consistent across a single combustion cycle and across four different combustion cycles, with expected fluctuations. The largest variation was seen in LOI, which fluctuated between 1.5% and 5% across four combustion cycles. Potentially, loss of efficiency in the fluidized bed boiler over time contributed to this variation, as the higher LOI corresponded with the later combustion cycles. All samples contained angular silica, woody ash, and aluminosilicate sphere morphologies.

Overall, the type of boiler used at the power generation facility had a significant effect on fly ash chemistry and morphology, but variations in wood source at the same facility had a limited impact on physical and chemical properties. A notable impact of the FBB was the inclusion of crystalline silica with the biomass fly ash which produced an ash with a higher silica content and angular silica particles. Lab-combusted samples did not contain this silica, and they had a correspondingly higher percentage of calcium and other alkaline metals. The FBB contributed to an efficient fuel combustion and ash with a low unburned carbon content, a particle size distribution in the silt range, and a low specific surface area. Woody biomass fly ash produced at a full-scale, biomass-only facility with a fluidized-bed boiler is a high-calcium, low-organic, silty material.

CHAPTER 5. SATURATED AND UNSATURATED HYDRAULIC PROPERTIES OF WEATHERED COAL FLY ASH

5.1 Introduction

Dewatering of ash disposal facilities is a critical issue in the current regulatory environment; ash impoundment facilities that are undergoing clean closure often require an extensive amount of water to be removed before the impoundment surface is able to support the weight of excavators and other heavy construction equipment. Ash impoundment facilities typically contain a combination of fly ash (a low plasticity silt) and bottom ash (a coarse sand), and hydraulic flow is preferential through the coarse-grained lenses. However, hydraulic properties will be controlled in part by the finer-grained material [103], particularly as the ash mixture becomes partially-saturated. Fly ash will retard hydraulic flow and increase the energy inputs necessary to dewater the ash pond to an acceptable level. Therefore, dewatering operations require an understanding of fly ash hydraulic properties, specifically saturated hydraulic conductivity and unsaturated matric potential.

As was summarized in the literature review (Chapter 2), fly ash is a low-plasticity silt, and the hydraulic conductivity of fly ash falls within the typical range of a material primarily comprised of silt-sized particles (on the order of 10^{-4} – 10^{-6} cm/s) [48,50,104,105]. Young et al. [50] reported hydraulic conductivities on the order of 10^{-5} cm/s for Class F fly ashes samples from a variety of sampling conditions, including samples that were compacted and tested in the laboratory, mostly undisturbed Shelby tube samples from the field (also tested

in the laboratory), and in-situ measurements of hydraulic conductivity using Guelph permeameters. Sample saturation and spatial variability within the ash disposal facility were reported to represent the two most important factors that contributed to hydraulic conductivity variability [50]. Others have found that chemistry of fly ash plays a role in hydraulic conductivity, particularly for high calcium fly ash (Class C, typically). Cementation decreased the hydraulic conductivity of high-calcium content fly ash, in one case to a magnitude of 10^{-7} cm/s [50,104,106]. Palmer et al. [104] reported that fly ash hydraulic conductivity was sensitive to both compaction water content and compaction energy (Standard versus Modified Proctor), as values fluctuated several orders of magnitude between 10^{-4} cm/s (for samples compacted at low water content (less than 5%) using Modified Proctor) and 10^{-6} cm/s (for samples compacted at high water contents and Modified Proctor). Samples compacted at Standard Proctor had less variability in hydraulic conductivity (all samples fell within the 10^{-5} cm/s order of magnitude) across the same range of water contents (approximately 5-25%). Palmer et al. [104] suggested that variation in fly ash hydraulic conductivity was due to cementation reactions. Webb et al. [105] observed that compaction density had an influence on hydraulic conductivity. An increase in compacted density had a corresponding decrease in hydraulic conductivity.

The unsaturated properties of fly ash are represented in this study as the relationship between matric potential and water content, known as the soil-water retention curve or the soil-water-characteristic-curve (SWCC). Key parameters for representing this curve include the saturated water content (Θ_s), the residual water content (Θ_r), and the air-entry suction [107,108]. The residual water content is not necessarily the minimum possible water content; rather, it is defined as the maximum water content not available for flow

(due to sorption onto particle surfaces or blocked pore throats) [107]. Air-entry suction, or the air-entry value, is defined as the applied pressure where water first begins leaving the largest pores; it is the "break" in the water retention curve where water content begins to decrease with additional matric potential. Coarse-grained soils are expected to have a low air-entry value; it takes very little pressure to begin removing water from the pore space [50,109]. Fly ashes exhibit a higher air-entry value than coarse-grained materials, but typically the slope of the curve after the break point will still be steep – the drainage of water occurs in a small matric suction range [50]. In this way, ashes present water-retention features of both sand (steep drainage curve) and silt (high air-entry pressure). Clayey soils, in contrast, show a much shallower water retention slope; it takes much more pressure to achieve the same water content as a coarser material [110]. Fly ash unsaturated behavior is characteristic of a fine-grained, uniformly-graded material with a narrow grain size distribution and a correspondingly narrow pore size distribution [50].

While some research on fly ash hydraulic properties exists, much of it is concerned with fly ash as a soil additive or focuses on mixtures of fly ash with coarser-grained material [48,111]. A limited number of studies focuses specifically on hydraulic properties of fly ash, and these studies have limited information on microscale and microstructure hydraulic interactions [50,104,105]. This chapter addresses gaps in literature by providing more detail on fly ash saturated and unsaturated hydraulic properties, as well as examining more closely the interaction between fly ash chemistry, surface charge, contact angle, water content, and matric potential.

5.2 Materials and Methods

5.2.1 Materials

The PY ash was chosen specifically for saturated and unsaturated hydraulic testing because plant operations personnel and consultants working on dewatering the ash disposal facility observed that ash from this particular site took considerably longer to dewater than ash from nearby disposal sites at the same facility (6 months of stockpiling and slow drying versus a few weeks). Also, this ash retained water for far longer than fly ash from other power generation facilities in Georgia. The PY ash was tested in the as-received condition as well as chemically altered before testing its hydraulic properties, in an attempt to isolate if chemical or physical factors contributed to the saturated and unsaturated properties of the ash. The PY ash was observed to contain aluminosilicate spheres, unburned carbon particles, sheeted particles comprised of aluminum, silicon, oxygen, and alkaline and alkaline earth elements (SEM EDS micrographs shown in Appendix B), and silicon dioxide diatom frustules (SEM EDS micrographs shown in Appendix B) (Figure 19).

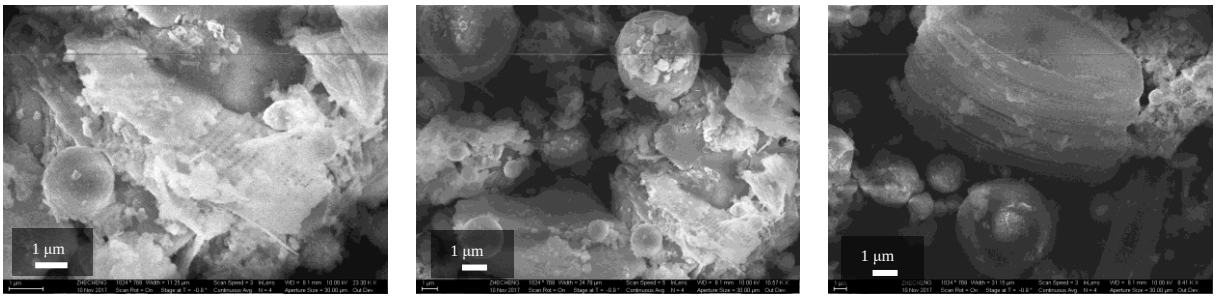

Figure 19. SEM micrographs of as-received PY ash, highlighting its various morphologies. Micrographs were used for descriptive analysis of ash samples

A series of four pre-treatments was performed on the as-received PY ash before testing, and a physical and chemical characterization of the treated samples was performed in

accordance with the methods outlined in the introduction. PY ash was rinsed with deionized water ($\Omega > 17.4$) for 18h at constant rotation, filtered, dried, crushed and stored (Y_DI). PY ash was rinsed with a 5% HNO_3 solution for 18h at constant rotation, filtered, rinsed for 2 hours with deionized water, filtered, dried, crushed and stored (Y_A). PY ash was calcined at 800°C, at a heating rate of 10°C/min and held at temperature for 2 hours, crushed, and stored (Y_C). Finally, crystalline and surface deposits of iron oxides were removed from PY ash using the citrate-bicarbonate-dithionite (CBD) method, and the resultant ash was filtered, dried, crushed, and stored (Y_CBD) [112,113].

These chemical treatments were chosen to remove soluble surface species (DI-water) without impacting the aluminosilicate spheres or degrading other PY morphologies, to potentially dissolve or degrade the flaky aluminosilicate particles and potentially alter the surface characteristics of the diatom frustules (5% HNO_3), and to remove porous unburned carbon particles and again, potentially alter the surface characteristics of the diatom frustules through high-temperature combustion (calcining).

The citrate-bicarbonate-dithionite (CBD) method was chosen for iron removal because this method removed free iron oxides from surface coatings and crystalline iron oxides, but not iron that had been bound in the lattice structure of particles [113]. Also, this method, in the literature, did not dissolve additional fly ash features, such as the aluminosilicate spheres. This method was highly effective for dissolving iron oxides because the sodium dithionite ($Na_2S_2O_4$) reduced the insoluble Fe(III) forms to soluble Fe(II) forms while the bicarbonate buffered the system at pH 7.3, to keep FeS and elemental S from precipitating [112], yet the combination of chemicals did not dissolve the silicate clay minerals. Crystalline hematite and goethite were both effectively removed in preliminary experiments performed

by Mehra and Jackson [112]. However, some amount of aluminum and silica complexes were reported to be removed, especially because Al substitutes for iron when iron is removed [114]. After CBD treatment using the as-received PY ash, ICP-OES analysis of the supernatant indicated that approximately 50 ppm of Fe was dissolved in solution, and SEM EDS imaging confirmed that the aluminosilicate spheres remained intact (Section 5.3.1).

5.2.2 Methods

The physical and chemical characterization techniques used for these materials can be referenced in the introduction. The point-of-zero charge (PZC) was measured by a zeta potential analyser (Brookhaven ZetaPALS) using an ash/water concentration of 1 mg/mL; samples were sieved across a #400 (0.037mm) sieve, and only particles less than 0.037mm were analyzed, as outlined in the Brookhaven manual. Before testing, sample solutions were adjusted to pH values ranging from 2 – 13 and adjusted until the pH stabilized.

Contact angle was determined using a Rame-Hart Model 250. A 10µL water droplet was carefully placed on the ash surface, and the included software automatically estimated the change in contact angle over a period of 50 s. Readings were taken at 1 s intervals.

Saturated hydraulic conductivity testing was performed using a flexible-wall permeameter and the falling-head, rising-tailwater method, as outlined in ASTM D5084 [115]. The permeating liquid was chosen as deaired 0.03 M $CaCl_2$ as a proxy for tap water because testing was performed over a six-month period, and standard Atlanta tap water was expected to fluctuate in composition during that time. Specimens were originally in the loose, ground, dried condition and compacted to a target dry density of 1.1 g/cm^3 and a

compacted water content of 30% (based on literature of optimum water content and dry densities of compacted samples of Class F fly ash) [104,108]. Samples had approximate dimensions of 6.6 cm (2.6") height and 3.3 cm (1.3") diameter; they were tested for saturated hydraulic conductivity under different confining pressures, to simulate the consolidation pressure experienced by an ash sample deposited with less than 4.5 m (15 ft, 2.5 psi), 7.9 m (26 ft, 5 psi), 11.9 m (39 ft, 7.5 psi) and 15.8 m of overburden (52 ft, 10 psi overburden pressure). Samples were tested when they had achieved a B value of 0.90 or above (>95% saturation) [116]. Hydraulic gradients were kept to less than 15 to mitigate effects of migration of particles and clogging of pores [117].

SWCC testing was performed at Daniel B. Stevens and Associates, Incorporated (DBS&A), using the same target dry density. Samples were tested for saturated hydraulic conductivity using the falling-head, rising-tailwater method and also tested for water retention during drying using four standard methodologies: hanging column (HC), pressure plate (PP), dew point potentiometer (DPP), and a relative humidity box (RH) [115,118]. However, for the Y-CBD sample, DBS&A reported that the DPP analysis was not appropriate, such that data is not available in the matric suction range between 10^3 and 10^5 cm^{-1}. The coefficient related to air-entry pressure (α, cm^{-1}), N (related to the pore size distribution, dimensionless), residual water content (Θ_r %), and saturated water content (Θ_s, %) were fitted from experimental data of water content versus matric suction (Θ, Ψ) using the Van Genutchen equation. In its generic form, k represents all integer values, expressed as a combination of the two unknown parameters, m and N, from the Van Genutchen equation ($k = m - (1+1/N)$). If k is assumed to be zero [107,119], $m = 1 + 1/N$, and the Van Genutchen equation becomes (Equation 2):

$$S_e = \frac{\theta(\psi) - \theta_r}{\theta_s - \theta_r} = \frac{1}{(1 + (\alpha\Psi)^N)^{1-\frac{1}{N}}} \quad (2)$$

5.3 Results and Discussion

5.3.1 Results of Chemical Treatments

Overall, chemical and thermal pretreatments had a limited influence on the inorganic chemistry of the ash, besides the increased percentage of sodium in the Y_CBD sample, due to the combination of sodium citrate, bicarbonate, chloride, and dithionite used during the treatment (Table 15). The ash was rinsed for 2 h with DI water after CBD treatment, but the sodium content remained elevated.

The treatments did influence the physical properties of the ash (Table 16; Figure 20). The calcining heat treatment decreased the LOI from 15.6% to 1.6%. Although this method is not as accurate for quantifying unburned carbon content compared to TOC, it is reasonable to assume that the unburned carbon content in Y_C was considerably less than in the as-received PY. The calcining treatment is discussed in greater detail below because the ash transformation after thermal treatment provided some insights into the water retention characteristics of the ash. The specific surface area of the Y_A sample decreased by a factor of 3, which was considerably higher than the other chemical treatments. However, the median particle size remained the same. This decrease may have been a reflection of the methylene blue method used to measure specific surface area, as this sample was hydrophobic (discussed below); the change in surface chemistry may have inhibited the sorption/ionic exchange of methylene blue species [10]. The treatments did influence the

liquid limit of the fly ash. The PY samples classified as MH, with a liquid limit of 59%. However, the treated samples tested for Atterberg classified as ML, with liquid limits below 50%.

Some morphologies were not impacted by the treatment processes (Figure 20). Although testing of the supernatant after CBD treatment using ICP-OES confirmed that iron was removed, SEM micrographs showed that the aluminosilicate spheres remained intact. Additionally, the diatom frustules remained intact throughout the treatment processes. These morphologies were observed in SEM micrographs of all treated and untreated ash samples.

Table 15. Physical Properties of Treated PY Ash

	PY	**Y_DI**	**Y_A**	**Y_C**	**Y_CBD**
SSA (m^2/g)	6.1	7.3	1.8	2.4	5.5
G_s	2.32	2.20	2.23	2.43	2.21
LOI (%)	15.3	12.4	14.8	1.60	26.8
D_{50} (μm)	21.7	20.8	21.1	24	29.2
u^4	1.13	1.17	1.06	0.94	0.88
LL (%)	59.1	-[1]	44.5	49.3	-
USCS	MH	-	ML	ML	-

[1]samples were consumed before LL could be tested

Table 16. Oxide Content of Treated PY Ash

	PY	Y_DI	Y_A	Y_C	Y_CBD
SiO2	58.0	59.5	54.5	57.7	46.5
Al_2O_3	25.5	25.6	27.2	25.5	20.0
Fe_2O_3	9.33	7.76	10.6	9.4	5.86
SO_3	0.09	0.15	0.09	0.07	3.24
CaO	0.99	0.84	1.07	1.03	3.55
Na_2O	0.64	0.75	0.61	0.75	16.1
MgO	1.02	1.08	1.05	1.06	0.82
K_2O	2.48	2.75	2.62	2.63	2.12
P_2O_5	0.62	0.28	0.75	0.55	0.29
TiO_2	1.17	1.2	1.22	1.13	0.91
SrO	0.07	0.08	0.08	0.07	0.07
BaO	0.17	0.16	0.19	0.19	0.13
POC (%)	92.9	92.8	92.3	92.6	72.4

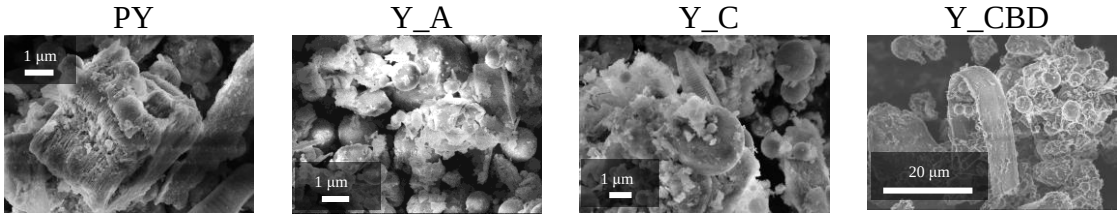

Figure 20. SEM micrographs of untreated and treated PY samples. Micrographs were used for descriptive analysis of ash samples

5.3.2 Calcined Ash

The PY ash exhibited an unusual transformation upon heating. Ignition in a muffle furnace for a loss-on-ignition (LOI) test (Method B, ASTM D7348) showed that the dried, powdered, grey ash turned bright red during high-temperature combustion (Figure 21) [62]. None of the other ashes studied in this dissertation (PW, PM, PV, and BH ashes) exhibited this behavior. The unaltered sample was subjected to a series of heat treatments, to better quantify the temperature at which observed changes occurred. As-received PY ash was heated to 400, 500, 600, 700, and 800°C respectively in a muffle furnace at a heating rate of 300°C/h, held at temperature for 1 hour, and allowed to cool overnight. The resulting samples (FA400, FA500, etc.) were ground with a mortar and pestle and stored.

Characterization was performed in accordance with the procedures outlined in the introduction.

A reddish color was observed after combustion of the ash at various temperatures ranging from 400-800°C (Figure 21). The transition was gradual, but by 700°C, the reddish color predominated. The reddish color is a result of the transformation of structural iron in kaolinite to hematite, as red is directly attributed to this specific iron oxide [120–124]. Structural iron refers to iron isomorphously substituted in the structure of the kaolinite alumina-silica sheets as well as any iron substituted in the structure of ancillary minerals (ex. mica, anatase) [121,125].

Figure 21. Color change associated with thermal treatment of fly ash

This particular ash sample was unique among the 30 weathered ashes featured in this dissertation because no crystalline iron oxides were identified using x-ray diffraction [87,126] (Table 17). Although the elemental iron content (as measured by x-ray fluorescence) was approximately 12%, no crystalline iron oxide phases (hematite, goethite, or magnetite) were found. Thermally treated samples had lower LOI values and lower specific surface areas than the as-received PY sample, but particle size distributions were similar (Table 17).

Table 17. Properties of As-Received and Thermally Treated Ash

Temperature (°C)	SSA (m^2/g)	LOI (%)	Particle Size Distribution		Crystalline minerals, XRD[1]
			d50 (μm)	Uniformity	
As-received	6.1	12.54	21.7	1.13	Q, M, K, Mu
400	3.7	4.73	17.8	1.11	Q, M, K
500	3.7	2.50	18.1	1.09	Q, M
600	4.3	0.79	17.6	1.05	Q, M, K
700	4.9	0.31	20.0	1.25	Q, M, H
800	2.4	1.60	24	0.936	Q, M, H

[1]Q = quartz, M = mullite, K = kaolinite, and Mu = muscovite, H = hematite

The kaolinite found in the fly ash may have come from either the bituminous fuel source or the surrounding geology. Some bituminous, semi-anthracite, and anthracite coals contain kaolinite as a major mineral (>1-10% by weight) [54], and kaolinite represents as a major mineral in fly ashes after combustion of these coals [54]. Kaolinite may have also been introduced after disposal, due to the presence of alluvial soils underlying the disposal facility [127]. Kaolinite may have been excavated along with the fly ash during the dewatering process.

High-temperature metamorphosis of kaolinite is a well-researched phenomenon in the ceramic and concrete beneficiation industries [120–122,124,125,128,129]. After removal of free water at low temperature heating (~100°C), dehydroxylation of the kaolinite structures occurs in the 350-550°C range. A poorly ordered, non-crystalline metakaolin phase is formed that is valuable in the concrete industries as a highly reactive pozzolanic material. At this point in the thermal treatment process, any structural iron contained in the metakaolin has a highly-distorted crystalline structure that is readily monitored using Mossbauer spectroscopy [124]. At temperatures above 550°C and up through ~1000°C, metakaolin breaks down further, forming more stable crystalline phases such as mullite (an aluminosilicate) and cristobalite (a high-temperature polymorph of SiO_2). Some of the

structural iron may substitute for aluminum in the mullite crystalline structure, but the rest forms iron oxides (often hematite) [120–122,124]. Iron may serve as a catalyst for the transformation of metakaolin at temperatures below 950°C [124].

The transformation of kaolinite to a non-crystalline metakaolin phase and the formation of hematite was confirmed by XRD (Figure 22). Crystalline kaolinite peaks at 12.5 and 20° 2Θ were replaced by a crystalline hematite peak forming at 35.5° 2Θ as the calcining temperature was increased to 800°C. Although the kaolinite peaks were low intensity compared to prevailing crystalline phases of quartz and mullite, there were no kaolinite peaks in the fully calcined ash (treated to 800°C). The XRD results were consistent with the literature on high-temperature metamorphosis of kaolinite to metakaolin above 550°C (listed above). Additionally, the low-intensity hematite peak at 35.5° 2Θ was not present in ashes heat-treated below 700°C.

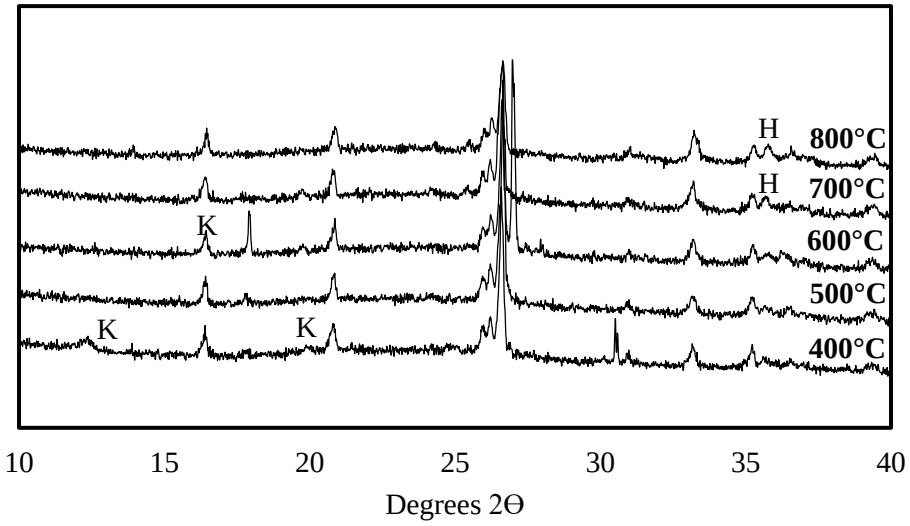

Figure 22. The appearance of crystalline hematite peaks (H) at higher temperatures during calcination of fly ash, and the corresponding disappearance of kaolinite peaks (K)

The contribution of kaolinite to the bulk specific surface area of the as-received PY ash was estimated to be approximately 15% of the total specific surface area (or 0.88 m^2/g), according to the following equation (Equation 3):

$$\%SSA_{kaolinite} = [\%Particles < 2\mu m \cdot SSA_{kaolinite}] \cdot \frac{1}{SSA_{PY}} \quad (3)$$

Where $SSA_{kaolinite}$ was the specific surface area of kaolinite (assumed to be 20 m^2/g) [130], SSA_{PY} was the measured specific surface area of PY (6.12 m^2/g), and %Particles < 2µm was 4.40%, taken from the laser particle size analysis. This estimation assumed that all particles smaller than 2 µm were kaolinite, but this assumption was not confirmed by another quantification method. However, this estimation was performed primarily to exemplify that a small quantity of high specific surface area clay (<5% of the cumulative volume of particles) may make a disproportionately large contribution to the bulk specific surface area of the fly ash.

5.3.3 Microscale Ash/Water Interactions

Further investigations on the microscale interactions between treated PY samples and water was performed, including measurements of point-of-zero-charge (PZC) and measurements of contact angle. The PZC pH fluctuated from less than 2 to approximately 5, in ascending order of Y_CBD (no PZC reached at low pH) < Y_C (no PZC reached at low pH) < Y_A (~3) < Y_DI (~4) < Y (~5) (Figure 23). Overall, acidic conditions produced a fly ash with a positive surface charge, but neutral and basic conditions resulted in a negative surface charge until conditions became highly basic (pH > 12). The pH conditions in four wet-disposed, alkaline Class F impoundment facilities were found to start as highly basic (pH

= 11.8) transitioning through near-neutral pH to finally acidic (pH = 4.3) as carbonates, aluminosilicates and silicates dissolve [80]. Under these conditions, the surface charge of weathered ash may fluctuate between slightly negative to slightly positive, although highly weathered fly ash may have different electrical responses to porewater and aqueous minerals than freshly-disposed ash. In the laboratory conditions used for hydraulic conductivity testing, however, PY samples were expected to have a negative surface charge because the pH of the saturating liquid (0.3 M $CaCl_2$) was above 5.

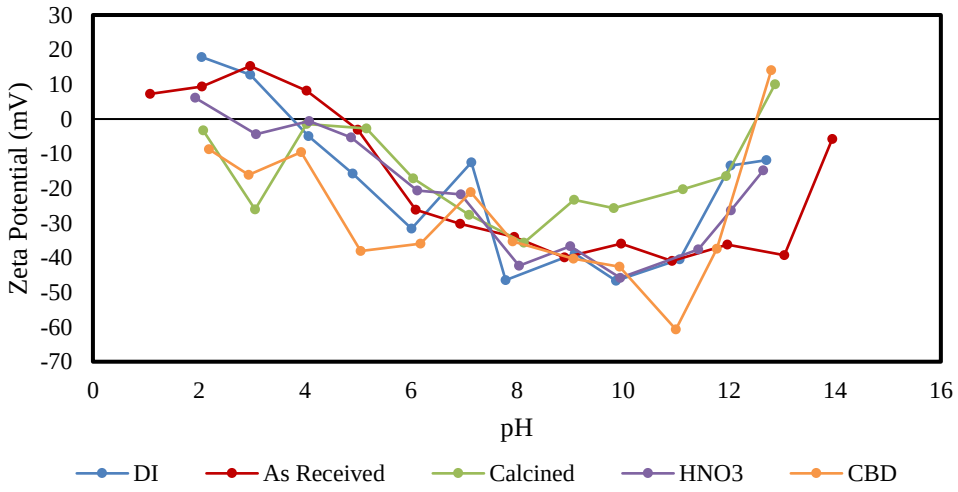

Figure 23. Zeta potential of treated ash samples over the pH range 2 – 14

Only one treated sample (PY_A) displayed hydrophobicity. The as-received PY sample and the other treated samples displayed no water droplet contact angle at all; the water droplet displayed purely wetting behavior. The PY_A, in contrast, displayed a marked hydrophobicity, enough for a contact angle measurement (Figure 24). The average contact angle after 50 measurements (1 per second) was 139° (left) and 138° (right) for the first test, and 158° (left) and 124° (right) for the second test. Over a period of 50 seconds after the initial wetting, the right-side contact angle decreased, and the left-side contact angle increased, indicating an uneven saturation front (Figure 24). The difficulty of wetting this

sample was also notable while achieving a 30% water content before the saturated hydraulic conductivity test and while measuring the liquid limit.

Test I	Test II
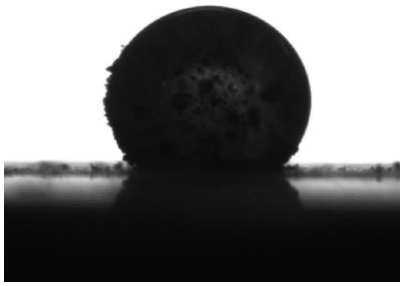	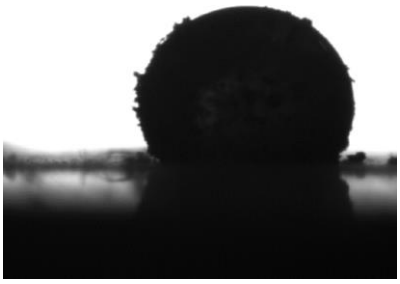
Average Contact Angle (L/R): 139°, 138°	Average Contact Angle (L/R): 158°, 124°

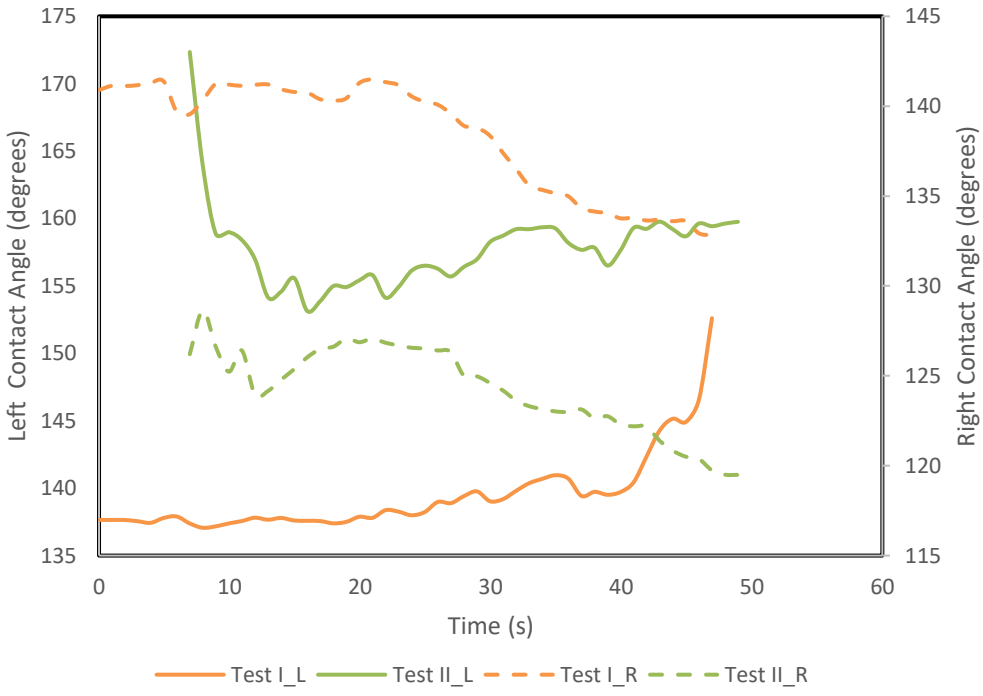

Figure 24. Change in contact angle of the left and right side (dual axes) for Y_A over a period of 50 seconds

5.3.4 Saturated Hydraulic Conductivity

Saturated hydraulic conductivity values were compared for the simulated overburden conditions (Table 18; Figure 25). Samples had, on average, hydraulic conductivities on the order of $1x10^{-5}$ cm/s, except for Y_CBD which had k_s on the order of $1x10^{-6}$ cm/s. There was no consistent trend of change in hydraulic conductivity with simulated overburden pressure. Microstructure adjustments in the sample fabric at higher pressures may have contributed to the variation in hydraulic conductivity with overburden, but flow was not significantly impeded by higher overburden pressure. In literature, higher initial compaction densities during sample preparation resulted in lower saturated hydraulic conductivities [105], but a similar correlation with simulated consolidation after saturation was not observed. The most significant influence was in the Y_A sample, where a small increase in overburden decreased the hydraulic conductivity from $1.88x10^{-5}$ cm/s to less than $1.0x10^{-5}$ cm/s. Overall, values for saturated hydraulic conductivity were consistent with literature on both fly ashes and silt-sized materials.

Table 18. Saturated Hydraulic Conductivity of Treated Fly Ashes ($x10^{-5}$ cm/s)

Simulated Overburden (ft)	PY	Y_DI	Y_A	Y_C	Y_CBD
12	1.25	1.13	1.88	1.15	0.232
26	1.36	1.27	0.81	0.94	0.23
39	1.29	1.09	0.46	0.94	0.253
52	0.81	1.31	0.98	1.78	0.159
Average	**1.13**	**1.20**	**1.33**	**1.80**	**0.219**

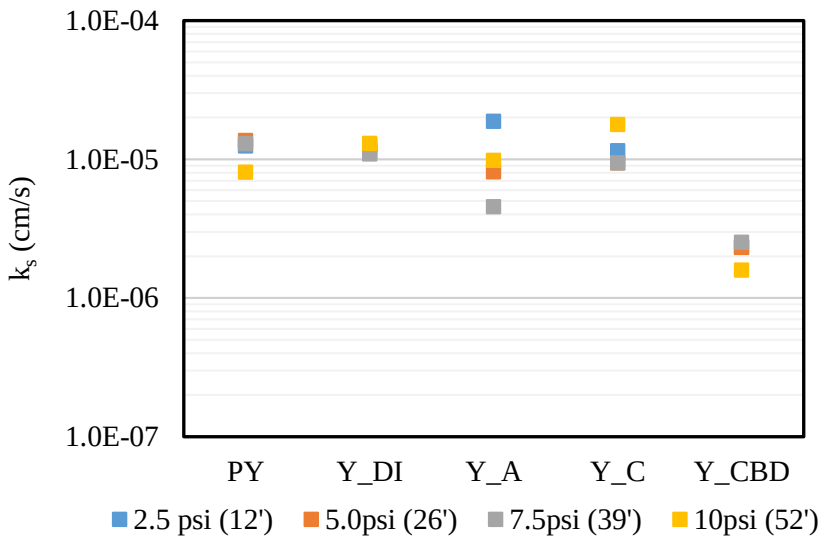

Figure 25. Hydraulic conductivity variation with simulated overburden pressure.

Treating the ash with sodium dithionite to reduce the iron into soluble Fe(II) forms had the most significant impact on saturated hydraulic conductivity. Although calcination changed the clay mineralogy and removed porous unburned carbon, the hydraulic conductivity remained in the same order of magnitude. The same hydraulic conductivity results were seen after rinsing the ash with DI water and 5% HNO_3. However, the removal of surface and crystalline iron, and the addition of sodium species (including halite and analcime) to the fly ash because of the CBD treatment had a strong influence on water flow. The k_s value dropped an order of magnitude from the as-received sample. Sodium compounds can act as deflocculating agents, so the addition of sodium to the porewater may have led to deflocculation and migration of kaolinite particles to the pore spaces, thus decreasing the saturated hydraulic conductivity.

Testing at various overburden pressures confirmed that hydraulic conductivity did change with pressure head, as mentioned in the literature, although the trend was not consistent [109]. Hydraulic conductivity has also been shown to change with chemistry for fly ash,

particularly for high calcium content fly ashes that exhibit self-hardening behavior [50,104]. These treated ashes did not have a high calcium content and, upon inspection after saturation and testing (a 7 to 10-day process), were deformable under slight applied pressure; they did not exhibit cementitious behavior.

5.3.5 Unsaturated Hydraulic Properties

The Van Genutchen SWCC was predicted using experimental matric suction and moisture content data for four of the five samples (

Table 19; Figure 26); Y_DI was excluded due to cost and time considerations. All samples had an initial plateau at low matric suction, indicating that additional air entry pressure was needed to begin desaturating the samples. Air-entry pressures ranged from 51-340 cm^{-1}; Young et al. [50] reported values between 100-400 cm^{-1} for fly ash. The PY sample (71 cm^{-1}) and the Y_CBD sample (51 cm^{-1}) were on the lower end of the range for fly ash, but Y_C (340 cm^{-1}) and Y_A (340 cm^{-1}) fell within the expected range. The higher air-entry pressure was a result of capillarity and small pore sizes within the fly ash matrix, though it may also be related to hydroscopic compounds (such as calcium oxides) and cation exchange capacity [50]. Higher values of air-entry pressure corresponded to finer-grained material.

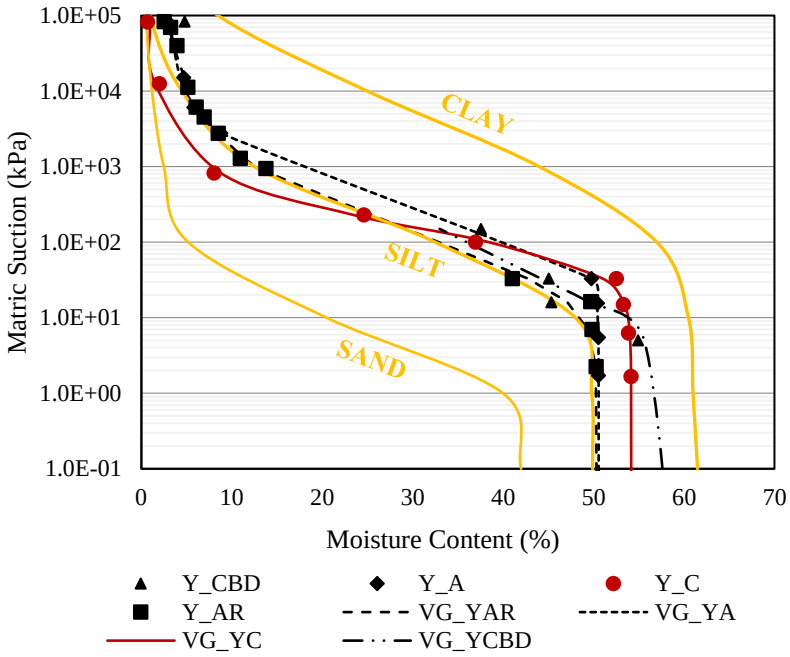

Figure 26. SWCC for four samples (Y_DI excluded) and the corresponding fitted Van Genutchen suction curves, compared to soil suction curves generated by Lu and Likos [131]

Table 19. Unsaturated Hydraulic Properties Calculated from the Van Genutchen Curve

	PY	**Y_C**	**Y_A**	**Y_CBD**
α (cm^{-1})	0.0024	0.001	0.0005	0.01
N	1.47	1.87	1.78	1.21
Θ_r (%)	1.60	0.79	2.68	-[1]
Θ_s (%)	50.5	54.2	50.6	59.3

[1]could not be predicted from the Van Genutchen curve

The as-received PY ash displayed, in general, unsaturated behavior characteristic of a silt [50]; the PY sample had a shallow drainage curve over the $10^2 – 10^6$ cm^{-1} matric suction range and a residual moisture content of 1.60%. The predicted α value was consistent with literature on fly ash SWCC, though the predicted residual water content was an order of magnitude higher than those reported for Class F fly ash by Abhijit and Sreedeep (2015) [47]. The higher residual water content was due to the combination of water-retentive diatoms and kaolinite present in the as-received PY ash [132].

There was some variation in unsaturated behavior due to treatment of PY. The Y_C sample had one of the highest air-entry pressures (336 cm^{-1}), and the sharpest drainage curve over the $10^2 – 10^6$ cm^{-1} matric suction range and a low residual moisture content (0.79%). The dewatering behavior of Y_C was comparable to the behavior of a sand, even though the high air entry pressure was characteristic of a silt [50,133]; the removal of porous carbons and transformation of kaolinite to metakaolin during calcination resulted in rapid drainage. In contrast, the Y_A and Y_CBD samples had higher residual or measured moisture contents (2.68 and 4.80%, respectively) and shallower drainage slopes, which was behavior more appropriate for a silt [50,110]. However, the Y_CBD and PY samples had the lowest air-entry pressures (51 cm^{-1} and 71 cm^{-1}, respectively). These samples did not easily retain excess water in bulk pore spaces but retained water within the kaolinite structures. Additional water was retained within the micropores of the diatom frustules [132]. The contradictions expressed by Y_C, PY, and Y_CBD confirmed that fly ash may exhibit characteristics of both sands and silts during dewatering.

The higher residual moisture content was attributed to both the kaolinite and the diatom frustules present in the as-received ash, neither of which were impacted by the acid-washing or CBD treatments. Dumenu et al. [133] observed that at high matric suction the SWCCs of fly ash tend to merge – this behavior was observed in PY, Y_A, and Y_CBD, even though the acid treatment shifted the drainage portion of the curve towards higher values of matric suction. The acid treatment resulted in an ash with the highest air-entry pressure (lowest α value), and the CBD treatment resulted in an ash with the highest measured water content at the maximum applied matric suction of $8.5x10^5$ cm^{-1}.

Overall, the calcining treatment shifted the unsaturated behavior of PY towards a sand, with lower matric suction required to achieve a specific water content. This ash has lower water retention capabilities than the as-received sample. The acid and CBD treatments shifted PY towards high water retention behavior and higher residual water content; the difference between the Y_C and Y_A was approximately half an order of magnitude during the drainage portion of the water retention curve. Calcination to transform the kaolinite to disordered metakaolin and remove some of the porous unburned carbon was an effective treatment for reducing the water retention capacity of PY, but treatments that did not remove or transform either the kaolinite or the diatom frustules, the two morphologies most likely to retain water, did not decrease the water retention capacity of PY.

5.4 Conclusions

The as-received PY sample exhibited a unique color transformation during thermal treatment (above 800°C). Further investigation indicated that this ash contained kaolinite which transformed into a combination of non-crystalline metakaolin and crystalline hematite (and potentially mullite and cristobalite) upon heating above 800°C. This hypothesis was confirmed by the shift in crystalline phases from kaolinite to hematite in x-ray diffraction analyses.

All PY samples displayed a hydraulic conductivity on the order of 10^{-5} or 10^{-6} cm/s, which was consistent with literature on silts. The CBD treatment represented the only treatment of the as-received PY sample that had a significant influence on hydraulic conductivity. The removal of crystalline and surface iron species and the inclusion of sodium compounds in the fly ash decreased the saturated hydraulic conductivity by an order of magnitude. For

all PY samples, however, there was no consistent trend between confining pressure (simulated overburden stress) and saturated hydraulic conductivity.

The influence of treatment was observed more strongly in the unsaturated behavior of the fly ash samples than in the saturated behavior. There was approximately a half an order magnitude difference in matric potential between the Y_A treated sample and the Y_C treated sample during drainage. The Y_C samples displayed unsaturated characteristics of a silty (high air-entry pressure) and sandy material (sharp drainage curve, low residual water content), whereas the PY, Y_A, and Y_CBD samples displayed more silt-like drainage characteristics, reflected in a shallower drainage curve and higher residual water content. The high-water retention capacity of the PY ash was due to the kaolinite and diatom frustules present in the ash. The calcining treatment transformed kaolinite into disordered metakaolin, reducing the water-retention capacity of the PY ash. However, no chemical treatments impacted the diatom frustules. Consequently, the acid and CBD treatments, which impacted neither the kaolinite nor the diatom frustules, did not decrease the water-retention capacity of the PY ash.

CHAPTER 6. EVALUATION OF ALTERNATIVE FLY ASHES AS SCMS

6.1 Introduction

Historically, coal has provided a significant percentage of the fuel used for energy generation in the United States. In the most recent decade, however, natural gas has rivaled coal as a primary fuel source, with each currently providing approximately 30% of the fuel used for domestic energy production [18]. This decrease in coal usage has contributed to shortages in domestically-produced fly ash [134], and along with other factors, including changes in emissions regulations and the practice of co-firing coal with other fuel sources, contribute to the increased variability in available fly ash resources. Consequently, the amount of fresh fly ash that meets specifications for use in concrete in the U.S. is reduced [8]. Nonetheless, fly ash continues to be one of the most broadly utilized supplementary cementitious materials (SCMs) worldwide. Fly ash is commonly used to reduce permeability, improve resistance to alkali-silica reaction and sulfate attack, and to reduce the heat of hydration in mass concrete elements [22,135–138]. Although a number of alternative SCMs are being explored, including calcined clays, crushed waste glass, and natural zeolites, it is also worthwhile to consider 'off-spec' ashes – or fly ashes and other fuel combustion by-products that do not meet current ASTM C618 specifications - as alternative pozzolans to augment the reduced supply of freshly produced or 'ordinary' coal ash [8,139–141].

Alternative ashes that may supplement inconsistent and inadequate supplies of fly ash include: (1) woody biomass ash, (2) ash from coal that has been co-fired with small amounts of biomass, and (3) previously geologically-disposed, weathered coal fly ashes. Each of these potential resources is abundant and geographically distributed, potentially representing a practical solution to the increasingly limited supply of 'on-spec' fly ash. Woody biomass ash, in the context of this study, is ash from the combustion of 100% wood and/or wood waste. These ashes are typically more enriched in alkaline earth metals and less enriched in iron, aluminum, and sulfur than coal fly ashes [5,13,41]. These ashes are excluded from use in concrete – either alone or in combination with other materials - by ASTM C618 by virtue of their non-coal source, independent of other characteristics. Co-firing coal with biomass is a more environmentally-friendly and renewable alternative to pure coal combustion because the addition of biomass waste offsets some of the greenhouse gas emissions from burning fossil fuels [4,142]. However, as ashes from co-firing are not derived 100% from coal, they are also excluded from ASTM C618.

Ash that was previously land disposed, weathered, or ponded represents a plentiful resource that is derived 100% from coal but is variable in composition and is not well-understood as a pozzolan. These ash deposits may be relatively new, or as much as 100 years old, and have a range of physical and chemical properties. Because these deposits accumulate over time and may include ashes derived from a variety of sources and burning conditions, including both on-spec ashes produced "off-season" (i.e., outside of periods of heavy construction demand) and off-spec ashes, their variability is likely much greater than ordinary fly ash produced at certain power generation facilities [82,143,144]. Exposure to water, minerals, and biological material during disposal and long-term submersion also

contribute to weathering the ash, changing its chemical and physical properties [56,59,82]. This ash may be a challenging material to use as an SCM, but it is a vast and underutilized resource – one that could be used as ordinary fly ash becomes scarcer.

Of the three potential alternative ash sources, relatively more research has been conducted on the use of biomass and co-fired ashes as cement replacements in concrete applications. For example, rice husk ash (RHA), due to its high amorphous silica content, has been successfully used as a pozzolan for decades [145–147]. However, woody biomass sources are typically low in amorphous silica or alumina, and as a result compressive strength is reduced in mortars with woody biomass fly ash as cement replacement [14,148–150]. In-turn, co-fired fly ashes have a less significant effect on compressive strength and may achieve the 28-day 75% strength activity requirement of ASTM C618 [102] or achieve even comparable strength to ordinary cement mixes by 28 days [150]. The co-fired ashes included here, previously studied by Shearer and Kurtis [12], successfully met the ASTM C618 strength requirements, although some samples were too high in LOI to meet the prescriptive requirements.

Weathered coal fly ash has only recently been considered as a resource for the concrete industry, and research on beneficiated weathered fly ash remains limited. However, weathered fly ash has been reclaimed and, after processing with heat treatments, marketed as a Class F fly ash for use in concrete [151].

ASTM C618 is the governing standard for “coal fly ash and raw or calcined natural pozzolan” usage in North American concrete [8]. Its prescriptive and performance-based metrics are meant to ensure suitable fly ash quality for fly ash suppliers and concrete

manufacturers. Certain chemical and physical requirements classify fly ashes as Class F (pozzolanic fly ash) and Class C (pozzolanic or latent cementitious fly ash) [8], as well as considering Class N (natural pozzolans), as shown in Table 20. The strength activity index (SAI) is performed on mortars produced with an 80:20 blend (by mass) of Portland cement:ash with water and sand and tested in compression at 7 and 28 days. It is the only required direct mechanical measure of performance [8]. The SAI must be 75% of the control, a mortar produced from the same Portland cement and water, at either 7 or 28 days. There are additional optional testing requirements not shown below. Given the scale of change in energy production and the need for SCMs for durable concrete, modernization of the guidance is needed to allow for the inclusion of alternative ashes for uses which enhance concrete quality.

Table 20. ASTM C618 Requirements

Chemical Requirements	Class		
	N	F	C
$SiO_2 + Al_2O_3 + Fe_2O_3$, %	70	70	50
SO_3, max, %	4	5	5
Moisture, %	3	3	3
LOI, max[1], %	10	6[1]	6
Physical Requirements	N	F	C
Fineness			
Amount retained when wet-sieved on 45 μm (No. 325) sieve, max, %	34	34	34
Strength activity index			
With portland cement, at 7 days, min, percent of control	75	75	75
With portland cement, at 28 days, percent of control	75	75	75
Water requirement, max, percent of control	115	105	105
Soundness			
Autoclave expansion or contraction, max %	0.8	0.8	0.8
Uniformity requirements			
Density, max variation from average, %	5	5	5
Percent retained on 45 μm (No. 325), max variation, percentage points from average	5	5	5

[1]LOI may be up to 12% for Class F pozzolans if acceptable performance records or laboratory tests results are made available

Because ASTM C618 specifies “coal fly ash”, it is generally accepted that co-fired and solely biomass ashes are excluded from use. However, other international governing standards do consider such materials. For example, the European standard EN450-1 already provides a specification to allow co-fired ashes as SCMs [41,148]. These requirements include the type and amount of biomass material, but provisions are explicit [152]. These provisions could serve as an example for adapting ASTM C618 to allow for co-fired ashes. Because ASTM C618 does not address reclaimed ashes explicitly, it is not clear if reclaimed ashes have been marketed as SCMs. To ensure an adequate supply of suitable ash for use in concrete, alternative ashes should be addressed by specifications applicable to construction in North America. This study was undertaken to determine if alternative fly ashes are suitable for use as SCMs in concrete. They would augment current seasonal shortages in fresh fly ash.

6.2 Materials and Methods

6.2.1 Materials

Ordinary coal fly ash (FA), co-fired ash (CA), woody biomass ash (BP1), and weathered coal fly ashes (WFA) were obtained from eight different U.S. power generation facilities (Table 21). All coal and co-fired samples (FA, CA, and WFA) were derived from eastern bituminous coals. BP was produced by combustion of a combination of forest, sawmill and urban wood waste. WFA samples were taken from four ash disposal facilities located at power generation facilities. PM samples were taken at depths between 0.15 – 1.5 m below ground surface (bgs) within the wet-storage facility with an estimated age of fewer than 10 years old. The ash produced at this facility was disposed because it was not consistently of

marketable quality. PW samples were taken from the ash delta, at a depth of 0.15-0.9 m bgs, where there was no standing water. The surficial ash crust was removed before sampling. Although PW ash was consistently of marketable quality, market demand was not sufficient to dry collect all of the ash. The PY sample was taken at shallow depth below the phreatic surface using a hydraulic excavator. Plant Y had no dry collection capacity. The PV samples were collected from a wet-storage facility at depths of approximately 3 m (PV1) and 4.6 m (PV2) bgs. PV samples are less than 20 years old. All WFA ashes were wet-sluiced to storage ponds that were exposed to the open air. They were weathered under southeastern U.S. (PM, PW, and PY) or central U.S. (PV) climatic conditions and partially saturated. Samples that represented a combination of bottom ash and fly ash were sieved through a No. 200 (45 μm) sieve to separate the fly ash from the bottom ash.

Table 21. Firing Conditions for Ash Samples

Plant ID	Location	Capacity (MW)	Boiler configuration[1]	Type of ash
PA	Georgia	3499	TF	FA
PB	Alabama	2013	OWF	FA, CA
PC	Alabama	138	TF	FA, CA
BP	Vermont	50	TGS	BP
PW	Georgia	952	TF	WFA
PM	Georgia	163	TF	WFA
PY	Georgia	952	TF	WFA
PV	Indiana	250	OWF	WFA

[1]OWF = opposed wall fired; TF = tangentially fired; TGS = travelling grate stoker

6.2.2 Methods

Characterization of the PW, PM, PY and PV samples was performed according to the methods outlined in the introduction. Characterization and strength activity testing of the PA, PB, PC, and BP1 samples were obtained previously [13,14]. Strength activity testing of WFA samples was performed by author Benkeser and described below.

The internal standard method was used to determine the amorphous content in the 13 WFA samples. Samples were spiked with 10% (by weight) of crystalline lanthanum hexaboride (LaB_6) and analyzed using x-ray diffraction. Phase quantification was performed using an automatic Rietveld analysis in HighScore Plus. A Pseudo-Voigt polynomial function was used with a split-width-and-shape asymmetry function. The standard weight of LaB_6 was manually set to 10%, and the software automatically calculated a correction factor from the overestimation of the internal standard [153]. This correction factor was then applied to each of the other crystalline phases, and the weight percent of the amorphous phase was calculated as the remaining difference to 100% (Equation 4).

$$\%\, amorphous = 100 - \sum_{i=1}^{n} Calculated\ Weight\%_i \cdot \frac{StandardWeight\%}{CalculatedWeight\%_{StandardPhase}} \quad (4)$$

The relative percentages of each crystalline and amorphous phase in the original sample was then calculated by removing the relative percentage of the LaB_6 standard (Equation 5).

$$OriginalPhase\%_i = MeasuredPhase\%_i \cdot \left(\frac{100}{100 - Standard\%}\right) \quad (5)$$

Two-inch (5 cm) mortar cubes were prepared with each fly ash sample for strength activity index (SAI) testing at both 7 and 28 days. These mixes were made with one water-to-cement (w/c) ratio (0.484) to guarantee that the only variable is the fly ash source/type. The fly ash replaced 20% of the mix by weight, in accordance to ASTM C618 [8] and was tested in accordance to ASTM C109 [154]. All specimens were stored in accordance to

ASTM C109. After mixing the mortar cubes were stored at a relative humidity of no less than 95% (ASTM C511) for 24 hours. The demolded specimens were then submerged in a saturated lime ($Ca(OH)_2$) solution until being removed for testing. The storage room was kept at a controlled temperature of 23 ºC [154].

6.3 Results and Discussion

6.3.1 Physical Characteristics of Alternative Fly Ashes

Weathered coal and co-fired samples displayed physical and morphological properties consistent with those for coal fly ashes [13,24] (

Table 22). These samples were fine-grained, grey in color and consisted primarily of glassy aluminosilicate spheres and unburned carbons [13] (Figure 27; Figure 28). The CA samples included some fibrous particles from the biomass fraction but also contained spherical particles. The WFA samples were similar in appearance to ordinary coal fly ash, but they contained more heavily encrusted aluminosilicate spheres. There were also many large agglomerations of smaller spheres held together by binding compounds (mostly sulfates), especially in the PW ashes. Evidence of diatoms was found in the PY sample. These morphological changes are likely due to weathering, precipitation, and biological infiltration happening in the ash pond [72,82].

Table 22. Physical Properties of Samples [13]

Sample	% biomass in fuel	d_{50} (μm)	SSA (m^2/g)	G_s
PA	-	16.2	1.3	2.63
PB-FA	-	29.9	4.6	2.47
PB-CA1	4	26.9	2.5	2.45
PB-CA2	8.2	23.3	3.5	2.39
PC-FA	-	17.3	7.5	2.15
PC-CA	15	11.4	6.1	2.20
BP1	100	168	12.7	1.87
PM1	-	45.7	2.6	2.26
PM2	-	28.2	12	2.26
PM3	-	24.5	1.3	2.39
PM4	-	23.8	3.2	2.35
PM5	-	30.5	2.2	2.38
PW3	-	24.3	0.90	2.72
PW6	-	29.7	1.2	2.91
PW8	-	18.3	2.3	2.42
PW9	-	12.7	2.0	2.48
PW10	-	23.4	1.9	2.67
PY	-	27.6	-[1]	2.32
PV1	-	18.2	-	2.51
PV2	-	17.9	-	2.58

[1]no data available

Figure 27. Color photos of ash samples: BP1 (left), WFA (middle), and CA (right)

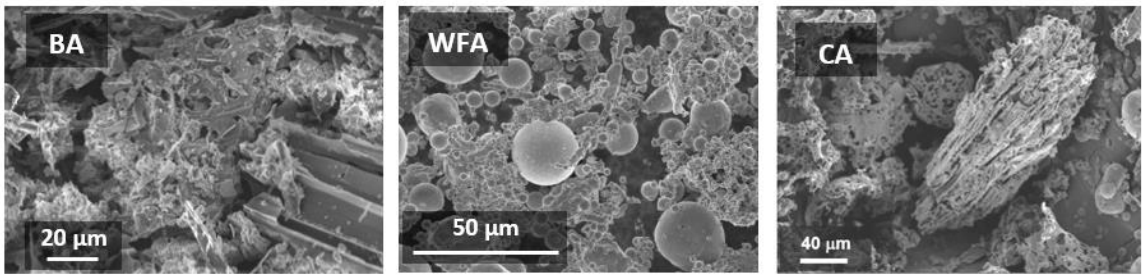

Figure 28. SEM micrographs of three alternative fly ashes: BP1 (left); WFA (middle); and CA (right). Micrographs were used for descriptive analysis of ash samples

In contrast, the BP1 morphology and physical properties were significantly different than the WFA, CA, and FA samples. The BP1 sample had the highest specific surface area, at 0.7 m2/g higher than the next highest sample (PM2) and 318% higher than the average (4.0 m2/g). The median particle size was increased by 544% from the average (30.9 μm), and the specific gravity was the lowest (77% of the average). BP1 was a black, coarse-grained ash comprised entirely of fibrous, woody particles. These larger, lightweight, carbonaceous particles are responsible for the difference in physical properties between the coal-derived and biomass-derived samples [13].

6.3.2 Chemical Characteristics of Alternative Fly Ashes

The WFA and CA samples have, in many aspects, chemical composition consistent with those classified as a Class F fly ash under ASTM C618, but the BP1 sample does not qualify as any of the three classes. The main inorganic constituents of the coal and co-fired ashes were silica, aluminum, and iron oxides, summed as the primary oxide content (POC) (Table 23; Table 24). The POC was over 70% for all FA, WFA, and CA samples.

Table 23. Chemical Composition of Non-Weathered Ash Samples [13]

Major Oxides (wt. %)	PA	PB			PC		BP1
	FA	FA	CA1	CA2	FA	CA	BA
SiO_2	55.3	45.3	47.9	48.0	47.0	48.6	6.43
Al_2O_3	27.2	23.4	24.7	24.4	22.9	23.4	0.75
Fe_2O_3	7.98	14.0	11.7	10.2	9.82	9.04	0.54
CaO	1.26	1.13	1.22	1.24	0.49	0.74	24.1
MgO	1.23	1.18	1.20	1.16	0.71	0.77	2.54
SO_3	0.07	0.06	0.10	0.07	0.04	0.05	2.88
Na_2O	0.47	0.68	0.62	0.80	0.19	0.23	0.40
K_2O	3.02	2.42	2.58	2.43	2.13	2.22	7.48
P_2O_5	0.19	0.33	0.37	0.34	0.34	0.42	2.18
POC	90.5	82.7	84.3	82.6	79.7	82.7	7.72
LOI (%)	1.4	5.9	5.5	5.2	15	15	47
TOC (%)	1.1	5.0	4.6	4.3	14	14	22

Table 24. Chemical Composition of Weathered Ash Samples

Major Oxides (wt. %)	PM					PW					PY	PV	
	1	2	3	4	5	3	6	8	9	10		1	2
SiO_2	54.45	52.43	52.40	53.65	54.77	46.62	38.45	55.58	54.43	40.05	49.6	47.0	46.8
Al_2O_3	28.89	30.48	28.34	30.08	28.94	21.21	17.40	25.99	24.53	17.90	27.6	18.7	18.8
Fe_2O_3	8.67	8.55	11.79	8.00	8.13	23.82	36.86	10.18	12.31	34.66	12.4	24.1	24.6
CaO	1.06	1.56	1.11	1.38	1.28	1.62	1.55	1.64	1.89	1.43	1.03	3.24	3.16
MgO	0.99	0.98	0.80	0.89	0.94	0.83	0.66	1.00	0.97	0.67	0.96	0.93	0.93
SO_3	0.10	0.14	0.05	0.07	0.05	0.10	0.12	0.12	0.12	0.28	0.87	0.57	0.53
Na_2O	0.35	0.43	0.31	0.31	0.38	0.60	0.48	0.68	0.77	0.41	0.47	0.57	0.56
K_2O	2.81	2.58	2.38	2.51	2.53	2.34	1.83	2.93	2.83	1.89	2.48	2.45	2.45
P_2O_5	0.47	0.90	0.31	0.75	0.56	0.20	0.17	0.25	0.22	0.16	0.96	0.22	0.22
POC (%)	92.01	91.46	92.53	91.73	91.84	91.65	92.71	91.75	91.27	92.61	89.7	89.8	90.3
LOI (%)	7.5	20	4.4	8.3	4.4	0.17	0.78	2.6	1.6	8.7	13	5.9	5.2
TOC (%)	5.2	12	3.6	7.5	5.4	0.14	0.25	3.0	0.89	5.1	3.7	3.8	3.6

Trace elements included alkaline and alkaline earth metals and sulfur, each not exceeding 3.5% of the total inorganic content. The BP1 sample does not meet Class N, C, or F compositional specifications. The POC is very low, less than 8%. The main inorganic constituent, making up 24% of the total inorganic elemental composition, is calcium oxide (CaO). The BP1 sample is enriched in other alkaline metals as well, compared to the coal and co-fired samples. The high alkaline content and the low POC would indicate, from the current prescriptive standards, that the biomass sample is unsuitable for use as an SCM in concrete. However, other applications related to concrete are possible, for example using woody biomass ash as an alkali-based activator.

The WFA and CA samples had inconsistent loss-on-ignition (LOI). Three of the five PM ashes, one PW ash, the PY ash, the two PC ashes and the BP1 ash exceeded the 6% LOI maximum requirement (Table 23; Table 24). The BP1 ash being high in LOI is not surprising, considering its morphology and source. The PC, PM, and PY ashes that had LOI over 10% were more interesting because they had similar morphologies to original coal fly ash. The consistently high LOI for PM and PY samples is a likely reason for why

these ashes were wet disposed instead of marketed as Class F fly ash. The PC ashes were burned at an older facility which uses lower temperatures than more modern facilities, resulting in a higher unburned carbon content.

It is worth noting, in a footnote to the tabulated compositional requirements for Class F ash in ASTM C618, that up to 12% LOI is permitted when the performance of the ash can be validated by laboratory testing or historical performance [8]. This suggests that reclaimed or co-fired ashes with LOI > 6% could be considered for use in concrete – with adequate evidence of their performance. Recent advances in beneficiation of high LOI fly ash and the common use of water-reducing and high-range water-reducing admixtures are both approaches which can ameliorate or compensate for adverse admixture interactions or reductions in workability associated with higher LOI ordinary fly ashes [155]. Additional effort should be put toward examining if the 12% LOI limit could be extended to ashes which are currently off-spec.

TOC measurements indicated that LOI overestimates carbon content in alternative ashes (Table 23; Table 24). LOI is a measurement of bulk mass loss between 23-950°C, including mass loss due to: (1) dehydration of hydrated mineral phases (gypsum and portlandite), (2) decomposition of carbonates, and (3) combustion of unburned carbon [25,63,68]. LOI will be artificially inflated for ashes that contain hydrated mineral phases, such as weathered fly ashes that were wet-disposed [54,68,126]. All of the high LOI samples had lower TOC values, and three (PM1, PW0, and PY) had TOC values below 6%. TOC methods mitigate the carbon overestimation effects, especially for alternative ashes that may have been exposed to water and may be more appropriate for quantifying carbon content than LOI.

6.3.3 Quantification of Crystalline and Amorphous Phases

The crystalline minerals of the CA, WFA, and FA samples were similar, but the BP1 sample had more crystalline phases with alkaline and alkaline earth metals and no amorphous phases. Quartz (SiO_2), mullite ($Al_6Si_2O_{13}$), hematite (Fe_2O_3), and magnetite (Fe_3O_4) were the major crystalline components of the coal and co-fired ashes (Figure 29), with the distinctive amorphous hump between 18° and 35° 2 Theta observed [102]. This broad peak arises from the poorly ordered crystalline structure of the glassy aluminosilicate spheres in the fly ash [156]. Low-intensity diffraction peaks associated with crystalline calcium phases were also seen in the PY and PV samples, including ettringite (3CaO•Al2O3•3CaSO4•32H2O) and calcite (CaCO3), respectively. The major crystalline forms in the BP1 sample were calcite and arcanite (K_2SO_4), and the amorphous silica hump was not observed. The XRD phase analysis complemented the SEM and XRF data on woody biomass ash composition; BP1 has low silica and aluminum content and no amorphous hump [13], which is consistent with the SEM characterization that showed no glassy aluminosilicate spheres.

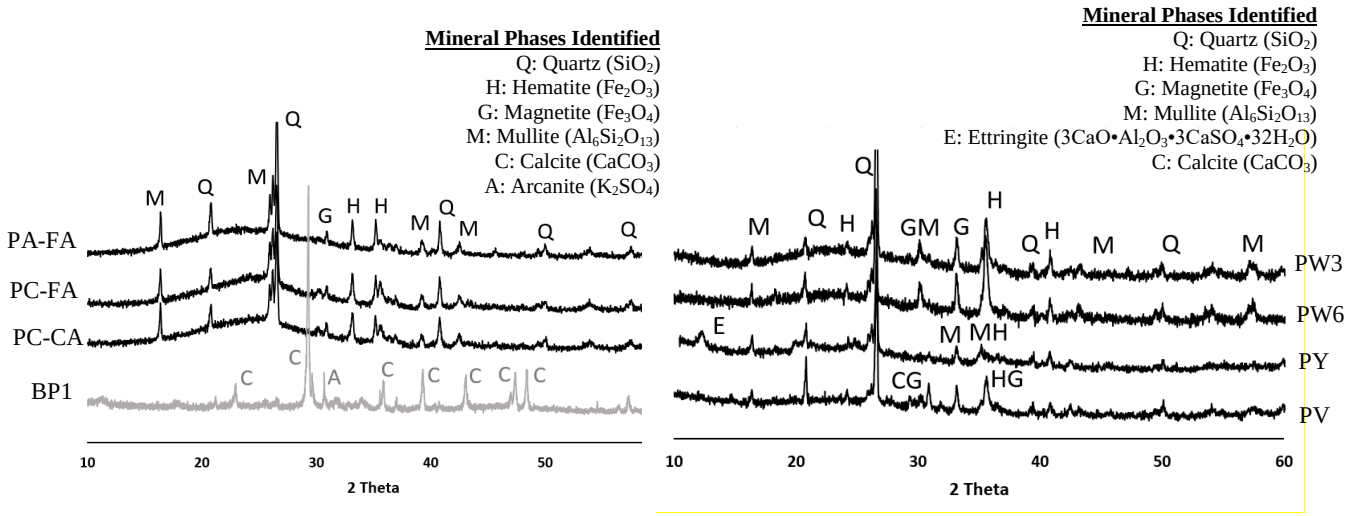

Figure 29. X-ray powder diffraction of FA, CA, and BP1 samples (left) and WFA samples (right)

Further crystalline and amorphous silica analyses were performed with the WFA samples to determine if they retain amorphous silica after weathering. Silicates will dissolve into ash pond pore water over time, as pH decreases to acidic values [59,80]. It is important to determine if weathered ashes retain enough amorphous glass to be pozzolanic. The range of amorphous content in Class F and co-fired coal fly ashes is large, 45-97% [153,157–159]. Chancey et al. [153] divided the amorphous content of Class F fly ashes into five categories based on composition: (1) three variations of calcium-aluminum-silica glass; (2) potassium-aluminum-silica glass; and (3) sodium-aluminum-silica glass. Yan et al. [160] subdivided the amorphous phases in pulverized coal fly ash into two categories: aluminum-silica glass and silica glass. Oey et al. [161] characterized the interaction between silica and aluminosilicate tetrahedra (network formers) and low valence metal cations (network modifiers) in amorphous glass. Their work defined a network ratio, N_r, that relates composition to glass structure and provides more information about pozzolanic reactivity than using POC alone.

Weathered fly ashes retained amorphous silica after weathering (Table 25). The range in amorphous silica content for samples from PM was 40-57%. For PW, the range was 69-82%, and PY and PV ashes had approximately 65% amorphous content by weight. On average, 63% of the inorganic minerals in WFA samples was made of amorphous material.

Table 25. Phase Quantification of Crystalline and Amorphous Phases in WFA

Phase	PM					PW					PY	PV	
(wt. %)	1	2	3	4	5	1	2	3	4	5		1	2
Mullite	34.2	27.2	35.8	33.9	35.7	8.11	7.89	10.2	8.33	8.0	17.4	13.4	13.1
Quartz	16.4	12.9	14.3	13.7	17.0	8.22	9.00	9.33	8.11	10.9	14.0	18.8	16.1
Magnetite	0.0	0.44	1.11	0.44	0.67	7.67	7.78	0.67	0.67	9.11	0.44	2.11	0.0
Hematite	0.56	0.44	1.00	0.44	0.67	2.44	3.44	0.0	0.78	3.11	0.33	3.33	4.33
Calcite	0.0	0.0	0.0	0.0	0.0	0.0	0.0	0.0	0.0	0.0	0.0	1.33	1.33
Ettringite	0.0	0.0	0.0	0.0	0.0	0.0	0.0	0.0	0.0	0.0	0.11	0.0	0.0
Amorphous	48.8	59.1	47.9	51.6	45.9	73.4	71.9	79.8	82.1	68.8	67.8	61.0	65.1

The crystalline data of the WFA samples, in conjunction with XRF, was used to calculate the network ratio (N_r) of aluminosilicates to the glass network modifiers (alkaline and alkaline earth metals), after Oey et al. [161]. However, WFA samples have low percentages of alkaline and alkaline earth metals (especially calcium), and N_r was zero for all samples. As a result, the proposed parameter was found not to be suitable for assessing the potential reactivity of these ashes.

6.3.4 Strength Activity Index

Of the 17 alternative ashes included in this study, five did not pass the SAI requirements at 7 and/or 28 days (Figure 30). The BP1 sample did not meet the compositional specifications in ASTM C618 and also failed the SAI at both ages. While the other ashes met compositional requirements, those that failed the SAI were not limited to one type of alternative ash. Two of the three co-fired ash samples failed at 28 days but passed at 7 days. Because of the language regarding SAI in ASTM C618, which requires

that the ash meet strength at *either* age, all three co-fired ashes fulfill the SAI requirements. Four of the 13 WFA samples failed at both ages, while the remaining met the requirement at both ages. It is notable that some of off-spec ashes outperformed FA at 7 (PM3, PC-CA) and 28 days (PM1).

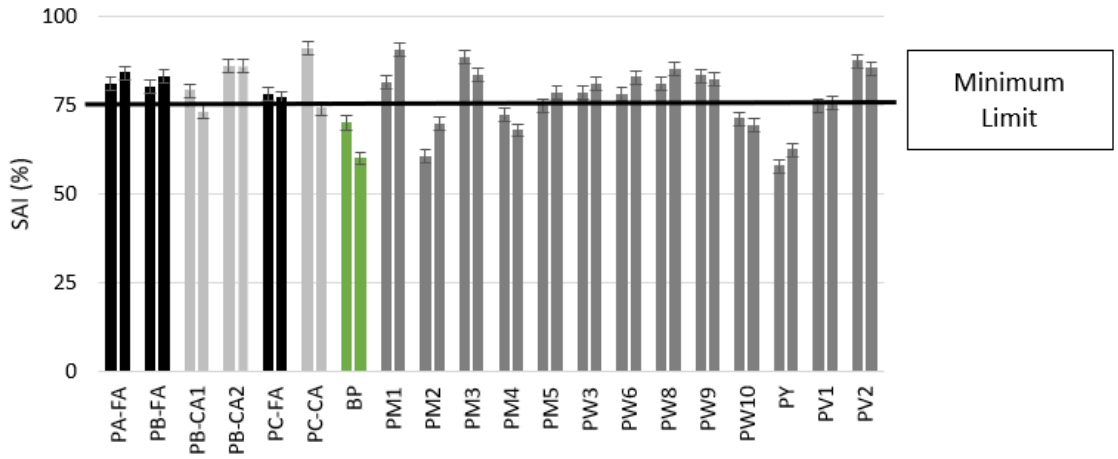

Figure 30. Strength activity index of 20 ashes at 7 days (left bar) and 28 days (right bar)

A rate of strength increase was calculated, to compare how quickly alternative fly ashes gain strength compared to ordinary fly ashes (Figure 31). This approach allows for the identification of faster and slower-reacting ashes. To calculate the rate, the 28-day SAI was divided by the 7-day SAI. Using this approach removed the influence of the ordinary portland cement on the SAI results. Nine of 20 samples gained strength with the additional 20 days of curing; of these, only two samples (PM2 and PY) did not pass the SAI requirement at both 7 and 28 days. The fact that these ashes gained strength in 20 days yet still failed the SAI requirement suggests that these ashes could be effective pozzolans, given longer curing times. However, this would need to be validated with testing the strength activity index after longer curing times.

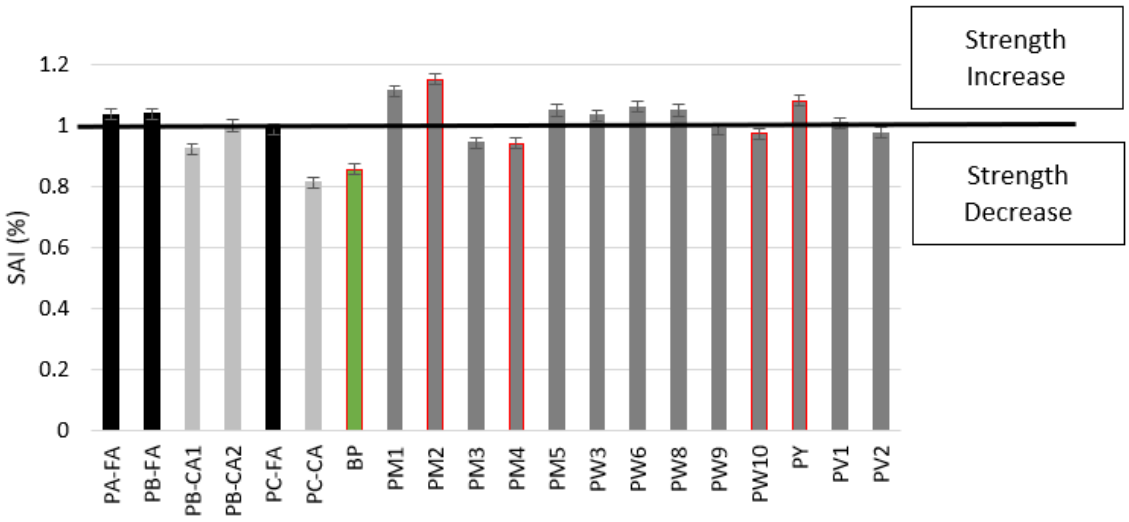

Figure 31. Ratio of SAI at 28 and 7 days for 20 ashes. Samples outlined in red failed the SAI requirement at 7 and 28 days

This analysis of alternative ashes from 8 different power facilities shows that many varieties of alternative ashes fulfill the prescriptive and performance requirements of ASTM C618. The co-fired and weathered coal fly ashes fulfill all the chemical and physical requirements of ASTM C618, except for loss-on-ignition. ASTM C618 specifies that up to 12% LOI is acceptable if "either acceptable performance records or laboratory test results are made available" [8]. There is room in ASTM C618 for alternative ashes that fulfill the prescriptive and performance requirements, as supplies of ordinary coal fly ash become scarcer, particularly if additional guidance on performance testing can be provided.

6.4 Conclusions

Based on the results of this experimental investigation of 20 coal, co-fired and woody biomass ashes fulfilling the requirements of ASTM C618, the following conclusions are drawn:

1. Woody biomass ashes that are low in silica and aluminum, high in calcium and are comprised primarily of coarse, fibrous unburned carbon particles are not suitable as pozzolanic supplementary materials in concrete.
2. Co-fired and weathered coal fly ashes can meet ASTM C618 requirements for chemical, physical, and mechanical properties for Class F fly ashes, even though these alternative ash sources are not currently directly addressed by the standard. Some of these ashes had LOI values that exceeded 6%.
3. 13 of 17 alternative coal fly ashes (a combination of weathered coal and co-fired ashes) met the strength requirements outlined in ASTM C618. These ashes have potential for use in concrete as supplementary cementitious materials.
4. Coal fly ashes retain amorphous pozzolanic glass (a range of 48-82% by weight for 13 samples), even after weathering.

Overall, results from this study demonstrate that ashes that are currently 'off-spec', because of their source, but meet physical, chemical and strength requirements in ASTM C618 could be used successfully in concrete. Thus, it is proposed that co-fired and weathered ashes should be specifically considered by the governing standards in North America.

CHAPTER 7. REMOVAL OF LEAD BY ALTERNATIVE FLY ASHES

7.1 Introduction

Various methods exist for removing heavy metals from wastewaters (e.g. chemical precipitation, ion exchange, and adsorption), but adsorption is one of the most popular due to its efficiency and cost-effectiveness compared to other methods [9,162]. Much work has been done in developing low-cost sorbents from beneficiated waste materials [162–169]. However, the bulk of work on novel adsorbents focuses on the performance of waste materials that were specifically designed (activated, treated, or combusted) with adsorption in mind [162–164,170]. This study focuses instead on testing the sorption capacity of waste materials in their natural condition. These fly ashes are waste materials from power generation facilities, but their higher organic content makes them undesirable for beneficial use in concrete applications. Yet this high organic content and other chemical or physical properties may be advantageous for sorption. It is worthwhile to study how natural, unmodified waste materials sorb heavy metals. Beneficial use of these materials in sorption applications would serve twofold purposes – it would reduce landfill space needed to dispose of these wastes while also treating wastewater contaminants.

Alternative fly ashes have geochemical and morphological properties that may be advantageous for heavy metal removal. Biomass fly ash typically has higher alkaline elements and carbon content and lower sulfur content than coal fly ash [13,171]. Its natural pH is > 7, in the basic range [93]. Additionally, it has carbon structures that resemble

activated carbon, an industry standard sorbent [13]. Both the carbon structures and the alkaline natural pH of these materials work favorably for the removal of divalent metal cations from aqueous solutions. The negatively-charged surfaces adsorb metal ions, and the alkaline pH favors eventual precipitation as hydroxides and carbonates [94]. Weathered coal fly ash, in the context of this paper, refers to fly ash that was previously geologically disposed. When geologically disposed, tertiary-formed mineral phases, especially phases that appear as encrustations on ash particle surfaces, may impact metal adsorption by chemically altering the adsorption solution chemistry [54]. For example, soluble tertiary-deposited surface phases such as sulfates, carbonates, and chlorides may dissolve in the adsorption solution and change the equilibrium solution pH [54]. These chemical changes may improve metal cation removal. As stated previously, these alternative ashes were not activated or adjusted for adsorption in any way, nor was the solution chemistry controlled.

Lead is a toxic heavy metal contaminant is efficiently removed from aqueous solution by both adsorption and precipitation mechanisms [94,164,172,173]. Hayes and Leckie (1988) inferred that lead adsorbed by forming strongly bound inner sphere complexes on metal oxide ligands because adsorption was not affected by changing the ionic strength of the background solution [174]. Srivastava et al. [166] reported Pb(II) uptake as high as 1865 mg/g for lignin extracted from paper mill waste and determined that lignin surface functional groups and ion exchange reactions were dominant mechanisms of lead adsorption. Surface complexation models are widely used for the adsorption of heavy metal cations because these models are effective at describing the adsorption of heavy metals to surface functional groups [175,176]. Type of surface functional group, surface site

densities, surface charge, and pH have all been shown to influence lead adsorption [94,166,170,175–178].

This work performed in this chapter studied lead removal by alternative fly ashes that are barred from use in concrete applications due to high organic content. This study focused on three biomass fly ashes, two weathered coal fly ashes, one non-weathered, high-carbon content coal fly ash, one commercially produced coal-derived activated carbon, and one commercially-produced woody biomass-derived activated carbon to determine how these materials perform as low-cost adsorbents.

7.2 Materials and Methods

Fly ash samples were obtained from six power generation facilities throughout the southern United States (Table 26). Three samples of pure biomass fly ash were taken from full-scale, biomass-only power facilities (BP1, BP2, and PN). Two weathered coal fly ash samples (PW8 and PM2) were taken from ash disposal facilities in the southeastern United States; these samples were weathered under southeastern United States (humid subtropical) climate conditions in saturated to partially saturated conditions [179]. A sample of unweathered, high carbon-content fly ash (CP4-1) was taken from another facility in the southeastern United States. Two commercially-produced activated carbons, one coal-derived (AC1 – Carbon Resources CR2050B) and one biomass-derived (AC2 - Carbon Resources CR2325W-CA) were selected as comparisons to the coal, weathered coal, and biomass samples.

Table 26. Physical Properties of Sorbents

Ash	BP1[1]	BP2	PN	AC1	AC2	PM2	PW8	CP4-1
Fuel	wood	wood	wood	coal	wood	coal	coal	coal
% Biomass	100	100	100	0	100	0	0	0
D_{50} (μm)	640	1440	19.1	151	33.7	28.2	18.3	21.7
TOC (%)	47.4	80.5	0.53	87.9	82.1	11.6	2.96	8.7
SSA (m^2/g)	180	687	1.50	893	1157	11.7	2.30	8.12

[1]Samples BP1, BP2, AC1, AC2, and CP4-1 were characterized by Yeboah [11]

Pb(II) solutions for batch sorption testing were prepared using lead nitrate - $Pb(NO_3)_2$ (Fisher Scientific) in deionized water ($\rho > 17$ MΩ.cm). For ICP-OES analysis, calibration solutions were prepared using EPA Method 200.7 Calibration Standard 10 (High Purity Standards). Leaching testing of the biomass and high-carbon content unweathered coal ashes [11] using the TCLP method [180] and of PM2 and PW8 using the SPLP method [181] confirmed that the leachable lead levels were less than 0.03 ppm (data referenced in Appendix B), far lower than the 5 – 200 ppm initial concentration range analyzed for adsorption.

Freestanding 50 ml polypropylene centrifuge tubes (Fisher Scientific) were used for batch sorption tests. The samples were suspended in heavy metal solutions at varying metal concentrations at a solid to liquid ratio of 10 g/L (500 mg in 50 ml). The samples were rotated at a rate of 18 revolutions per minute for 24 hours at room temperature (21 ± 0.5° C). Samples were centrifuged at 3000 rpm and filtered across nylon membrane syringe filters (EMD Millipore Millex) with a 45 μm pore opening. The filtered supernatants were acidified for ICP-OES analysis in 5% nitric acid using trace metal grade nitric acid – HNO_3 (Fisher Scientific) and 1 mg/L yttrium internal standard (Ultra Scientific – 1000 μg/ml). ICP-OES analysis was conducted on a dual view Perkin Elmer Optima 8000 with argon torch gas and compressed air shear gas.

Kinetic Pb(II) sorption tests were performed on all samples to confirm that that the equilibrium time of 24 hours was sufficient for equilibrium conditions to be reached.

The Langmuir (Equation 6) and Freundlich (Equation 7) isotherms were fitted using the Solver add-in from Microsoft Excel.

$$Q = Q_{max}\frac{K_L C}{1 + K_L C} \tag{6}$$

$$Q = K_D C^{\frac{1}{n}} \tag{7}$$

Where Q_{max} is the maximum predicted sorption capacity (mg/g), K_L is the Langmuir sorption coefficient (L/mg), C is the equilibrium concentration (mg/L), K_D is the distribution coefficient (L/mg), and n is a correction factor. The linear isotherm was fitted as a linear regression line.

A non-linear regression analysis method was used for the Langmuir and Freundlich isotherms in which the sum of squared errors (SSE) (Equation 8) was minimized between the predicted isotherm values and the experimental data.

$$SSE = \sum \left(q_{exp} - q_{pred}\right)^2 \tag{8}$$

Where q_{exp} is the experimental sorption capacity (mg/g) and q_{pred} is the predicted sorption capacity from the isotherm equation. The Pearson Product-Moment Correlation Coefficient was then calculated using the Excel function RSQ (Equation 9).

$$R^2 = \left[\frac{\sum(x-\bar{x})(y-\bar{y})}{\sqrt{\sum(x-\bar{x})^2 \sum(y-\bar{y})^2}}\right]^2 \quad (9)$$

The concentration of soluble cations (Mg^{2+}, Ca^{2+}, K^+, and Na^+) was determined according to a modified version of the procedure outlined in ASTM D7503 [182]. Ash was added to a 100 mg/L Pb(II) solution, rotated for 24 hours, centrifuged, and filtered. The supernatant was acidified with 5% HNO_3 and tested for Mg^{2+}, Ca^{2+}, K^+, and Na^+ using inductively coupled plasma optical emission spectrometry (ICP-OES, Perkin Elmer Optima 800).

Samples BP1, BP2, AC1, AC2, and CP4-1 were characterized and tested for Pb(II) sorption by Yeboah [11] using a similar methodology to that listed here. Additional testing on these samples, including measurement of soluble cations and sorption thermodynamic modeling, was performed by author Wirth.

7.3 Results and Discussion

7.3.1 Experimental Sorption Data

The removal capacity for Pb(II) ions varied among the samples (Figure 32). Two of three biomass fly ashes (BP1, BP2) showed linear removal capacity for lead, with a maximum capacity (in the tested concentration range) of approximately 40 mg/L. These samples outperformed the coal and wood-derived activated carbons. The third biomass ash sample (PN) showed good removal capacity for Pb(II), but the Langmuir isotherm was a better fit than the linear isotherm, with a maximum predicted capacity of 27 mg/L. All biomass and activated carbon samples outperformed the coal and co-fired fly ashes by a wide margin (Figure 32). The maximum removal capacity for the coal ashes was 5.6 mg/L

(PW8). In their natural, untreated state coal and weathered coal fly ashes show limited removal capacity for Pb(II).

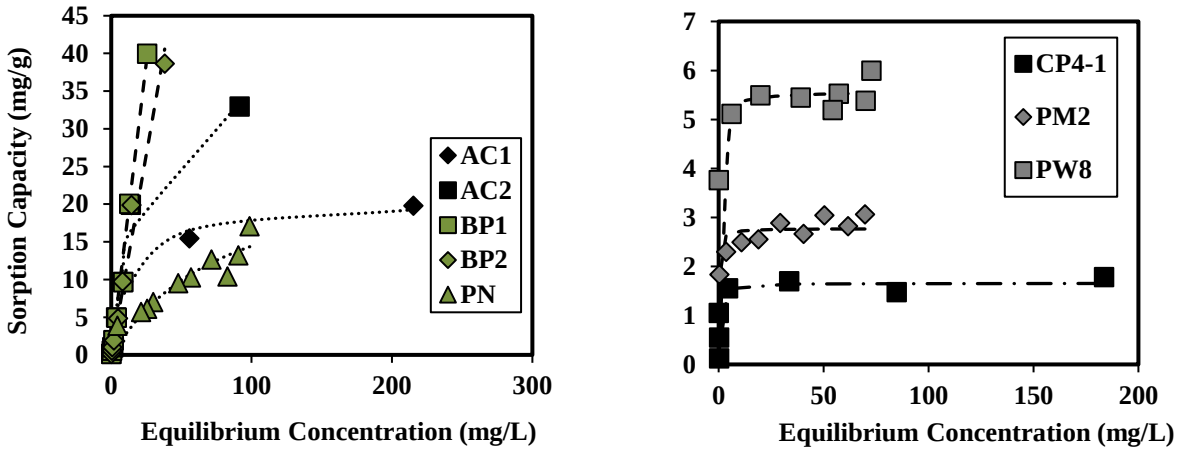

Figure 32. Pb(II) adsorption behavior of three biomass fly ashes (left), two activated carbons (left), one unweathered coal fly ash (right), and two weathered coal fly ashes (right), with their corresponding Langmuir or linear isotherms

Langmuir, Freundlich, and linear (where appropriate) sorption isotherms were fit from the experimental data (Table 27). These are commonly used in sorption literature as predictive models for equilibrium sorption, and details on their parameters and derivations are reported elsewhere [9,11,183]. In general, both the Langmuir and Freundlich isotherms fit well. The Langmuir isotherm is a theoretically derived model which has the advantage over the empirical Freundlich model of predicting a maximum sorption capacity for the adsorbate/sorbent system. All references to q_{max} later in this Chapter are predicted from the Langmuir isotherm or taken as the maximum of the linear isotherm. This model will also be used later in the chapter for quantifying sorption energy.

Table 27. Isotherm Parameters for Sorbents

		BP1	BP2	PN	AC1	AC2	PM2	PW8	CP4-1
Linear	K_D (L/mg)	1.55	1.07						
	R^2	0.998	0.979						
Langmuir	q_{max} (mg/g)			26.5	20.5	41.1	2.77	5.58	1.66
	K_L (L/mg)			0.012	0.075	0.048	5.26	1.81	3.15
	R^2			0.864	0.982	0.980	0.946	0.987	0.677
Freundlich	n	0.950	1.16	1.70	2.71	1.96	11.0	30.7	7.77
	K_D	1.25	1.72	0.969	2.94	3.41	2.03	4.85	0.946
	R^2	0.999	0.990	0.882	0.923	0.934	0.916	0.987	0.648

7.3.1.1 Alkaline, water-soluble ions in fly ash

Although biomass ashes demonstrated good removal capacity for Pb(II), additional investigations are needed to determine if sorption was the dominant removal mechanism. Ashes with high CaO concentrations (such as the three biomass ashes) are typically alkaline, and ashes with low CaO and high Al_2O_3 concentrations are typically acidic [94]. Soluble alkaline ions on the particle surface dissolve in the slightly acidic Pb(II) solution, raise the equilibrium pH of the aqueous Pb/ash system, and contribute to the precipitation of Pb(II) as lead carbonates and hydroxides [94,177].

Additional experiments were conducted to determine if soluble alkaline cations influenced Pb(II) removal. Biomass fly ash samples were enriched in alkaline and alkaline earth metals compared to coal-derived ashes (Table 28) [13,43]. These ashes had correspondingly higher conductivities and higher equilibrium pH (after 24-hour sorption with Pb = 100 mg/L). The variation in aqueous chemistry between the biomass and coal fly ashes had significant implications for Pb(II) removal. It is likely that the equilibrium aqueous conditions contributed to precipitation of Pb(II) compounds in the Pb(II)/biomass ash system, though this is discussed in more detail below [94].

Table 28. Soluble Cations and Conductivity of Fly Ash

	Soluble Cation Concentrations in Pb(II) solution (mg/L)					
Ash	Eq pH	Ca	Na	Mg	K	Conductivity (uS/mL)
BP1	10.9	7.76	17.2	0.82	633	2220
BP2	10.7	1.30	12.8	1.80	890	980
PN	11.8	161	1.84	2.05	38.1	446
AC1	5.96	8.17	0.82	0.73	0.0	57.8
AC2	5.53	15.4	1.33	6.43	0.0	180
PM2	4.54	25.1	3.70	1.50	0.64	163
PW8	5.44	35.1	0.0	0.66	0.0	176
CP4-1	5.61	26.8	5.62	1.32	4.03	160

The predicted q_{max} was compared to both the sum of soluble cation concentrations (Mg^{2+}, Ca^{2+}, K^{+}, and Na^{+}) and to the total organic carbon content (TOC) of the ash (Figure 33; Figure 34). A strong positive correlation between soluble ion concentration and Pb(II) removal for the biomass and coal samples was observed, but an inverse relationship was observed for the activated carbons. For the activated carbons, even the wood-derived one (AC2), measured soluble cation concentrations were the lowest (less than 25 ppm total cation concentration) while Pb(II) removal was the highest. This correlation suggested that lead was not precipitating but was sorbing to the activated carbon surface. A positive correlation between organic carbon content and q_{max} was also found for most of the samples; sorption of heavy metal cations was related to the availability of carbon surfaces. Coal-derived AC1 and pure biomass sample PN did not follow the general q_{max}/TOC trend, though the very low carbon content of PN compared to the other biomass sample suggested that sorption to carbon functional groups did not contribute to the removal of Pb(II) from solution.

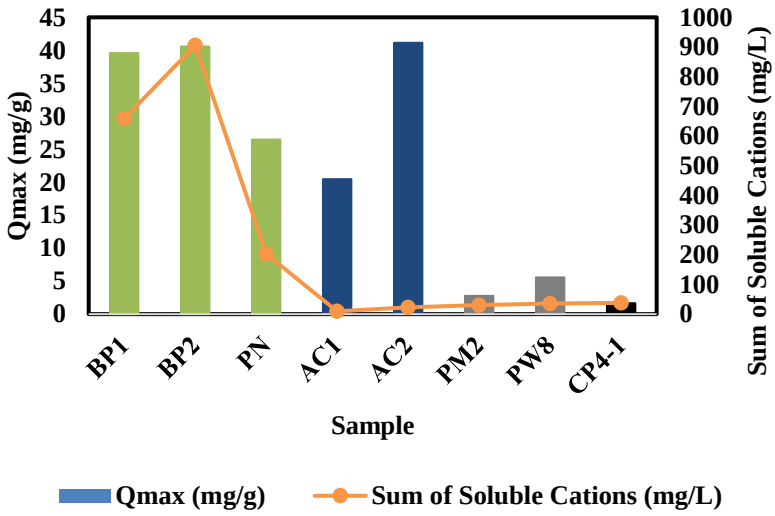

Figure 33. Q_{max} (mg/L) of the biomass ashes (green), the activated carbons (blue), the weathered coal ashes (grey), and the high-carbon content coal ash (black) compared to the sum of soluble cations in solution after equilibrium with 100 mg/L of Pb(II) solution

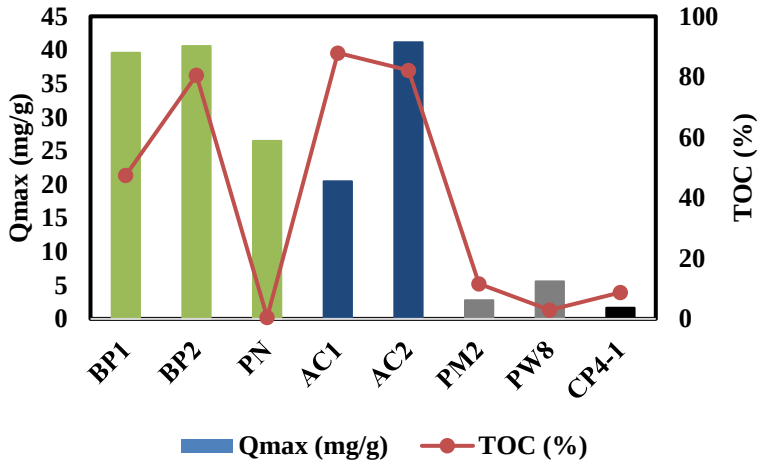

Figure 34. Q_{max} (mg/L) of the biomass ashes (green), the activated carbons (blue), the weathered coal ashes (grey), and the high-carbon content coal ash (black) compared to TOC (%)

The high concentration of soluble cations in the biomass ashes raised the equilibrium pH of the Pb(II)/ash system for the biomass samples and contributed to Pb(II) removal due to lead precipitation [94]. For samples BP1 and BP2, the high soluble cation concentration combined with a high carbon content indicated that both sorption and precipitation

removed Pb(II) species. In contrast, the dominant removal mechanism for the PN sample was lead precipitation. The low soluble cation concentrations for the AC and coal fly ashes indicated that the dominant removal mechanism for these samples was likely sorption/ion exchange mechanisms involving the carbon functional groups [164,170,175].

7.3.2 PHREEQC Speciation Modeling

7.3.2.1 Pb(II) Speciation

PHREEQC was used to confirm that precipitation effects played a significant role in lead removal from solution in alkaline environments. First, PHREEQC was used to predict the speciation of aqueous Pb(II) over a wide range of pH (Figure 35). Solid Pb(II) species were not allowed to precipitate, as this analysis was performed to identify which aqueous lead species dominate at acidic and basic pH ranges.

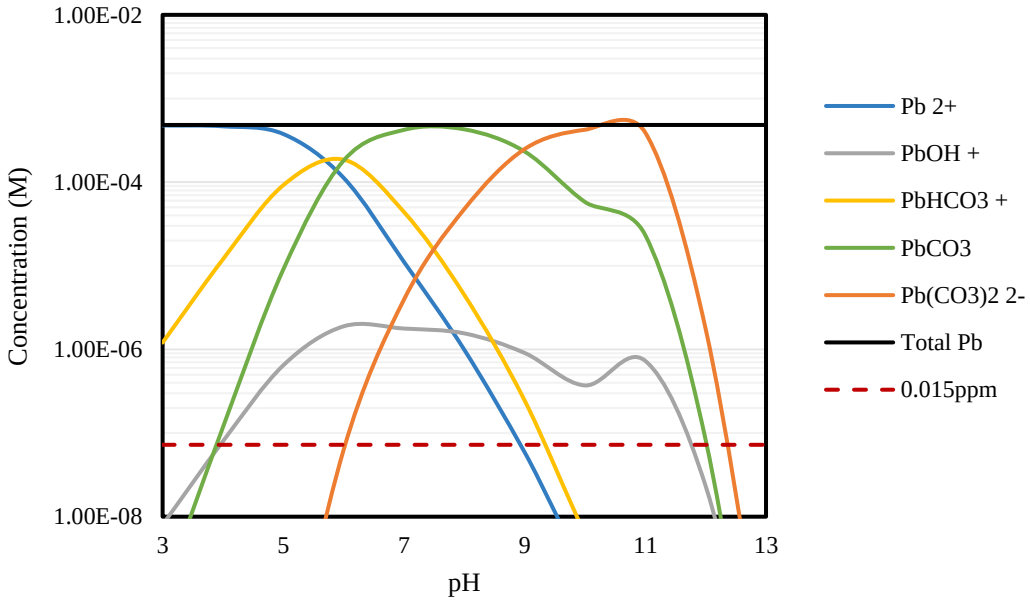

Figure 35. Lead speciation across the pH spectrum, with the EPA lead action level of 0.015 ppm (7.24×10^{-8} M) included for reference (the dashed red line). The total lead concentration was 100 ppm (4.83×10^{-3} M), represented by the solid black line

In the pH range of activated carbon and coal fly ash samples (4.5 – 6.0), Pb^{2+}, $PbHCO_3^+$, and $PbCO_3$ dominated. In contrast, in the pH range of the biomass samples (10.7 – 11.8), $PbCO_3$ and $Pb(CO_3)_2^{2-}$ dominated. This may have implications for sorption, if sorbents are more attracted to the positively-charged Pb^{2+} and $PbHCO_3^+$ ions. The equilibrium chemical conditions for biomass samples did not fall within the range of positively-charged Pb(II) aqueous species.

7.3.2.2 Pb(II) Precipitation

The data provided by PHREEQC was also used to determine if precipitation of lead phases was likely in the range of chemical conditions used during the sorption experiments. The measured cation, lead, and nitrate concentrations and the measured equilibrium pH (Table 28) were charge balanced with concentrations of chloride and sulfate ions in 0.05 L of water. The concentrations of chloride and sulfate ions (10 mg/L and 400 mg/L, respectively) were not measured directly but estimated based upon values from literature of ash pondwater [184]. PHREEQC provided saturation indices (SI) for solid mineral phases (Equation 10). A mineral phase with a SI >0 was supersaturated in solution and likely to precipitate.

$$SI = \log\left(\frac{IAP}{K_{sp}}\right) \tag{10}$$

Where IAP is the ion activity product and K_{sp} is the solubility product [185].

The most likely minerals to precipitate from Pb/ash solutions were lead sulfate (anglesite) and lead hydroxide (Table 29). In the case of PN, which had a high concentration of

calcium ions in solution (161 mg/L), calcite was also likely to precipitate. An additional PHREEQC simulation (not shown) confirmed that the initial Pb(II) solution (before ash was added) was not supersaturated (SI > 0) for any precipitated species. The addition of the soluble cation concentrations and equilibrium pH, which simulated the equilibrium sorption conditions, was enough to produce SI values above 2 for the biomass supernatant solutions. The soluble cations had a direct influence on the lead removal mechanism. The AC and coal ashes showed slight supersaturation of lead sulfates (1.3 < SI < 1.9), but the SI values were much lower than the lead hydroxide saturation values for the biomass ashes (4.6 < SI < 5.8). The AC and coal samples also had a limited quantity of soluble cations and slightly acidic equilibrium pH.

Table 29. Saturation Indices for Fly Ash Supernatants

Ash	Anglesite $PbSO_4$	Calcite $CaCO_3$	Lead Hydroxide $Pb(OH)_2$
BP1			5.75
BP2			5.68
PN		0.158	4.61
AC1	1.86		0.622
AC2	1.87		
PM2	1.33		
PW8	1.44		
CP4-1	1.87		

The high positive value for SI for the three biomass ashes confirm that precipitation was a dominant mechanism for Pb(II) removal in the Pb(II)/biomass ash system. In comparison, the low positive SI values, low equilibrium pH, and low aqueous cation concentration in weathered and high carbon content coal fly ashes indicated the sorption and/or ion exchange processes were the dominant removal mechanisms for Pb(II) in coal fly ash.

7.3.3 Statistical Mechanics Adsorption Model

Additional analyses on adsorption mechanisms were performed using a Langmuir sorption isotherm derived from statistical mechanics. Statistical mechanics describes the thermal properties of materials using a statistical analysis of their molecular interactions [186]. The derived formula looked similar to the traditional aqueous chemistry Langmuir model, but the thermodynamic derivation had a meaningful advantage over the original theoretical derivation, namely the coefficient K^0 (Table 30). This coefficient (as outlined in greater detail below) was used to approximate the energy associated with adsorption. The full derivation of the formula can be referenced in Appendix A.

Table 30. Derivations of the Langmuir Isotherm

Original Langmuir derivation [183]	Aqueous chemistry derivation [9]	Statistical mechanics derivation
$\frac{N}{N_0} = \frac{\sigma_1 \mu}{1 + \sigma_1 \mu}$	$\frac{Q}{Q_{max}} = \frac{K_L C_e}{1 + K_L C_e}$	$\frac{N}{N_{site}} = \frac{K^0 \cdot a_{solute}}{1 + K^0 \cdot a_{solute}}$

K^0 is a unitless parameter, as is the activity of the solute (a_{solute}) (Equation 11). While a_{solute} is the most accurate representation of the behavior of aqueous ions, it is sometimes difficult to calculate activity in a complex aqueous solution. If an infinitely dilute solution is assumed, the ratio of equilibrium concentration to a standard reference concentration (c/c_0) can be substituted for activity, which was advantageous because the equilibrium concentration, c, can be measured experimentally. The statistical mechanics derivation of the Langmuir isotherm becomes (Equation 12):

$$\frac{N}{N_{site}} = \frac{\mathrm{Q}}{\mathrm{Q}_{max}} = \frac{K^0 \cdot \mathrm{a}_{\mathrm{solute}}}{1 + K^0 \cdot \mathrm{a}_{\mathrm{solute}}} \tag{11}$$

$$\frac{Q}{Q_{max}} = \frac{K^0 \cdot \frac{c}{c_0}}{1 + K^0 \cdot \frac{c}{c_0}} = \frac{\frac{K^0}{c_0} c}{1 + \frac{K^0}{c_0} c} \tag{12}$$

Similar to the aqueous chemistry derivation of the Langmuir isotherm, Q_{max} and K^0 are fitted from experimental data. However, unlike the traditional Langmuir parameter K_L, K^0 is a unitless parameter that is related to the change in energy associated with the sorption process (ΔG^0, the standard state Gibbs free energy). ΔG^0 is readily calculated using K^0, temperature (T = 298 K), and Boltzmann's constant ($k = 1.38 \cdot 10^{-23}$ J/K) (Equation 13).

$$K^0 = \exp\left(-\frac{U_{ads} - \mu_0}{kT}\right)\frac{c_0}{c_{tot}} H = \exp\left(-\frac{\Delta G^0}{kT}\right); \Delta G^0 = -kTln(K^0) \tag{13}$$

The change in energy associated with sorption was calculated for the activated carbon, coal and weathered coal fly ashes. The biomass fly ashes were excluded from this analysis because a primary mechanism for Pb(II) removal was precipitation. K^0 was determined for three scenarios (Figure 36): (A) using the equilibrium concentration of Pb(II) measured by ICP-OES (Equation (12)); (B) using the activity of the Pb(II) ions, calculated using PHREEQC, but not including any soluble cation information in the model (Equation (11)); and (C) using the activity of the Pb(II) ions, calculated using PHREEQC but also including the equilibrium pH and soluble cations of the Pb(II)/ash system (Equation (11)).

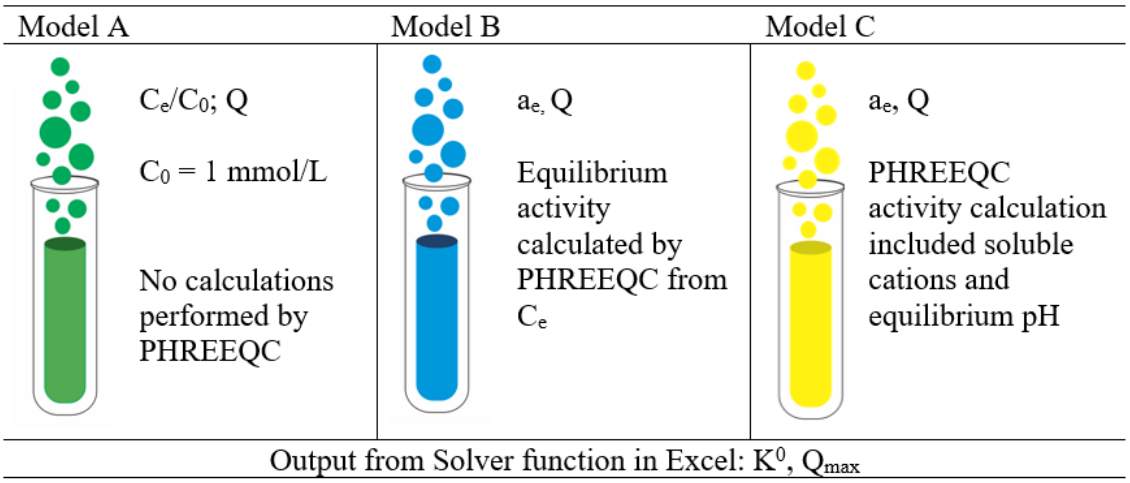

Figure 36. Three scenarios used to calculate the K^0 and Q_{max} sorption parameters

The K^0 or K^0/c_0 parameters were fitted using the Solver function in Excel, and K^0 was used to calculate the energy change associated with sorption. For the molar isotherm fitting, a c_0 of 1 mmol/L was chosen as a representative concentration for the equilibrium sorption system.

PHREEQC provided the necessary activities of aqueous Pb(II) species to check the assumption that the Pb(II) solutions were infinitely dilute (i.e. $a = c/c_0$) because high concentrations of ionic species in solution can have a significant impact on overall solution activity [187]. PHREEQC used the Davies equation for calculation of the activity coefficient of aqueous species [185] (Equation 14); this approach has been used by others to calculate the activity of aqueous Pb(II) ions [176].

$$\log \gamma = -Az_e^2 \left(\frac{\sqrt{\mu}}{1+\sqrt{\mu}} - 0.3\mu \right) \quad (14)$$

Where A is a constant at a given temperature, γ is the activity coefficient, μ is the ionic strength, and z_e is the number of equivalents of exchanger in the exchange species [185].

The change in energy associated with sorption was calculated for the activated carbon, coal and weathered coal fly ashes (Table 31). Strong adsorption (chemisorption) is typically in the range of 1-10 eV range, and weak adsorption (physisorption) is typically in the ~10-100 meV range. The negative value for Gibbs free energy indicates a more favorable energy state for the sorbate after adsorption onto the fly ash surface. Values for ΔG^0 indicate the adsorption onto activated carbon surfaces is due to weak, electrostatic bonds between surface sites and Pb(II) ions, and adsorption onto coal fly ashes is due to stronger, more chemical-type bonding between surface sites and Pb(II) ions. Coal fly ashes would be less advantageous as sorbents if multiple adsorption/desorption cycles are required, because it is difficult to remove the chemically-bonded Pb(II) ions without further input of energy. However, the activated carbons (unsurprisingly, considering that these materials are designed for sorption applications) are much more likely to effectively desorb Pb(II) ions and can be used for multiple adsorption/desorption cycles.

Table 31. Energy Change due to Sorption for Coal Fly Ashes and Activated Carbon

	Ash	AC1	AC2	PM2	PW8	CP4-1
Molar	K_0 ()	15.6	9.87	1089	376	653
	ΔG^0 (meV)	-70.6	-58.9	-180	-152	-167
Activity (no soluble cations)	K_0 ()	19.9	9.93	186	156	652
	ΔG^0 (meV)	-76.9	-59.0	-134	-130	-167
Activity (soluble cations)	K_0 ()	15.8	11.5	216	453	774
	ΔG^0 (meV)	-71.0	-62.7	-138	-157	-171

7.4 Conclusions

Alkaline, biomass fly ashes showed high removal capacity for aqueous Pb(II) species, but high-carbon content coal and weathered coal fly ashes showed low removal capacity. The high equilibrium pH and high soluble cation concentrations of biomass fly ash indicated

that a primary removal mechanism for Pb(II) was precipitation of lead hydroxides. Adsorption onto carbon surface and precipitation of lead solids seemed to be responsible for Pb(II) removal with the high-carbon content biomass fly ash samples BP1 and BP2. For PN, lead precipitation was the only removal mechanism.

Coal fly ashes had a stronger binding energy associated with adsorption than activated carbon, as predicted by a statistical mechanics derivation of the Langmuir isotherm. These materials would not be productive as adsorbents used for multiple adsorption/desorption cycles, due to their strong binding affinity for Pb(II). Overall, alternative ashes were not suitable if Pb(II) adsorption was the specific goal of a water treatment process, but if lead removal was the final goal, alkaline, high-carbon content biomass fly ashes may be economical alternatives to activated carbon.

CHAPTER 8. CONCLUSIONS

Previously-geologically disposed, weathered fly ash is a potential new source of Class C and Class F fly ash; however, there is limited data in the literature on how weathering has affected the morphology of the ash. The work performed in Chapter 3 of this study on 22 weathered fly ashes indicated that volatile mineral phases present in weathered ash include hydrated calcium sulfates, hydrated clays, portlandite, carbonates, iron oxides, and unburned carbon. Weathered fly ashes include, on average, more hydrated mineral phases that unweathered fly ashes, most likely because they were wet-disposed and exposed to precipitation. In some weathered ash samples, greater than 6% of the total sample mass was lost due to dehydration (heating in the 200-400 °C range). Additionally, weathered fly ashes contained large, highly porous carbon particles, even after weathering. Samples that were disposed for longer than ten years included more degraded carbon structures and exposed carbon surfaces than younger samples.

Final closure for ash impoundments often requires the use of heavy construction equipment to be placed on the ash surface, but this involves dewatering of the impoundment. Dewatering an ash impoundment requires extensive knowledge of ash saturated and unsaturated hydraulic properties, but there is limited data in literature on unsaturated behavior of weathered fly ash. This study was undertaken to determine if chemical and physical treatments of a high-water-retention capacity weathered coal fly ash (PY) influence ash hydraulic characteristics. Color transformation during thermal treatment of the as-received PY sample was due to the transformation of kaolinite present in the ash into non-crystalline metakaolin and crystalline hematite (and potentially mullite and

cristobalite). This hypothesis was confirmed by the shift in crystalline phases from kaolinite to hematite in x-ray diffraction analyses.

All PY samples had a hydraulic conductivity on the order of 10^{-5} or 10^{-6} cm/s, which was consistent with literature on silts. The only treatment of the as-received PY sample that had a significant influence on hydraulic conductivity was the CBD treatment; the saturated hydraulic conductivity dropped by an order of magnitude. There was no consistent trend between confining pressure (simulated overburden stress) and saturated hydraulic conductivity.

The influence of treatment was observed in the water retention characteristics of the fly ashes. The as-received PY sample had unsaturated behavior consistent with a fine-grained silt; its water-retention profile characterized by a shallow drainage curve and a high residual water content. The high residual water content was attributed to the kaolinite and diatom frustules present in the ash. The calcined sample displayed unsaturated characteristics of a silty (high air-entry pressure) and sandy material (sharp drainage curve, low residual water content), whereas the Y_CBD sample displayed the opposite characteristics. It had a sand-like low air-entry pressure but a silt-like shallower drainage curve and high residual water content. The acid-treated sample displayed purely silt-like water retention behavior, reflected in the high air-entry pressure, a shallower drainage curve and higher residual water content. Chemical treatments that did not alter the surface characteristics of either the kaolinite or the diatom frustules (HNO_3, CBD treatments) did not reduce the water-retention capacity of the PY ash. However, the calcining treatment, that transformed the kaolinite, resulted in a fly ash with reduced water-retention capabilities.

In terms of beneficial use, weathered coal fly ashes can meet ASTM C618 requirements for chemical, physical, and mechanical properties for Class F fly ashes, though some of these ashes had LOI values that exceeded 6%. Coal fly ashes retain amorphous pozzolanic glass (a range of 48-82% by weight for 13 samples), even after weathering. When used in concrete mortars, per ASTM C109, 9 of 13 weathered ash samples met the strength requirements per ASTM C618. These ashes have the potential for use in concrete as supplementary cementitious materials. However, the effectiveness of weathered coal fly ashes in sorption applications is limited. These ashes have a limited total removal capacity for Pb(II) (<6 mg/g). Additionally, they have stronger binding energy associated with adsorption than activated carbon, as predicted by a statistical mechanics derivation of the Langmuir isotherm. These materials would not be productive as adsorbents used for multiple adsorption/desorption cycles, due to their strong binding affinity for Pb(II).

Woody biomass fly ash is a more renewable, almost carbon-neutral fuel alternative to coal combustion for electricity generation. However, the waste materials generated must also be geologically disposed or beneficially used, so it is worthwhile to characterize woody biomass fly ash and explore potential beneficial use sectors. A woody biomass fly ash (PN) produced at a power generation facility equipped with a fluidized bed (FB) boiler was chemically and morphologically very distinct from three other woody biomass ash samples produced at power generation facilities with other boiler configurations. The PN ash displayed a lower unburned carbon content, a lower specific surface area, a higher specific gravity, and a lower median particle size compared to three other samples. The FB boiler contributed to an efficient fuel combustion and ash with a low unburned carbon content, a

particle size distribution in the silt range, and a low specific surface area. The type of boiler and the corresponding combustion conditions had a significant impact on ash morphology.

Although the woody fuel mixture varied across different combustion cycles at the PN facility, the physical and chemical properties of the PN samples were consistent across a single combustion cycle and across four different combustion cycles, with expected fluctuations. The largest variation was seen in LOI, which fluctuated between 1.5% and 5% across four combustion cycles. All samples contained angular silica, woody ash, and aluminosilicate sphere morphologies. A notable impact of the FB boiler was the inclusion of crystalline silica with the biomass fly ash which produced an ash with a higher silica content and angular silica particles. Lab-combusted samples did not contain this silica, and they had a correspondingly higher percentage of calcium and other alkaline metals. Woody biomass fly ash produced at a full-scale, biomass-only facility with a fluidized-bed boiler is consistently a high-calcium, low-organic, silty material.

Alkaline, biomass fly ashes, even though they have very different morphologies, show high removal capacity for aqueous Pb(II) species. The high equilibrium pH and high soluble cation concentrations of biomass fly ash indicate that a primary removal mechanism for Pb(II) is precipitation of lead hydroxides. Adsorption onto carbon surface and precipitation of lead solids are assumed to be dual mechanisms for Pb(II) removal for high-carbon content biomass fly ash samples BP1 and BP2. For PN, lead precipitation was the only removal mechanism. Wastewater treatment applications may be a beneficial use sector for woody biomass fly ash if metal removal is the primary objective for the treatment, and if the specific removal mechanism does not have to be sorption onto solid surfaces.

CHAPTER 9. FUTURE WORK

Proposed future work expands the characterization work summarized in this dissertation by including additional weathered fly ash and biomass fly ash samples, as this dissertation was limited in scope to only four different types of woody biomass fly ash, five weathered fly ash impoundments, and two beneficial use applications. Specific future work opportunities include:

- Further experimental testing on weathered coal fly ashes, to expand the current work on characterization of these materials. To validate the conclusions mentioned in this dissertation concerning the chemical and physical composition of weathered coal fly ashes, additional samples from geographical areas outside the southeastern United States would be helpful, as various climatic conditions may slow or accelerate the weathering process. Characterizing both shallow and deeply buried samples would be useful, to evaluate the time effects of aging.
- Further laboratory testing on the unsaturated hydraulic properties of weathered coal fly ash. First, testing additional weathered fly ashes for water-retention characteristics would augment the limited scope of this dissertation. Ideally, some of the additional samples would not have kaolinite or diatom frustules. Additionally, artificially adding a known quantity of kaolinite or diatomaceous earth to fly ash to increase its water-retention capacity would provide quantitative data on the effects of these morphologies on the water-retention capacity of fly ash. Lastly, additional work on chemical treatments of water-retentive morphologies to reduce their water-retention characteristics would be helpful. Ideally, these

chemical treatments could be implemented in field studies, to aid plant operations personnel in the dewatering of ash impoundment facilities.

- Testing additional weathered coal fly ashes for use as SCMs in concrete. Ideally, both weathered Class C ashes and Class F ashes would be tested for SAI in concrete mortars, to augment the limited scope of this dissertation, which included only 13 Class F weathered fly ash samples. This study could also include an exploration into how hydrated mineral phases, volatile mineral phases, and unburned carbon content influence mortar strength and durability. It is still unknown whether a potentially large quantity of hydrated and other volatile mineral phases in weathered fly ashes negatively impacts concrete performance.
- Characterization of additional woody biomass fly ashes from power generation facilities both within and outside of the United States, to validate the conclusion that combustion conditions and boiler efficiency have a strong impact on biomass ash properties. This study represented a limited scope of biomass fly ashes from the United States only. Additional characterization on woody biomass fly ash from other power generation facilities would augment the database of woody biomass fly ashes.
- Additional laboratory testing on woody biomass combustion, to quantify the effects of temperature on woody biomass fly ash morphology. Woody biomass fuel would be combusted in a temperature-controlled furnace, at temperatures between 600 and 900°C, and the resultant biomass ashes would be characterized. Examining the relationships between carbon content, combustion temperature, and biomass ash

properties would validate the conclusion that combustion conditions have a strong impact on biomass ash properties

- Additional testing of woody biomass fly ashes for heavy metal removal, to augment the current study on lead removal. Other divalent metal cations such as copper, cadmium, and chromium could be analyzed. Additionally, the removal capacity of alternative ashes for multi-metal solutions could be analyzed, as most wastewater streams contain more than one heavy metal. The metal removal capacity of biomass ashes in a multi-metal system would provide additional insight into the effectiveness of using biomass ashes for wastewater treatment.
- Additional geochemical modeling of the heavy metal/ash system, to quantify the precipitation and adsorption mechanisms. PHREEQC was used in this dissertation to model solely the precipitation reactions associated with Pb(II) removal at high pH, but PHREEQC also is capable of modeling adsorption using surface complexation models [185,188,189]. However, the surface complexation models associated with PHREEQC require additional experimental analysis of the quantity and type of adsorption surface sites. Future work with biomass and high-carbon content coal fly ashes would include finding the quantity and type of adsorption sites and the protonation constants of the adsorption site experimentally using titration [175] and then modeling the surface complexation of Pb(II) ions to ash functional groups.

APPENDIX A. DERIVATION OF THE THERMODYNAMIC LANGMUIR ISOTHERM

This expression was derived with the assistance of Dr. Laurent Brochard at Ecole des Ponts Paris Tech and is based on expressions from statistical mechanics. For a system of N_{site} number of adsorption sites with no interaction between adsorbed molecules, and N_u number of molecules adsorbed onto $N_u \leq N_{site}$ number of sites, the probability of there being a u microstate with N_u number of adsorbed molecules is:

$$p_u = \frac{1}{Z_{GC}} \exp(-N_u \frac{U_{ads} - \mu}{kT})$$

Where ZGC is the Grand Canonical Partition Function,

$$Z_{GC} = [1 + \exp\left(-\frac{U_{ads} - \mu}{kT}\right)]^{N_{site}}$$

At a fixed T and μ, the fraction of sites that are occupied can be determined from the Grand Potential $\Lambda = E - TS - \mu N = -kT\ln(Z_{GC})$ and the thermodynamic definition of the number of molecules, N, in the ensemble.

$$N = \frac{-\partial \Lambda}{\partial \mu};\ \Lambda = -kTln(Z_{GC})$$

$$\frac{N}{N_{sites}} = \frac{1}{1 + \exp(\frac{U_{ads} - \mu}{kT})}$$

$$U_{ads} - kTln\left[\frac{N_{site}}{N} - 1\right] = \mu_{ads}$$

The thermodynamic definition of chemical potential of an adsorbed species refers to a standard state chemical potential and a deviation from standard state, expressed by the activity of the adsorbed species.

$$\mu_{ads} = \mu_{ads}^{0} + kTln(a_{ads})$$

$$\mu_{ads}^{0} = \mu\left(N = \frac{N_{site}}{2}\right) = U_{ads}$$

One may set the statistical mechanics relationships between adsorbed sites and chemical potential equal to the thermodynamic relationship between chemical potential and activity.

$$U_{ads} - kTln\left[\frac{N_{site}}{N} - 1\right] = \mu_{ads} \quad (1)$$

$$U_{ads} + kTln(a_{ads}) = \mu_{ads} \quad (2)$$

$$\ln(a_{ads}) = -\ln\left[\frac{N_{site}}{N} - 1\right]$$

$$a_{ads} = \frac{1}{\frac{N_{site}}{N} - 1}$$

The Gibbs free energy of the adsorption process is the derivative of the free energy of the system with respect to the advancement of the solution, ξ.

$$\Delta G = \frac{\delta G}{\delta \xi}$$

$$dG = VdP - SdT + \mu_{solute} dN_{solute} + \mu_{ads} dN_{ads}$$

The rate of advancement, δξ, is related to the number of adsorbed molecules N_{ads} and the number of molecules of solute still in solution, N_{solute}.

$$\delta\xi = -dN_{solute} = dN_{ads}$$

$$\Delta G = \mu_{ads} - \mu_{solute}$$

The relationship between Gibbs free energy and the chemical potential of the adsorbed and dissolved species can be used to find another expression for a_{ads}. The change in free energy is represented by the free energy of a standard state, ΔG^0, and the chemical potentials of the adsorbed and solute species.

$$\Delta G = \mu_{\text{ads}} - \mu_{solute} = \Delta G^0 + kTln(a_{ads}) - kTln(a_{solute})$$

The standard state of a dilute solution is assumed to be a solution of a standard concentration, c_0. The system is assumed to be at equilibrium, and the change in Gibbs free energy for a solution at equilibrium is zero.

$$\Delta G = -\text{kTln}(\text{K}^0) + kTln(a_{adsorbed}) - kTln(a_{solute}) = 0$$

$$kTln(K^0) = kTln\left(\frac{a_{ads}}{a_{solute}}\right)$$

$$K^0 = \frac{a_{ads}}{a_{solute}}; a_{ads} = K^0 a_{solute}$$

A Langmuir-like relationship between the adsorbed species and activity of the solute emerges.

$$a_{ads} = \frac{1}{\frac{N_{site}}{N} - 1} = K^0 \cdot a_{solute}$$

$$\frac{N}{N_{site}} = \frac{K^0 \cdot a_{solute}}{1 + K^0 \cdot a_{solute}}$$

APPENDIX B. ADDITIONAL DATA AND FIGURES

Table B1. Characterization Data for PN_M17 Daily Samples

Major Oxides	5.10	5.11	5.12	5.13	5.14
SiO_2	66.78	64.79	74.12	61.06	71.05
Al_2O_3	4.53	4.84	4.08	5.52	4.58
Fe_2O_3	4.5	4.77	3.54	4.35	3.53
SO_3	1.01	1.01	0.65	1.16	0.81
CaO	15.29	16.69	11.93	19.55	13.68
Na_2O	0.33	0.34	0.22	0.33	0.29
MgO	1.32	1.46	0.97	1.58	1.18
K_2O	2.7	2.82	2.16	3.06	2.37
P_2O_5	0.61	0.66	0.45	0.73	0.57
TiO_2	0.41	0.46	0.42	0.44	0.41
SrO	-	0.09	0.07	0.09	0.08
BaO	0.1	0.11	0.07	0.1	0.09
LOI (%)	1.74	2.10	0.98	1.19	0.40
POC (%)	75.81	74.4	81.74	70.93	79.16
G_s	2.70	2.72	2.68	2.72	2.87
d_{50}	24.2	24.0	28.1	25.3	27.6

Table B2. Characterization Data for PN_N17 Daily Samples

Major Oxides	11.9	11.10	11.11	11.12	11.13	11.14	11.15	11.16	11.17
SiO_2	64.1	55.6	57.2	58.1	57.9	67.1	62.5	59.1	53.1
Al_2O_3	4.69	5.19	4.88	4.79	4.82	4.07	4.36	4.52	4.49
Fe_2O_3	3.78	4.25	4.22	4.17	4.18	2.97	3.25	3.64	4.52
SO_3	1.64	2.13	1.79	1.7	1.73	1.17	1.44	1.59	62.1
CaO	18.1	24.1	23.1	22.6	22.7	17.6	20.5	22.6	2.24
Na_2O	0.48	0.45	0.4	0.4	0.39	0.28	0.31	0.36	0.34
MgO	1.67	2.15	2.13	2.04	2.05	1.56	1.77	2.00	2.76
K_2O	3.18	3.59	3.57	3.5	3.56	3.07	3.31	3.52	5.21
P_2O_5	0.93	1.15	1.07	1.05	1.05	0.78	0.88	1.01	1.40
TiO_2	0.37	0.41	0.44	0.43	0.42	0.44	0.44	0.42	0.38
SrO	0.11	0.12	0.14	0.13	0.12	0.11	0.11	0.11	0.14
BaO	0.12	0.14	0.12	0.13	0.13	0.11	0.12	0.13	0.16
LOI (%)	6.17	7.60	5.76	6.12	5.64	4.24	3.89	5.64	5.94
POC (%)	72.6	65.0	66.3	67.1	66.9	74.1	70.1	67.3	62.1
G_s	2.80	2.91	2.65	2.93	2.69	2.67	2.74	2.83	2.76
d_{50}	22.7	21.0	22.9	24.4	22.8	22.8	23.5	22.7	21.3

Table B3. Characterization Data for PN_A18 Daily Samples

Major Oxides	3.28	3.29	3.30	3.31	4.1	4.2	4.3	4.4	4.6
SiO_2	61.87	60.51	84.96	53.41	64.46	62.54	62.8	62.12	71.51
Al_2O_3	4.2	4.31	2.62	4.11	3.78	3.75	3.49	3.65	3.11
Fe_2O_3	3.43	3.55	2.46	3.45	3.28	3.32	2.96	2.94	2.72
SO_3	1.72	1.71	0.15	2.15	1.51	1.64	1.57	1.64	0.88
CaO	18.68	20.12	5.58	24.71	17.93	19.07	19.13	19.7	13.61
Na_2O	0.25	0.31	0.18	0.25	0.27	0.26	0.23	0.23	0.22
MgO	2.19	2.19	0.6	2.52	2.07	2.21	2.13	2.15	1.54
K_2O	4.06	3.89	2.18	4.54	3.67	4.05	4.24	4.32	4.09
P_2O_5	1.15	1.11	0.37	1.29	1.08	1.13	1.11	1.11	0.83
TiO_2	0.47	0.45	0.31	0.42	0.39	0.36	0.35	0.36	0.28
SrO	0.1	0.1	0.04	0.12	0.09	0.1	0.1	0.1	0.07
BaO	0.14	0.14	0.07	0.16	0.14	0.15	0.15	0.15	0.13
LOI (%)	4.6	6.4	1.8	6.8	5.2	7.8	7.0	6.6	3.8
POC (%)	69.5	68.37	90.04	60.97	71.52	69.61	69.25	68.71	77.34
G_s	2.81	2.81	2.76	2.92	2.94	3.06	2.93	2.90	2.80
d_{50}	26.9	23.0	59.0	21.5	22.9	18.4	23.3	23.1	37.0

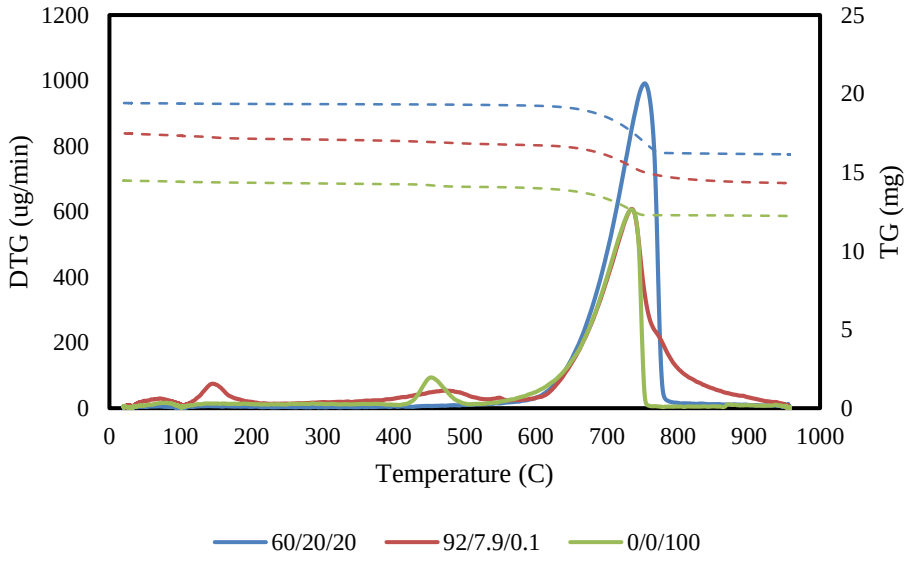

Figure 1B. Thermogravimetry analysis of three lab combusted samples identifying mass loss occurring in the N_2 atmosphere (below 950°C) and corresponding to the decomposition of carbonates. Peaks correspond to the DTG curve, and dashed lines correspond to the mass curve

Table B4. Lead leaching results from TCLP and SPLP methods [11,180,181]

Ash	Method Used	Lead Results (ppm)
BP1	TCLP	0.024
BP2	TCLP	nd (none detected)
CP4-1	TCLP	0.012
PM2	SPLP	0.018
PW8	SPLP	0.00027

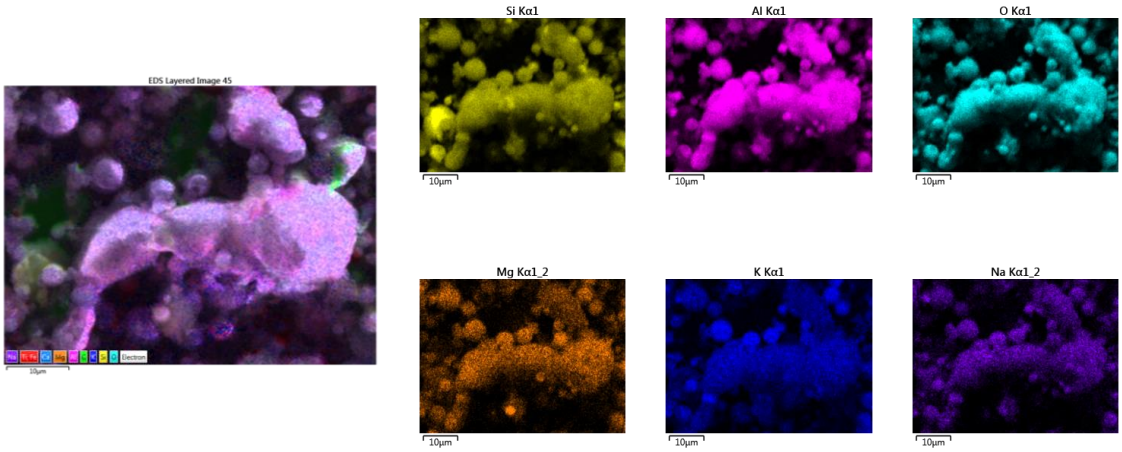

Figure 2B. SEM EDS micrographs representing the elemental composition of the as-received PY ash

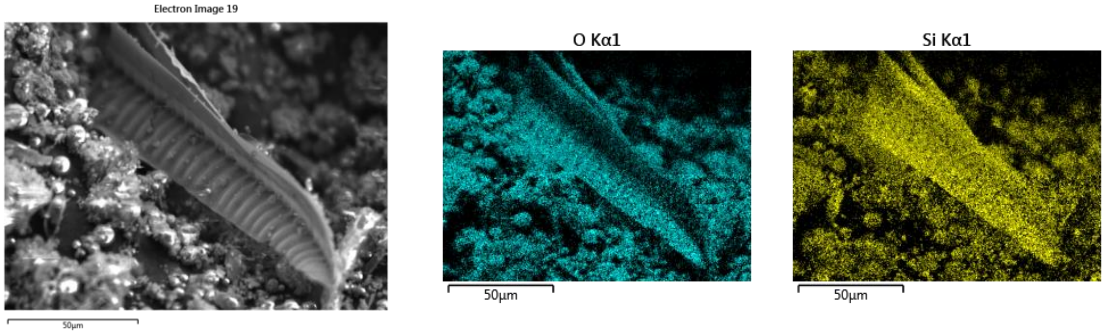

Figure 3B. SEM EDS micrograph of PY ash showing the elemental composition of diatom frustule

REFERENCES

[1] EPA. Disposal of Coal Combustion Residuals From Electric Utilities. Fed Arch 2015;80:21302–501.

[2] American Coal Ash Association. 2017 production and use survey report. Prod Use Reports 2017:1.

[3] Vassilev S V., Baxter D, Andersen LK, Vassileva CG, Morgan TJ. An overview of the organic and inorganic phase composition of biomass. Fuel 2012;94:1–33. doi:10.1016/j.fuel.2011.09.030.

[4] Vassilev S V., Baxter D, Andersen LK, Vassileva CG. An overview of the chemical composition of biomass. Fuel 2010;89:913–33. doi:10.1016/j.fuel.2009.10.022.

[5] Girón RP, Ruiz B, Fuente E, Gil RR, Suárez-Ruiz I. Properties of fly ash from forest biomass combustion. Fuel 2013;114:71–7. doi:10.1016/j.fuel.2012.04.042.

[6] UNEP. Fluidized Bed Combustion Boiler Technology For Cogeneration. Tech Study Rep 2007:1–68.

[7] Mahalle L, Berch S, Dymond C, Tedder S, Titus B, Todd M. Life cycle sustainability analysis sub-project of the woody biomass innovative project: a preliminary assessment. Tech Rep 2013:1–83.

[8] ASTM. Standard specification for coal fly ash and raw or calcined natural pozzolan for use in concrete. Annu B ASTM Stand 2017:3–6. doi:10.1520/C0618.

[9] Zhao G, Wu X, Tan X, Wang X. Sorption of heavy metal ions from aqueous solutions: A review. Open Colloid Sci J 2011;4:19–31.

[10] Santamarina JC, Klein KA, Wang YH, Prencke E. Specific surface: determination and relevance. Can Geotech J 2002;39:233–41. doi:10.1139/T01-077.

[11] Yeboah NNN. Characterization and productive reuse of high carbon content coal and biomass combustion residuals From energy production. Thesis 2014:1–204.

[12] Shearer CR. The productive reuse of coal, biomass, and co-fired fly ash. Thesis 2014:1–242.

[13] Yeboah NNN, Shearer CR, Burns SE, Kurtis KE. Characterization of biomass and high carbon content coal ash for productive reuse applications. Fuel 2014;116:438–47. doi:10.1016/j.fuel.2013.08.030.

[14] Shearer CR, Kurtis KE. Use of biomass and co-fired fly ash in concrete. ACI Mater J 2015;112:209–18. doi:10.14359/51686827.

[15] Sarkar DK. Thermal power plant: design and operation. 1st ed. Amsterdam: Elsevier; 2015.

[16] A.M DiGioia J, R.J. M, L.R. T. Fly ash structural fill handbook. EPRI 1979:1–223.

[17] Fisher GL, Chang DPY, Brummer M. Fly ash collected from electrostatic precipitators: microcrystalline structures and the mystery of the spheres. Science (80-) 1976;192:553–5.

[18] U.S. Energy Information Administration. Electric power monthly. Tech Rep

2018:1–222. doi:10.2172/123200.

[19] Thomas M. Optimizing the use of fly ash in concrete. Portl Cem Assoc 2007:1–24.

[20] Swamy RN. Design for durability and strength through the use of fly ash and slag in concrete. ACI Spec Publ Concr Technol 1997;171:1–72. doi:http://dx.doi.org/10.2471/BLT.06.038414.

[21] Gopalan MK. Sorptivity of fly ash concrete. Cem Concr Compos 1996;26:1189–97.

[22] Dinakar P, Babu KG, Santhanam M. Durability properties of high volume fly ash self compacting concretes. Cem Concr Compos 2008;30:880–6. doi:10.1016/j.cemconcomp.2008.06.011.

[23] Vassilev S V., Vassileva CG, Vassilev VS. Advantages and disadvantages of composition and properties of biomass in comparison with coal: An overview. Fuel 2015;158:330–50. doi:10.1016/j.fuel.2015.05.050.

[24] McCarthy GJ, Solem JK, Manz OE, Hassett DJ. Use of a database of chemical, mineralogical, and physical properties of North American fly ash to study the nature of fly ash and its utilization as a mineral admixture in concrete. Mater Res Soc Symp Proc 1990;178:3–33. doi:10.1017/CBO9781107415324.004.

[25] Fan M, Brown RC. Comparison of the loss-on-ignition and thermogravimetric analysis techniques in measuring unburned carbon in coal fly ash. Energy and Fuels 2001;15:1414–7. doi:10.1021/ef0100496.

[26] Brown RC, Dykstra J. Systematic errors in the use of loss-on-ignition to measure

unburned carbon in fly ash. Fuel 1995;74:570–4. doi:10.1016/0016-2361(95)98360-Q.

[27] Hill RL, Sarkar SL, Rathbone RF, Hower JC. An examination of fly ash carbon and its interactions with air entraining agent. Cem Concr Res 1997;27:193–204. doi:10.1016/S0008-8846(97)00008-2.

[28] Payá J, Monzó J, Borrachero M V., Amahjour F, Peris-Mora E. Loss on ignition and carbon content in pulverized fuel ashes (PFA): Two crucial parameters for quality control. J Chem Technol Biotechnol 2002;77:251–5. doi:10.1002/jctb.590.

[29] Schure MR, Soitys PA, Natusch DFS, Mauneys T. Surface area and porosity of coal fly ash. Environ Sci Technol 1985;19:82–6.

[30] Jones MR, McCarthy A, Booth APPG. Characteristics of the ultrafine component of fly ash. Fuel 2006;85:2250–9. doi:10.1016/j.fuel.2006.01.028.

[31] Kim B, Prezzi M. Evaluation of the mechanical properties of class-F fly ash. Waste Manag 2008;28:649–59. doi:10.1016/j.wasman.2007.04.006.

[32] Ngu LN, Wu H, Zhang DK. Characterization of ash cenospheres in fly ash from Australian power stations. Energy and Fuels 2007;21:3437–45. doi:10.1021/ef700340k.

[33] Musić S, Filipović-Vinceković N, Sekovanić L. Precipitation of amorphous SiO2 particules and their properties. Brazilian J Chem Eng 2011;28:89–94. doi:10.1590/S0104-66322011000100011.

[34] Das SK, Yudhbir. A simplified model for prediction of pozzolanic characteristics of fly ash, based on chemical composition. Cem Concr Res 2006;36:1827–32. doi:10.1016/j.cemconres.2006.02.020.

[35] Chandrasekaran SR, Hopke PK, Rector L, Allen G, Lin L. Chemical composition of wood chips and wood pellets. Energy & Fuels 2012;26:4932–7. doi:10.1021/ef4013328.

[36] Pettersen R. The chemical composition of wood. Chem Solid Wood 1984:1–9. doi:10.1021/ba-1984-0207.

[37] Ragland KW, Aerts DJ, Baker a. J. Properties of wood for combustion analysis. Bioresour Technol 1991;37:161–8. doi:10.1016/0960-8524(91)90205-X.

[38] Zule J, Dolenc J. Distribution of mineral substances in different wood tissues of European larch (Larix decidua Mill.). Drv Ind 2012;63:19–25. doi:10.5552/drind.2012.1117.

[39] McKendry P. Energy production from biomass (Part 1): Overview of biomass. Bioresour Technol 2002;83:37–46.

[40] Aho M, Gil A, Taipale R, Vainikka P, Vesala H. A pilot-scale fireside deposit study of co-firing Cynara with two coals in a fluidised bed. Fuel 2008;87:58–69. doi:10.1016/j.fuel.2007.03.046.

[41] van Eljk RJ, Obernberger I, Supancic K. Options for increased utilization of ash from biomass combustion and co-firing. IEA Bioenergy Task 32 Rep 2012:1–39.

[42] Girón RP, Gil RR, García AB, Fuente E, Nacional I, Csic I, et al. Preparation and charaterization of adsorbents/catalysts from forest biomass fly ash. 1st Spanish Natl. Conf. Adv. Mater. Recycl. Eco-Energy, 2009, p. 12–3.

[43] Vassilev S V., Baxter D, Andersen LK, Vassileva CG. An overview of the composition and application of biomass ash. Part 1. Phase–mineral and chemical composition and classification. Fuel 2013;105:40–76. doi:10.1016/j.fuel.2012.09.041.

[44] EPRI. Geotechnical Properties of Fly Ash and Potential for Static Liquefaction: Volume 1 - Summary and Conclusions. 2012. doi:1023743.

[45] Walton WH, Butler W. Root cause analysis of TVA Kingston dredge pond failure on December 22, 2008. AECOM Rep 2009:1–121.

[46] Kim B, Prezzi M. Compaction characteristics and corrosivity of Indiana class-F fly and bottom ash mixtures. Constr Build Mater 2008;22:694–702. doi:10.1016/j.conbuildmat.2006.09.007.

[47] Abhijit D, Sreedeep S. Evaluation of measurement methodologies used for establishing water retention characteristic curve of fly ash. J Test Eval 2015;43:20130091. doi:10.1520/JTE20130091.

[48] Kim B, Prezzi M, Salgado R. Geotechnical properties of fly and bottom ash mixtures for use in highway embankments. J Geotech Geoenvironmental Eng 2005:914–24.

[49] Malaya C, Sreedeep S. Effect of fertilizers and fly ash addition on suction–water

content relationship of a sandy soil. Indian Geotech J 2016;46:327–33. doi:10.1007/s40098-015-0174-2.

[50] Young SC, Schmidt-Petersen R, Ankeny M, Stephens DB. Physical and hydraulic properties of fly ash and other by-products from coal combustion. EPRI Rep 1993:1–73.

[51] Bachus RC, Santamarina JC. Geotechnical properties and diagenesis of ponded fly ash. Geo-Congress 2014 Tech Pap 2014:326–33. doi:10.1061/9780784413272.032.

[52] Foster KM, Rodriguez-marek A, Green R a, Sanchez RL. Dynamic geotechnical laboratory testing of coal combustion products. World Coal Ash Conf., 2013, p. 1–15.

[53] Marto A, Awang AR. Compaction characteristics and permeability of Tanjung Bin coal ash mixtures. 2011 Int Conf Environ Sci Eng 2011;8:134–7.

[54] Vassilev S V., Menendez R, Alvarez D, Diaz-Somoano M, Martinez-Tarazona MR. Phase-mineral and chemical composition of coal fly ashes as a basis for their multicomponent utilization. 1. Characterization of feed coals and fly ashes. Fuel 2003;82:1793–811. doi:10.1016/S0016-2361(03)00123-6.

[55] Akinyemi SA, Ojo OI, Gitari WM, Akinlua A, Fatoba OO, Petrik LF. Mobility and transport of inorganic species in weathered hydraulic disposed coal fly ash : An insight from geochemical fractionation and statistical evaluation. Energy Sci Technol 2012;3:10–20. doi:10.3968/j.est.1923847920120301.154.

[56] Akinyemi SA, Akinlua A, Gitari WM, Petrik LF. Mineralogy and mobility patterns of chemical species in weathered coal fly ash. Energy Sources, Part A Recover Util Environ Eff 2011;33:768–84. doi:10.1080/15567030903261881.

[57] EPRI. Weathering processes and secondary minerals formed in coal ash. Tech Rep 2006:1–50.

[58] Hosseini T, Han B, Selomulya C, Haque N, Zhang L. Chemical and morphological changes of weathered Victorian brown coal fly ash and its leaching characteristic upon the leaching in ammonia chloride and hydrochloric acid. Hydrometallurgy 2015;157:22–32. doi:10.1016/j.hydromet.2015.07.012.

[59] Zevenbergen C, Bradley JP, Van Reeuwijk LP, Shyam a K, Hjelmar O, Comans RNJ. Clay formation and metal fixation during weathering of coal fly ash. Environ Sci Technol 1999;33:3405–9.

[60] Mccarthy GJ, Grier DG, Wisdom M a, Renee B, Lerach SL, Jarabek RL, et al. Coal combustion by-product diagenesis II. 1999 Int. Ash Util. Symp., 1999, p. 1–9.

[61] Gitari MW, Fatoba OO, Nyamihingura A, Petrik LF, Vadapalli VRK, October A, et al. Chemical weathering in a dry ash dump: an insight from physicochemical and mineralogical analysis of drilled cores. 2009 World Coal Ash Conf., 2009, p. 1729–47.

[62] ASTM. Standard Test Methods for Loss on Ignition (LOI) of Solid Combustion Residues. 2013. doi:10.1520/D7348-08.2.

[63] Mohebbi M, Rajabipour F, Scheetz BE. Evaluation of two-atmosphere thermogravimetric analysis for determining the unburned carbon content in fly ash. Adv Civ Eng Mater 2017;6:20160052. doi:10.1520/ACEM20160052.

[64] Külaots I, Hurt RH, Suuberg EM. Size distribution of unburned carbon in coal fly ash and its implications. Fuel 2004;83:223–30. doi:10.1016/S0016-2361(03)00255-2.

[65] Engbrecht DC, Hirschfeld DA. Thermal analysis of calcium sulfate dihydrate sources used to manufacture gypsum wallboard. Thermochim Acta 2016;639:173–85. doi:10.1016/j.tca.2016.07.021.

[66] Payá J, Monzó J, Borrachero M V., Perris E, Amahjour F. Thermogravimetric methods for determining carbon content in fly ashes. Cem Concr Res 1998;28:675–86. doi:10.1016/S0008-8846(98)00030-1.

[67] Kobyłecki R. Unburned carbon in the circulating fluidised bed boiler fly ash. Chem Process Eng 2011;32:255–66. doi:10.2478/v10176-011-0020-8.

[68] Straka P, Náhunková J, Žaloudková M. Analysis of unburned carbon in industrial ashes from biomass combustion by thermogravimetric method using Boudouard reaction. Thermochim Acta 2014;575:188–94. doi:10.1016/j.tca.2013.10.033.

[69] Villain G, Thiery M, Platret G. Measurement methods of carbonation profiles in concrete: Thermogravimetry, chemical analysis and gammadensimetry. Cem Concr Res 2007;37:1182–92. doi:10.1016/j.cemconres.2007.04.015.

[70] Kumpiene J, Robinson R, Brannvall E, Nordmark D, Bjurstrom H, Andreas L, et al. Carbon speciation in ash, residual waste and contaminated soil by thermal and chemical analyses. Waste Manag 2011;31:18–25. doi:10.1016/j.wasman.2010.06.011.

[71] Styszko-Grochowiak K, Gołłaś J, Jankowski H, Koziński S. Characterization of the coal fly ash for the purpose of improvement of industrial on-line measurement of unburned carbon content. Fuel 2004;83:1847–53. doi:10.1016/j.fuel.2004.03.005.

[72] Yeheyis MB, Shang JQ, Yanful EK. Chemical and mineralogical transformations of coal fly ash after landfilling. World Coal Ash Conf., 2009, p. 1–13.

[73] Bray HJ, Redfern SAT. Kinetics of dehydration of Ca-montmorillonite. Phys Chem Miner 1999;26:591–600. doi:10.1007/s002690050223.

[74] Kristóf J, Frost RL, Kloprogge JT, Horváth E, Makó É. Detection of four different OH-groups in ground kaolinite with controlled-rate thermal analysis. J Therm Anal Calorim 2002;69:77–83. doi:10.1023/A:1019981505712.

[75] Sarikaya Y, Onal M, Baran B, Alemdaroglu T. The effect of thermal treatment on some of the physicochemical properties of a bentonite. Clays Clay Miner 2000;48:557–62.

[76] Bernal SA, Juenger MCG, Ke X, Matthes W, Lothenbach B, De Belie N, et al. Characterization of supplementary cementitious materials by thermal analysis. Mater Struct 2017;50:26. doi:10.1617/s11527-016-0909-2.

[77] Beck CW. Differential thermal analysis curves of carbonate minerals. Am Mineral 1950:985–1013.

[78] Levandowski J, Kalkreuth W. Chemical and petrographical characterization of feed coal, fly ash and bottom ash from the Figueira Power Plant, Parana, Brazil. Int J Coal Geol 2009;77:269–81. doi:10.1016/j.coal.2008.05.005.

[79] Shimadzu. TOC-V Series - Total Organic Carbon Analyzer 5000A. Manual 2008:1–20.

[80] Stefaniak S, Miszczak E, Szczepanska-Plewa J, Twardowska I. Effect of weathering transformations of coal combustion residuals on trace element mobility in view of the environmental safety and sustainability of their disposal and use. I. Hydrogeochemical processes controlling pH and phase stability. J Environ Manage 2015;156:128–42. doi:10.1016/j.jenvman.2015.03.046.

[81] Peel MC, Finlayson BL, McMahon TA. Updated world map of the Köppen-Geiger climate classification. Hydrol Earth Syst Sci 2007;11:1633–44. doi:10.5194/hess-11-1633-2007.

[82] Eze CP, Nyale SM, Akinyeye RO, Gitari WM, Akinyemi SA, Fatoba OO, et al. Chemical, mineralogical and morphological changes in weathered coal fly ash: A case study of a brine impacted wet ash dump. J Environ Manage 2013;129:479–92. doi:10.1016/j.jenvman.2013.07.024.

[83] Kim K, Kim SH, Park SM, Kim J, Choi M. Processes controlling the variations of pH, alkalinity, and CO2 partial pressure in the porewater of coal ash disposal site. J

Hazard Mater 2010;181:74–81. doi:10.1016/j.jhazmat.2010.04.089.

[84] Griffin JJ, Goldberg ED. Sphericity as a characteristic of solids from fossil fuel burning in a Lake Michigan sediment. Geochim Cosmochim Acta 1981;45:763–9. doi:10.1016/0016-7037(81)90047-8.

[85] Lu Y, Rostam-Abadi M, Chang R, Richardson C, Paradis J. Characteristics of fly ashes from full-scale coal-fired power plants and their relationship to mercury adsorption. Energy and Fuels 2007;21:2112–20. doi:10.1021/ef070145s.

[86] Vassilev S V., Menendez R, Borrego AG, Diaz-Somoano M, Martinez-Tarazona MR. Phase-mineral and chemical composition of coal fly ashes as a basis for their multicomponent utilization. 3. Characterization of magnetic and char concentrates. Fuel 2004;83:1563–83. doi:10.1016/j.fuel.2004.01.010.

[87] Wirth X, Benkeser D, Yeboah NNN, Shearer CR, Kurtis KE, Burns SE. Evaluation of alternative fly ashes as SCMs. ACI Mater J 2019;Accepted:1–25.

[88] FHWA. Petrographic methods of examining hardened concrete: A petrographic manual. Tech Rep 2006:221–45.

[89] Altman N, Krzywinski M. Analyzing outliers: Influential or nuisance? Nat Methods 2016;13:281–2. doi:10.1038/nmeth.3812.

[90] Vassilev S V., Baxter D, Andersen LK, Vassileva CG. An overview of the composition and application of biomass ash. Fuel 2012;105:19–39. doi:10.1016/j.fuel.2012.10.001.

[91] Schiemenz K, Eichler-Löbermann B. Biomass ashes and their phosphorus fertilizing effect on different crops. Nutr Cycl Agroecosystems 2010;87:471–82. doi:10.1007/s10705-010-9353-9.

[92] Risse LM, Gaskin JW. Best management practices for wood ash as agricultural soil amendment. Univ Georg Coop Ext Bull 2002;1142:1–4.

[93] Gitari WM, Petrik LF, Etchebers O, Key DL, Okujeni C. Utilization of fly ash for treatment of coal mines wastewater: Solubility controls on major inorganic contaminants. Fuel 2008;87:2450–62. doi:10.1016/j.fuel.2008.03.018.

[94] Erol M, Küçükbayrak S, Ersoy-Meriçboyu A, Uluba T. Removal of Cu2+ and Pb2+ in aqueous solutions by fly ash. Energy Convers Manag 2005;46:1319–31. doi:10.1016/j.enconman.2004.06.033.

[95] Renew JE, Huang C, Burns SE, Carrasquillo M, Sun W, Ellison KM. Immobilization of heavy metals by solidification/stabilization of co-disposed flue gas desulfurization brine and coal fly ash. Energy & Fuels 2016;30:5042–51. doi:10.1021/acs.energyfuels.6b00321.

[96] Goldsworthy P, Eyre D. Chapter 17: Value-in-use (VIU) assessment for thermal and metallurgical coal. Coal Handb 2013:455–96. doi:10.1533/9781782421177.3.455.

[97] Jaworek A, Czech T, Sobczyk AT, Krupa A. Properties of biomass vs. coal fly ashes deposited in electrostatic precipitator. J Electrostat 2013;71:165–75. doi:10.1016/j.elstat.2013.01.009.

[98] Cordeiro GC, Filho RDT, Fairbairn EMR. Effect of calcination temperature on the pozzolanic activity of sugar cane bagasse ash. Constr Build Mater 2009;23:3301–3. doi:10.1016/j.conbuildmat.2009.02.013.

[99] Zhao M, Han Z, Sheng C, Wu H. Characterization of residual carbon in fly ashes from power plants firing biomass. Energy & Fuels 2013;27:898–907. doi:10.1021/ef301715p.

[100] Vassilev S V., Baxter D, Vassileva CG. An overview of the behaviour of biomass during combustion: Part I. Phase-mineral transformations of organic and inorganic matter. Fuel 2013;112:391–449. doi:10.1016/j.fuel.2013.05.043.

[101] Vassilev S V., Baxter D, Vassileva CG. An overview of the behaviour of biomass during combustion: Part II. Ash fusion and ash formation mechanisms of biomass types. Fuel 2014;117:152–83. doi:10.1016/j.fuel.2013.09.024.

[102] Johnson A, Catalan LJJ, Kinrade SD. Characterization and evaluation of fly-ash from co-combustion of lignite and wood pellets for use as cement admixture. Fuel 2010;89:3042–50. doi:10.1016/j.fuel.2010.05.027.

[103] Ren, W., Santamarina JC. The hydraulic conductivity of sediments: A pore size perspective. Eng Geol 2017;223:48–54. doi:10.1016/j.enggeo.2017.11.022.

[104] Palmer BG, Edil TB, Benson CH. Liners for waste containment constructed with class F and C fly ashes. J Hazard Mater 2000;76:193–216.

[105] Webb RW, Stormont JC, Stone MCS, Thomson BM. Characterizing the unsaturated

and saturated hydraulic properties of coal combustion by-products in landfills of northwestern New Mexico. Am Soc Min Reclam 2014;3:70–99. doi:10.21000/JASMR14010070.

[106] Zabielska-Adamska K. Fly ash as a barrier material. Geo-Frontiers 2011, 2011, p. 947–56.

[107] Van Genuchten MT, Leij FJ, Yates SR. The RETC code for quantifying the hydraulic functions of unsaturated soils. EPA Rep 1991:1–85.

[108] Malaya C, Sreedeep S. Critical evaluation of the drying water retention characteristics of a Class F Fly ash. J Mater Civ Eng 2012;24:451–9. doi:10.1061/(ASCE)MT.1943-5533.

[109] Roberts DW. Soil properties, classification, and hydraulic conductivity testing. EPA Tech Resour Doc 1984:1–138.

[110] Minasny B, McBratney AB. Integral energy as a measure of soil-water availability. Plant Soil 2003;249:253–62. doi:10.1023/A.

[111] Ghodrati M, Sims JT, Vasilas BL. Evaluation of fly ash as as soil amendment for the Atlantic coastal plain: I. Soil hydraulic properties and elemental leaching. Water Air Soil Pollut 1995;81:349–61.

[112] Mehra OP, Jackson ML. Iron oxide removal from soils and clays by a dithionite-citrate system buffered with sodium bicarbonate. Clays Clay Miner 1958;7:317–27. doi:10.1346/CCMN.1958.0070122.

[113] Fan SS, Chang FH, Hsueh HT, Ko TH. Measurement of total free iron in soils by H2S chemisorption and comparison with the citrate bicarbonate dithionite method. J Anal Methods Chem 2016:1–7. doi:10.1155/2016/7213542.

[114] Ramaroson VH, Becquer T, Sá SO, Razafimahatratra H, Delarivière JL, Blavet D, et al. Mineralogical analysis of ferralitic soils in Madagascar using NIR spectroscopy. Catena 2018;168:102–9. doi:10.1016/j.catena.2017.07.016.

[115] ASTM. Standard test methods for measurement of hydraulic conductivity of saturated porous materials using a flexible wall permeameter. Annu B ASTM Stand 2016:1–24. doi:10.1520/D5084-16A.1.

[116] Skempton AW. the Pore-Pressure Coefficients a and B. Geotechnique 1954:65–9. doi:10.1680/sposm.02050.0010.

[117] Dunn RJ. Laboratory measurement of fine-grained soil fluid conductivity. Eng Geol 1985;21:215–23.

[118] ASTM. Standard test methods for determination of the soil water characteristic curve for desorption using hanging column, pressure extractor, chilled mirror hygrometer, or Centrifuge 1. Annu B ASTM Stand 2016:1–22. doi:10.1520/D6836-02R08E02.characteristic.

[119] Van Genuchten MT. A closed-form solution for predicting the hydraulic conductivity of unsaturated soils. Soil Sci Soc Am 1980;44:892–8. doi:doi:10.2136/sssaj1980.03615995004400050002x.

[120] Hofstetter TB, Schwarzenbach RP, Haderlein SB. Reactivity of Fe(II) species associated with clay minerals. Environ Sci Technol 2003;37:519–28. doi:10.1021/es025955r.

[121] Jepson WB. Chapter 15: Structural iron in kaolinites and in associated ancillary minerals. Iron Soils Clay Miner 1988:467–536. doi:10.1017/CBO9781107415324.004.

[122] Chotoli FF, Quarcioni VA, Lima SS, Ferreira JC, Ferreira GM. Clay activation and color modification in reducing calcination process: development in lab and industrial scale. Calcined Clays Sustain Concr 2018;16. doi:10.1007/978-94-024-1207-9.

[123] Thomas RE. High temperature processing of kaolinitic materials. Thesis 2010:1–324.

[124] Murad E, Wagner U. Pure and impure clays and their firing products. Hyperfine Interact 1989;45:161–77.

[125] Chandrasekhar S, Ramaswamy S. Iron minerals and their influence on the optical properties of two Indian kaolins. Appl Clay Sci 2006;33:269–77. doi:10.1016/j.clay.2006.06.008.

[126] Wirth X, Glatstein DA, Burns SE. Mineral phases and carbon content in weathered fly ashes. Fuel 2018;236:1567–76. doi:10.1016/j.fuel.2018.09.106.

[127] Georgia Power. Plant Yates history of constru. Report 2018:1–10.

[128] Rozenson I, Spiro B, Zak I. Transformation of iron-bearing kaolinite to iron-free kaolinite, geothite, and hematite. Clay Clay Miner 1982;30:207–14.

[129] Sengupta P, Saikia PC, Borthakur PC. SEM-EDX characterization of an iron-rich kaolinite clay. J Sci Ind Res (India) 2008;67:812–8.

[130] Santamarina JC, Klein KA, Fam MA. Soils and Waves. John Wiley and Sons, Inc.; 2001.

[131] Lu N, Likos WJ. Unsaturated Soil Mechanics. John Wiley and Sons, Inc.; 2004.

[132] Burger BCA, Shackelford CD, Member A. Soil-water characteristic curves and dual porosity sand – diatomaceous earth mixtures. J Geotech Geoenvironmental Eng 2001;8:790–800.

[133] Dumenu L, Pando MA, Ogunro VO, Daniels JL, Moid MI, Rodriguez C. Water retention characteristics of compacted coal combustion residuals. Geo-Frontiers 2017, 2017, p. 403–13.

[134] AASHTO Subcommittee on Materials. 2016 fly ash task force report. Report 2016:1–22.

[135] American Coal Ash Association. Fly ash facts for highway engineers. 2003. doi:10.1017/CBO9781107415324.004.

[136] Gopalan MK. Sorptivity of fly ash concretes. Cem Concr Res 1996;26:1189–97.

[137] Nath P, Sarker P. Effect of fly ash on the durability properties of high strength concrete. Procedia Eng 2011;14:1149–56. doi:10.1016/j.proeng.2011.07.144.

[138] Swamy RN. Design for durability and strength through the use of fly ash and slag in concrete. ACI Spec Publ Concr Technol 1997;171:1–72. doi:http://dx.doi.org/10.2471/BLT.06.038414.

[139] Burris LE. Increasing the reactivity of natural zeolites used as supplementary cementitious materials. Thesis 2014:1–274.

[140] Cancio Díaz Y, Sánchez Berriel S, Heierli U, Favier AR, Sánchez Machado IR, Scrivener KL, et al. Limestone calcined clay cement as a low-carbon solution to meet expanding cement demand in emerging economies. Dev Eng 2017;2:82–91. doi:10.1016/j.deveng.2017.06.001.

[141] Maraghechi H, Salwocki S, Rajabipour F. Utilisation of alkali activated glass powder in binary mixtures with Portland cement, slag, fly ash and hydrated lime. Mater Struct Constr 2017;50. doi:10.1617/s11527-016-0922-5.

[142] van Loo S, Koppejan J, Tustin J, Carling N. Biomass combustion and co-firing. IEA Bioenergy Rep 2002:1–16.

[143] Georgia Power. Plant Wansley history of Construction. Report 2018:1–19.

[144] Mccarthy GJ, Grier DG, Wisdom M a, Renee B, Lerach SL, Jarabek RL, et al. Coal combustion by-product diagenesis II. Int. Ash Util. Symp., 1999, p. 1–9.

[145] Zhang MH, Malhotra VM. High-performance concrete incorporating rice husk ash as a supplementary cementing material. ACI Mater J 1996;93:629–36. doi:10.14359/9870.

[146] Zareei SA, Ameri F, Dorostkar F, Ahmadi M. Rice husk ash as a partial replacement of cement in high strength concrete containing micro silica: Evaluating durability and mechanical properties. Case Stud Constr Mater 2017;7:73–81. doi:10.1016/j.cscm.2017.05.001.

[147] Isaia GC, Gastaldini ALG, Moraes R. Physical and pozzolanic action of mineral additions on the mechanical strength of high-performance concrete. Cem Concr Compos 2003;25:69–76. doi:10.1016/S0958-9465(01)00057-9.

[148] Berra M, Mangialardi T, Paolini AE. Reuse of woody biomass fly ash in cement-based materials. Constr Build Mater 2015;76:286–96. doi:10.1016/j.conbuildmat.2014.11.052.

[149] Ukrainczyk N. Reuse of woody biomass ash waste in cementitious materials. Chem Biochem Eng Q 2016;30:137–48. doi:10.15255/CABEQ.2015.2231.

[150] Wang S, Miller A, Llamazos E, Fonseca F, Baxter L. Biomass fly ash in concrete: Mixture proportioning and mechanical properties. Fuel 2008;87:365–71. doi:10.1016/j.fuel.2007.05.026.

[151] Fedorka W, Knowles J, Castleman J. Reclaiming and recycling coal fly ash for beneficial reuse with the STAR^{TM} process. 2015 World Coal Ash Conf., 2015, p. 1–10.

[152] EN. Fly ash for concrete (EN 405-1:2005). Br Stand 2005:1–34.

[153] Chancey RT, Stutzman P, Juenger MCG, Fowler DW. Comprehensive phase

characterization of crystalline and amorphous phases of a Class F fly ash. Cem Concr Res 2010;40:146–56. doi:10.1016/j.cemconres.2009.08.029.

[154] ASTM. Standard test method for compressive strength of hydraulic cement mortars (2-in or 50mm cube specimens). 2016. doi:10.1520/C0109.

[155] Plunk GC. How PACT was used to avoid 5 million tons of landfilled fly ash. Appl Sci Sustain Coal Ash 2015:14–7.

[156] van Roode M, Douglas E, Hemmings RT. X-ray diffraction measurement of glass content in fly and slags. Cem Concr Res 1987;17:183–97. doi:10.1016/0008-8846(87)90101-3.

[157] Van Der Merwe EM, Prinsloo LC, Mathebula CL, Swart HC, Coetsee E, Doucet FJ. Surface and bulk characterization of an ultrafine South African coal fly ash with reference to polymer applications. Appl Surf Sci 2014;317:73–83. doi:10.1016/j.apsusc.2014.08.080.

[158] Font O, Moreno N, Querol X, Izquierdo M, Alvarez E, Diez S, et al. X-ray powder diffraction-based method for the determination of the glass content and mineralogy of coal (co)-combustion fly ashes. Fuel 2010;89:2971–6. doi:10.1016/j.fuel.2009.11.024.

[159] Ibáñez J, Font O, Moreno N, Elvira JJ, Alvarez S, Querol X. Quantitative Rietveld analysis of the crystalline and amorphous phases in coal fly ashes. Fuel 2013;105:314–7. doi:10.1016/j.fuel.2012.06.090.

[160] Yan K, Guo Y, Ma Z, Zhao Z, Cheng F. Quantitative analysis of crystalline and amorphous phases in pulverized coal fly ash based on the Rietveld method. J Non Cryst Solids 2018;483:37–42. doi:10.1016/j.jnoncrysol.2017.12.043.

[161] Oey T, Timmons J, Stutzman P, Bullard JW, Balonis M, Bauchy M, et al. An improved basis for characterizing the suitability of fly ash as a cement replacement agent. J Am Ceram Soc 2017;100:4785–800. doi:10.1111/jace.14974.

[162] Feng Q, Lin Q, Gong F, Sugita S, Shoya M. Adsorption of lead and mercury by rice husk ash. J Colloid Interface Sci 2004;278:1–8. doi:10.1016/j.jcis.2004.05.030.

[163] Xu X, Cao X, Zhao L. Comparison of rice husk- and dairy manure-derived biochars for simultaneously removing heavy metals from aqueous solutions: Role of mineral components in biochars. Chemosphere 2013;92:955–61. doi:10.1016/j.chemosphere.2013.03.009.

[164] Kongsuwan A, Patnukao P, Pavasant P. Binary component sorption of Cu(II) and Pb(II) with activated carbon from Eucalyptus camaldulensis Dehn bark. J Ind Eng Chem 2009;15:465–70. doi:10.1016/j.jiec.2009.02.002.

[165] Strawn DG, Sparks DL. The use of XAFS to distinguish between inner- and outer-sphere lead adsorption complexes on montmorillonite. J Colloid Interface Sci 1999;216:257–69. doi:10.1006/jcis.1999.6330.

[166] Srivastava SK, Singh AK, Sharma A. Studies on the uptake of lead and zinc by lignin obtained from black liquor - a paper industry waste material. Environ Technol (United Kingdom) 1994;15:353–61. doi:10.1080/09593339409385438.

[167] Anis M, Haydar S, Bari AJ. Adsorption of lead and copper from aqueous solution using unmodified wheat straw. Environ Eng Manag J 2013;12:2117–24.

[168] Castaldi P, Silvetti M, Garau G, Demurtas D, Deiana S. Copper(II) and lead(II) removal from aqueous solution by water treatment residues. J Hazard Mater 2015;283:140–7. doi:10.1016/j.jhazmat.2014.09.019.

[169] Zhou YF, Haynes RJ. Sorption of heavy metals by inorganic and organic components of solid wastes: Significance to use of wastes as low-cost adsorbents and immobilizing agents. Crit Rev Environ Sci Technol 2010;40:909–77. doi:10.1080/10643380802586857.

[170] Moreno-Barbosa J, López-Velandia C, Maldonado A, Giraldo L, Moreno-Piraján J. Removal of lead(II) and zinc(II) ions from aqueous solutions by adsorption onto activated carbon synthesized from watermelon shell and walnut shell. Adsorption 2013;19:675–85. doi:10.1007/s10450-013-9491-x.

[171] Shao Y, Wang J, Preto F, Zhu J, Xu C. Ash deposition in biomass combustion or co-firing for power/heat generation. Energies 2012;5:5171–89. doi:10.3390/en5125171.

[172] Al-Degs YS, El-Barghouthi MI, Issa AA, Khraisheh MA, Walker GM. Sorption of Zn(II), Pb(II), and Co(II) using natural sorbents: Equilibrium and kinetic studies. Water Res 2006;40:2645–58. doi:10.1016/j.watres.2006.05.018.

[173] Hayes KF, Leckie JO. Modeling ionic strength effects on cation adsorption at hydrous oxide/solution interfaces. J Colloid Interface Sci 1987;115.

[174] Hayes KF, Papelis C, Leckie JO. Modeling ionic strength effects on anion adsorption at hydrous oxide/solution interfaces. J Colloid Interface Sci 1988;125:717–26. doi:10.1016/0021-9797(88)90039-2.

[175] Pesavento M, Profumo A, Alberti G, Conti F. Adsorption of lead(II) and copper(II) on activated carbon by complexation with surface functional groups. Anal Chim Acta 2003;480:171–80. doi:10.1016/S0003-2670(02)01597-0.

[176] Merdy P, Gharbi LT, Lucas Y. Pb, Cu and Cr interactions with soil: Sorption experiments and modelling. Colloids Surfaces A Physicochem Eng Asp 2009;347:192–9. doi:10.1016/j.colsurfa.2009.04.004.

[177] Singh A, Kumar D, Gaur JP. Removal of Cu(II) and Pb(II) by Pithophora oedogonia: sorption, desorption and repeated use of the biomass. J Hazard Mater 2008;152:1011–9. doi:10.1016/j.jhazmat.2007.07.076.

[178] Wang J, Teng X, Wang H, Ban H. Characterizing the metal adsorption capability of a class F coal fly ash. Environ Sci Technol 2004;38:6710–5. doi:10.1021/es049544h.

[179] National Weather Service. Addition Köppen Climate Subdivisions n.d. https://www.weather.gov/jetstream/climate_max.

[180] EPA. Toxicity characteristic leaching procedure. EPA Tech Resour Doc 1992:1–35.

[181] EPA. Synthetic precipitation leaching procedure. EPA Tech Resour Doc 1994:1–30.

[182] ASTM. Standard test method for measuring the exchange complex and cation exchange capacity of inorganic fine grained soils. Annu B ASTM Stand 2018:1–4. doi:10.1520/D7503.

[183] Langmuir I. The adsorption of gases on plane surfaces of glass, mica, and platinum. Dtsch Phys Gesellschaft 1918;16:1361–403.

[184] Chu J, Panzion P, Bradley L. An approach to using geochemical analysis to evaluate the potential presence of coal ash in drinking water. World Coal Ash Conf., 2017, p. 1–13.

[185] Parkhurst DL, Appelo CAJ. Description of input and examples for PHREEQC version 3 — A computer program for speciation, batch-reaction, one-dimensional transport, and inverse geochemical calculations. Groundw. B. 6, Model. Tech., 2013, p. 1–497. doi:10.1016/0029-6554(94)90020-5.

[186] Kardar M. Statistical Physics of Particles. Cambridge University Press; 2007.

[187] Atkins P, Paula JDE. Physical Chemistry. 8th Editio. Oxford University Press; 2006.

[188] Wilson T, Velleux M, Hallden J, Filardi M, Nolan PJ, Miller B. Surface Complexation Model Use and Sorptive Capacity Evaluations for Inorganic Constituents From Coal Combustion Residuals to Guide Monitored Natural Attenuation Assessment 2017.

[189] Ma SC, Zhang JL, Sun DH, Liu GX. Surface complexation modeling calculation of Pb(II) adsorption onto the calcined diatomite. Appl Surf Sci 2015;359:48–54.

doi:10.1016/j.apsusc.2015.09.133.